DE-LUBRICATION DURING SINTERING OF P/M COMPACTS:

OPERATIVE MECHANISM AND PROCESS CONTROL STRATEGY

by

Deepak Saha

A Thesis

Submitted to the Faculty

of the

WORCESTER POLYTECHNIC INSTITUTE

in partial fulfillment of the requirements for the

Degree of Masters of Science

in

Material Science and Engineering

by

_____

May 2001

APPROVED:

_____

Dr. Diran Apelian, Major Advisor

_____

Dr. Richard D. Sisson, Program Head

ABSTRACT

De-lubrication is the first stage in a sintering operation, where the lubricants (higher weight hydrocarbons) are removed from the parts by controlled heating. Improper de-lubrication leads to defects such as blistering, sooting, micro-porosity etc in a sintered part. Most of these problems arise, as there exists a gap in the present understanding of de-lubrication. The primary motive of this work is to direct research towards the development of sensors and controls and thus, mitigate the various problems due to improper de-lubrication. Currently, there exists a myriad of lubricants being used during the process of compaction. They include metallic based lubricants, polymers and non-metallic lubricants. In this work, research was limited in understanding the de-lubrication of EBS (Ethylene Bisstearimide), as, it the most commonly used lubricant in the industry. It has replaced commonly used lubricant due to cleaner burnouts, absence of metallic residue and, cost effectiveness. The entire work is divided into three phases:

- Phase 1: Ascertained the most important parameters that affect the kinetics of de-lubrication.
- Phase 2: Investigated the type of gases released during the decomposition of EBS.
- Phase 3: Recommended a control strategy.

TGA (Thermo-gravimetric analysis) was used in the phase I, the results clearly show that the rate of heating is the most important parameter during de-lubrication. Identification of gases was performed using the FTIR (Fourier transform infrared spectroscopy) and DUV (Deep ultraviolet spectroscopy). This constituted the second phase of our experiments. The primary gases identified in Phase II were carbon dioxide and a hydrocarbon (hepta-decane). Finally, an empirical model for de-lubrication has been proposed in Phase III. The model was verified in an industrial furnace. It has been observed that there exists a very good correlation between the proposed empirical model and the experiments performed in Phase II of this study.

This study lays down the following guidelines for the development of future sensors and controls:
- The development of future sensors should focus in the detection of CO_2 and hepta-decane.
- Rate of heating determines how fast or slow the lubricant decomposes and finally escapes form the compacted part.
- The empirical model may be used, as a means to determine the time a part should reside in a furnace for complete lubricant burnout at a given heating rate.

ACKNOWLEDGEMENTS

TABLE OF CONTENTS

LIST OF FIGURES

LIST OF TABLES

1.0 INTRODUCTION AND OVERVIEW

A typical sintering furnace is divided into three zones. The first zone of a sintering furnace is solely used for the removal of lubricants from the compacted part. This is achieved by heating the part to temperatures in the range of 500-600^{0}C at a controlled rate and atmospheric conditions. The de-lubricated part then enters the hot zone where it is heated to higher temperatures (close to its melting point) for sintering. The third zone or the cooling zone cools the sintered part at a desired rate to get the requisite micro structural properties. Proper de-lubrication is an important issue for the following reasons:

1. The end temperature of the first zone is normally 550-600 ^{0}C. Figure 1 shows a typical temperature furnace profile across the length of the furnace. As the part enters the hot zone (temperatures of 1200-1300 ^{0}C), it experiences a temperature gradient in a very short time, which causes the left over lubricant to expand rapidly and introduce cracks on the surface (blistering).
2. Improper gas flows and belt speeds can lead to the deposition carbon on the part. This is called sooting.
3. Most lubricants are hydrocarbons and improper removal can lead to carbon segregation at the grain boundaries.

Micro-cracks, carbon segregated grain boundaries and sooting are strong quality detractors of sintered parts. Very little knowledge base in the various parameters and kinetics of the reactions during de-lubrication has stymied the development of effective control systems for this process. Manufacturers follow different strategies to alleviate this problem. These vary from longer de-lubrication zones to increased amount of moisture in the furnace.

The literature review and the plant visits we carried out have confirmed that the "physics" of de-lubrication are not well established and the reason why there exists so many approaches. The objective of this work is to understand the physics of de-lubrication, and based on this knowledge, to recommend a control strategy.
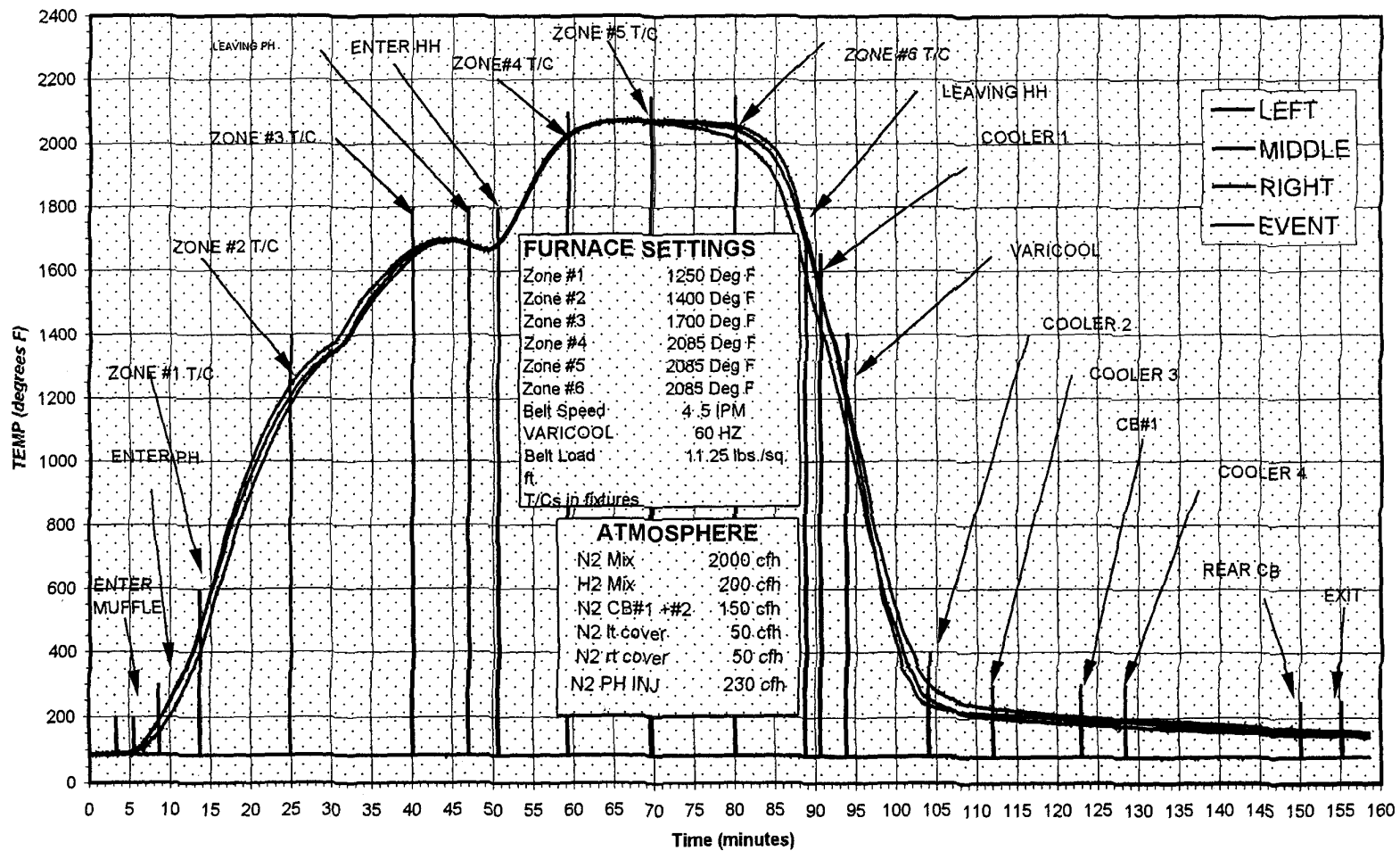
Figure 1: Typical temperature profile in a furnace

1.1 _Organization of Work_

According to this objective, i.e., to understand the de-lubrication process and to develop control systems for effective de-lubrication we subdivided the project in three phases.

Phase 1:   Ascertain the most important parameters that affect the kinetics of de-lubrication.

Phase 2:   Investigate the type of gases released during de-lubrication. This is required to control the process.

Phase 3:   Recommend a control strategy.

2.0   **LITERATURE REVIEW**

The critical literature review is divided into three sections. Section 2.1 addresses the need of lubrication in sintering. Section 2.2 gives the properties required in a lubricant and lists some of the most common lubricants used in the industry. Section 2.3 presents the various key parameters, which affect the removal of lubricants.

2.1   _Need For Lubrication_

All powder metallurgical parts are compacted to get the desired shape and green density prior to sintering. During the process of compaction, the powder is subjected to enormous pressures as the powder is pressed in a die to achieve the required green density. The frictional forces can be categorized as: The friction between the powder particles as they flow with increasing pressure.

1.   The friction between the die wall and the powder as the powder is compacted.
2.   The frictional forces generated when the compacted part is ejected from the die.

The frictional forces between the powder particles deter achievable higher and uniform density. Frictional forces between the walls and the powder reduce die life. These disadvantages are alleviated by the use of lubricants during compaction.

Lubrication is normally achieved by die wall lubrication or powder lubrication. Die wall lubrication is preferred in theory, but is not easy to incorporate into the

compaction equipment. Thus, lubricants are usually mixed with the metal powder before pressing. Typical concentrations of added lubricants vary between 0.5 and 1.5 % by weight.

2.1.1 Effect of Lubrication

Lubricants reduce frictional forces between the powder particles and between the powder particles and die wall by forming a thin layer of liquid on the surface [1]. When appropriately admixed with the powder, lubricants also help increase the green density of the component. Figure 2 shows the effect of powder lubrication on the green properties of pressed iron.
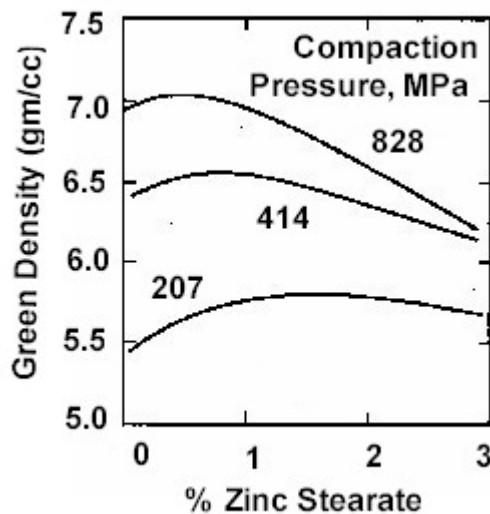
Figure 2:   Green density with% lubricant & compaction pressure [1]

Though the gain in green density is not appreciable, the ejection force necessary to remove the compact from the die decreases exponentially with the addition of lubricants. Figure 3 shows the ejection force as a function of the amount of lubricant.

The lowering of ejection pressure after compaction has made the addition of lubricants during compaction attractive. Lower ejection pressure also ensures the integrity of the compacted part as it is ejected out of the die [1].
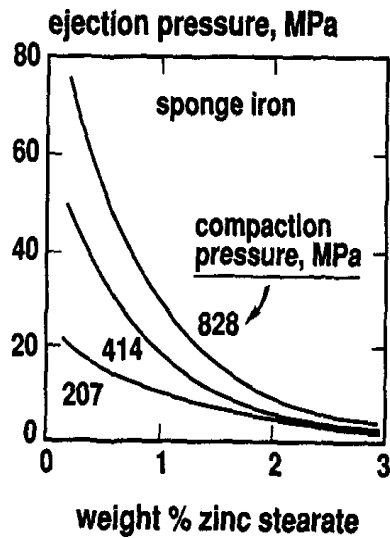
Figure 3:   Ejection force as a function of % lubricant [1]

2.2   *Properties Required In a Lubricant*

Addition of lubricant ensures lower friction between the die walls and during ejection by forming a thick film of high viscosity polymer on the particle surface. During compaction, the powder is subjected to enormous pressures. These high compaction pressures require lubricants with high viscosity; low viscosity fluids are forced away from the friction points under high pressures. Another important requirement is the ease of removal during sintering. Some of the common lubricants, used commercially are given in Table I.

Table I.   Melting ranges and 50% decomposition temperatures for common lubricants

Material	Melting Range, ^{0}C	$T_{1/2}$,^{0}C
Linear Polyethylene	95 – 115	390 – 405
Ethylene Bi-Steariamide	135 – 145	410 – 435
Zinc Stearate	115 – 125	440 – 460

Zinc Stearate has been used in the powder metallurgical industry for many years; however there have been some recent developments and an interest in moving away from zinc stearate since the latter decomposes during sintering into volatile zinc compounds. In addition, tougher environment laws and the availability of cheap lubricant such as ethylene bi-steariamide, has forced industries to shift to ethylene bi-steariamide (Industrial name 'Acrawax').

5

2.2.1 Structure and Thermal Decomposition of Ethylene Bi-Steariamide

Ethylene Bi-steariamide has 76H, 38C, 2O and 2N molecules in its molecule. The schematic diagram of its molecular chain is shown in Figure 4.
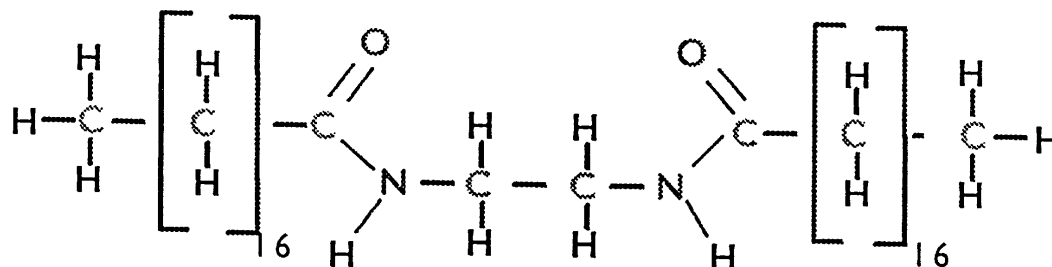
Figure 4:   Schematic of EBS molecule

The most interesting aspect of EBS lies in its varying bond strength. The bond strengths in its molecules range from 78 kcal to 130-kcal **[2]**. The weakest bonds are the C-N bonds, which are the bonds that break first. The next strongest bonds are the C-C bonds in the center followed by the C-H, and finally the strongest bonds are the C=O bonds which break the last. The continual thermal decomposition of the Acrawax lubricant was shown by DTA analysis carried out by Harb Nayar and George White **[2]**. Figure 5 shows the results of their DTA analysis. The DTA analysis shows 4 endothermic and 1 exothermic peak. Three of the four endothermic peaks are below 200 ^{0}C, while the exothermic peak is at the 550-600 ^{0}C. The authors concluded that the endothermic peaks are associated with melting of EBS and the other constituents, which are added in the manufacturing of EBS. The exothermic peak is the point where the strong bonds (here, C=0 bonds) break away to ethylene, CO and CO_2.
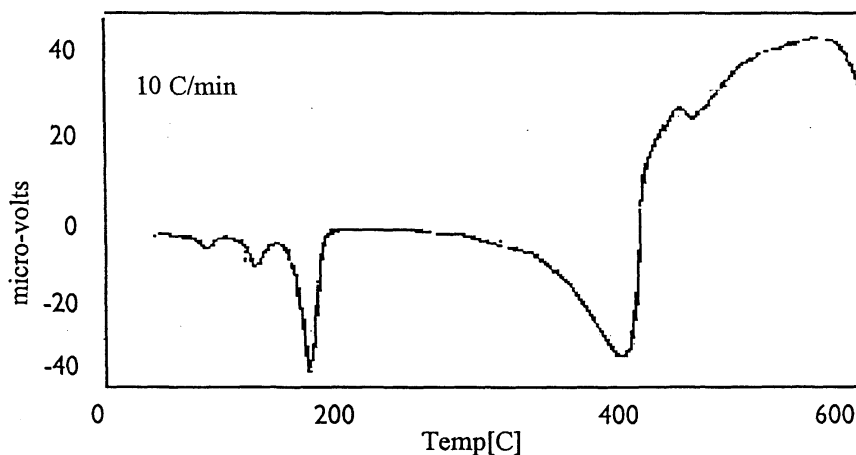
Figure 5:   DTA analysis of EBS [2]

However, most industries have an atmosphere of hydrogen and moisture in the de-lubrication zone. Understanding the decomposition of this molecule in the presence of moisture and hydrogen will aid the understanding of its thermal decomposition.

2.3   *Parameters Affecting De-Lubrication*

2.3.1   *Rate of Heating*

De-Lubrication is the process of thermal decomposition of the higher molecular weight hydrocarbon under controlled conditions. Heating rate or the rate of heat supplied affects the decomposition kinetics of the lubricant. If the heating rate is very high it leads to a very rapid decomposition of the lubricant and the associated volume change introduces micro-cracks in the parts. The decomposition of a large chain varies from one polymer to another. Poly-vinyl alcohol decomposes by side chain group elimination; polyacetal requires a reactive atmosphere to break up; paraffin wax decomposes by oxidation, etc. **[3]**. The difference is due to chemical bonding and the structure of the polymer **[4].** Work done by J. Woodthorpe et al **[5]** has shown that the final weight loss shows no correlation to defect formation. However, slope of the weight loss curve gives a very good indication about the type of lubricant to be used for easy removal. They concluded that lubricants, which decompose into small chains, are easier to remove. The slope of the decomposition curve changes by varying the heating rate.

DTA analyses done by Harb Nayar & George White **[2]** on EBS indicate that the breakdown of the Lubricant occurs in successive steps of endothermic reactions followed by an exothermic reaction [Figure 5]**.** The kinetics of the decomposition is complex, as EBS breaks into smaller hydrocarbons throughout the heating cycle. The kinetics of decomposition, to smaller and more thermally stable hydrocarbons, will depend on the amount of energy supplied.

2.3.2 *Flow Rate of Gases*

The sequence of events that lead to lubricant removal is melting, vapor formation, vapor diffusion through the pores and finally the lubricant vapor being swept away by the gases in the furnace. The most common problem during de-lubrication due to improper atmospheric conditions and gas flow rates is 'Sooting'. Sooting is the deposition of carbonaceous material from the lubricant on the part surface. Sooting is also associated with the migration of de-lubrication products into the sintering zone of the furnace, insufficient gas flow and down draughts in the exhaust stacks of the de-lubrication zone. The melting points and vaporization temperatures of lubricants vary greatly according to their

composition. For example, Acrawax and the organic part of Zinc Stearate can be removed by the time the part temperature reaches 550 ^{0}C. If there is a stagnant gas layer on the part it can lead to de-caburization defects [6]. It has also been shown that C/H ratio and oxygen are critical in the formation of soot [7]. Analysis done by Colllen and Samrasekera [6] has shown the linear dependence of gas velocity on the mass transfer phenomena. As the thermal pyrolysis of lubricants are very rapid, insufficient gas flows lead to a stagnant layer of the lubricant vapor on the part which increase the localized C/H ratio to greater than 1. This leads to 'sooting' or deposition of C on the surface of the part. The H to C ratio in a molecule determines the tendency of a hydrocarbon to generate 'soot'. EBS has an inherent disadvantage because it has an H to C ratio of 2, whereas cleaner hydrocarbons generally have an H to C ratio of 4 [8]. The tendency to form soot is therefore more prevalent in EBS. Controlling the gas flow during sintering is therefore essential.

2.3.3   Green Density

The amount of compaction pressure determines the green density of a part. The green density is an indication of the internal porosity in part. As discussed in the previous section, one of the steps in lubricant removal is its diffusion trough these internal pores to the surface. As the pressure for densification is increased the number of pores on the surface shows a dramatic decrease [9]. Auborn and Joon have also shown that the top surfaces contain more porosity compared to side surfaces. This was attributed to the smearing of the side surface as the part was ejected from the die. There was an observed delay in the start of de-lubricant at higher green densities. This was due to the reduced porosity in a higher green porosity. Figure 6 clearly shows that there is a change in the de-lubrication profile once the compaction pressures are increased. Increasing compaction pressures in Figure 6 shows a reduction in the internal and external porosity (for 'smearing'). There seems to be a delay in the temperature at which the lubricant first escapes by more than 50^{0}C. The slopes of the curve show a dramatic difference with higher compaction pressures. The relationship shown in Figure 6 clearly explains the effect of porosity on the migration of lubricant to the surface.
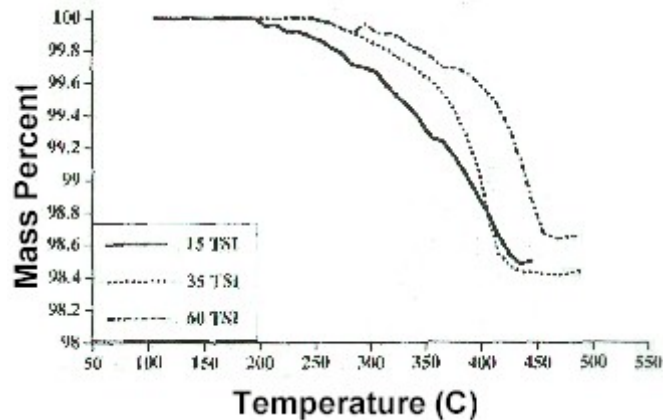
Figure 6:   Effect of compaction pressure on de-lubrication [9]

2.3.4 Atmospheric Conditions

As the lubricant vaporizes and migrates to the surface, presence of oxidizing atmospheres help in cracking up the hydrocarbon molecule. Three types of gases are used to achieve this end. They are oxygen, carbon dioxide and water vapor. Most powder metallurgical industries have shifted to the use of water vapor for cost, hazards of oxygen, and a low oxidizing potential of carbon dioxide. Studies done in this field have shown conflicting results. Studies carried out by Renowden and Pourtalet **[10]** have shown that de-lubrication is mostly unaffected by the use of moisture. Their experiments showed that hydrogen affects the process of lubricant breakdown. They concluded that Hydrogen breaks down the hydrocarbon by diffusing into the product and at the same time reduce the oxides. Studies done by George White, Antony Griffo and Harb Nayar **[11]** on the effect of atmosphere showed that the addition of water vapor with hydrogen had the greatest increase in efficiency.

3.0 PHASE I: EFFECT OF VARIOUS PARAMETERS ON THE DE-LUBRICATION OF EBS

In Phase 1, our goal is to determine the most important parameter affecting the kinetics of de-lubrication. Previous researchers have shown that the parameters affecting the process of de-lubrication are the rate of heating, molecular structure, green density, atmospheric composition and the flow rate of gases. Typically work on de-lubrication involves the measurement of weight loss as the selected lubricant is heated. A typical weight loss curve as a function of temperature is shown in Figure 7.
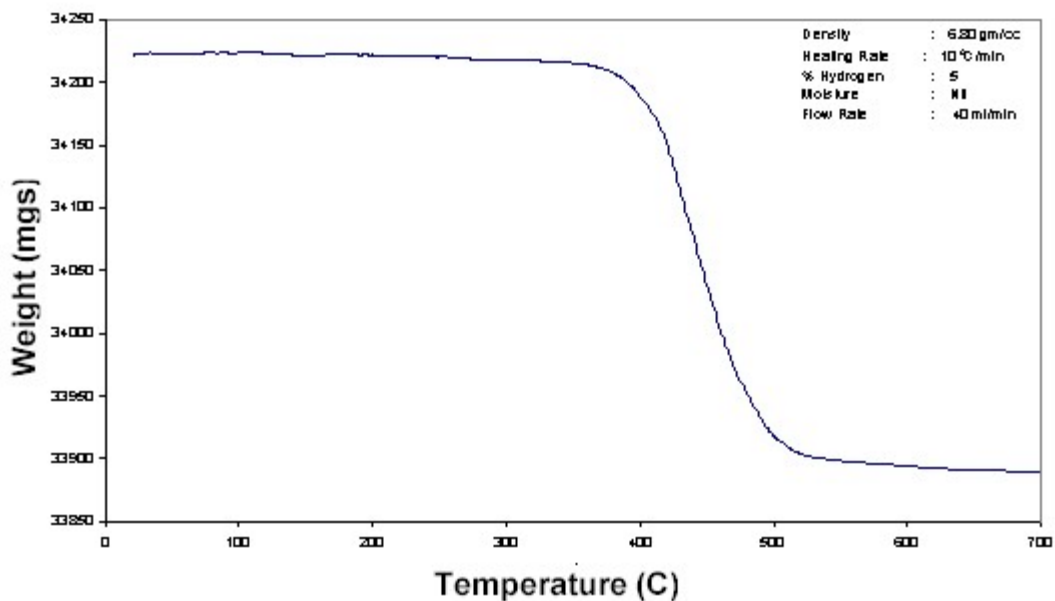
Figure 7:   Typical weight loss curve of EBS

Researchers have used the TGA machine (see Appendix **A**) for the determination of lubricant removal. As the weight losses are minute, the TGA machine with a resolution of 10^{-6} gm provides good accuracy. As the bulk of the work has been done in ferrous systems, the weight loss curve also incorporates in it the weight loss due to the reduction of iron oxide by hydrogen. The actual weight loss of the lubricant is obtained by subtracting the weight loss due to FeO reduction, from the total weight loss. The potential flaw with this approach is that one is assuming a fixed volume of iron oxide reduced (in this case, 0.2 - 0.3 % of the total weight of the sample) during the TGA run. However, this is not always a fixed amount, and in the analysis of the results, this should be taken in consideration.

Other researchers have alleviated this problem by measuring the weight loss of only EBS. This again simplifies the process of de-lubrication, as one of the main

factors' affecting the smooth removal of lubricants is the availability of open channels/pores in the compact. In order to eliminate this subtraction of weights and to simulate industrial conditions, we instead focused on the slope of the curve (dW/dT), or the rate of change in weight with temperature. Such an approach eliminates the calculation of weight losses due to the presence of hydrogen.

The Taguchi analysis was utilized to determine the role of the key process parameters on the kinetics of de-lubrication. The details of our experimental plans and procedures are discussed in section 3.1.

3.1   *Experimental Plan And Procedure*

3.1.1 *Experimental Design and Control*

The parameters selected are heating rate, % hydrogen, moisture and gas flow. Most TGA samples are in the 1 – 2 gm range; however the surface to volume ratio in such samples does not simulate industrial conditions. Accordingly, we used larger samples; 35 – 37 gm. TRS bars of dimensions ½" square base and height 1 ¼" were used. This allowed us to have weights ranging from 35-37 gm per sample (depending on the green density). The capability of the TGA machine at WPI (which can take weights as high as 100 gm) has permitted the evaluation of such large samples. We limited our experiments to compacts of Fe-0.8%C. Three levels for each parameter was selected. The experimental variables and their levels are shown in Table II. The levels were selected so that the middle level, here LEVEL # 2 simulates industrial operations. The flow rates were however limited due to the constraints of the TGA machine. The maximum permissible flow rate in this TGA machine is 100 ml/min. The amount of lubricant added to all the samples was 1% by weight.

Table II.   Experimental variables and levels

VARIABLE	LEVEL # 1	LEVEL # 2	LEVEL # 3
Heating Rate (^{0}C/min)	10	20	30
% Hydrogen	5	15	30
Moisture	-	Low	High
Flow Rate (ml/cc)	40	60	80

The samples were prepared in cooperation with Mr. Fred Semel of Hoeganaes Corporation. Taguchi L9 matrix was used for the experiments. The experimental conditions followed are shown in. Table III.

Table III.   Taguchi matrix to determine the rate of de-lube

Run Trial *	Factors			
	Heating rate (^{0}C/min)	% H$_2$	Moisture	Flow rate (ml/min)
1	10	5	-	40
2	10	15	Low	60
3	10	30	High	80
4	20	5	Low	80
5	20	15	High	40
6	20	30	-	60
7	30	5	High	60
8	30	15	-	80
9	30	30	Low	40

* The experimental conditions given for each run trial, was carried three times (for each density 6.8 gm/cc, 6.95gm/cc and 7.04 gm/cc). Due to the dependence of de-lubrication on green density, an L9 matrix was used for 3 different densities 6.8 gm/cc, 6.95 gm/cc and 7.04 gm/cc (27 trial runs all together). This was done to examine the delay in the lubrication burnout for the higher densities. The primary gas used in the experiments was nitrogen. Controlling the flow rate of gases controlled the composition of the atmosphere. For example, for a flow rate of 80 ml/min and a required hydrogen composition of 5%, hydrogen was controlled at 4 ml/min, the reminder (76 ml/min) being nitrogen. Passing nitrogen through a sealed water bath controlled the amount of moisture. For low amounts of moisture, nitrogen was passed through water at room temperature. For high moisture, nitrogen gas was passed through the bath of boiling water held at 80-85 ^{0}C. To prevent condensation of water before it entered the TGA furnace, the tubes were pre-heated.

3.1.2 Experiments to determine the decomposition kinetics of EBS

The TGA (see Appendix A) allows one to heat a sample and progressively measure the change in weight of the sample. Using this apparatus, samples of ½" square base and 1 ¼" height were put in the atmosphere dictated by the L9 Taguchi matrix. All the samples have the same composition Fe-0.8% C with 1% lubricant (EBS).

The samples were placed in the crucible, which hung from end of the TGA balance. The furnace cover was then brought up around the "hanging" crucible such that it completely surrounds the crucible. This also ensured an airtight compartment for atmosphere control. The final temperature of all the samples was fixed at 700 ^{0}C. The detailed furnace method is shown in Table IV.

Table IV.   Method used for heating rates of 10^0C/min

Segments	Schedule						
	Rate (^{0}C/min)	Temp (^{0}C)	Time (h:m:s)	Helium	Nitrogen	Hydrogen	Data Save
1	0	25	0:01:0	On	On	On	On
2	10	700	01:07:30	On	On	On	On
3	-20	25	0:33:30	On	On	Off	Off

The sampling interval was 8 s, i.e., data was collected by the software every 8 s. The flow of Hydrogen gas was put off as soon the temperature reached 700 ^{0}C for safety reasons.

The weight loss curves of the raw data are given in Appendix B. The onset of de-lubrication, end of de-lubrication and the slope of the weight loss curve were obtained from the data analysis software provide by the TGA. The data obtained from these experiments are profiled by curves similar to the one shown in Figure 7. The critical information obtained from the TGA data are: Start temperature, Onset temperature, Slope (dW/dt), Final temperature, End temperature; these are shown pictorially in Figure 8.
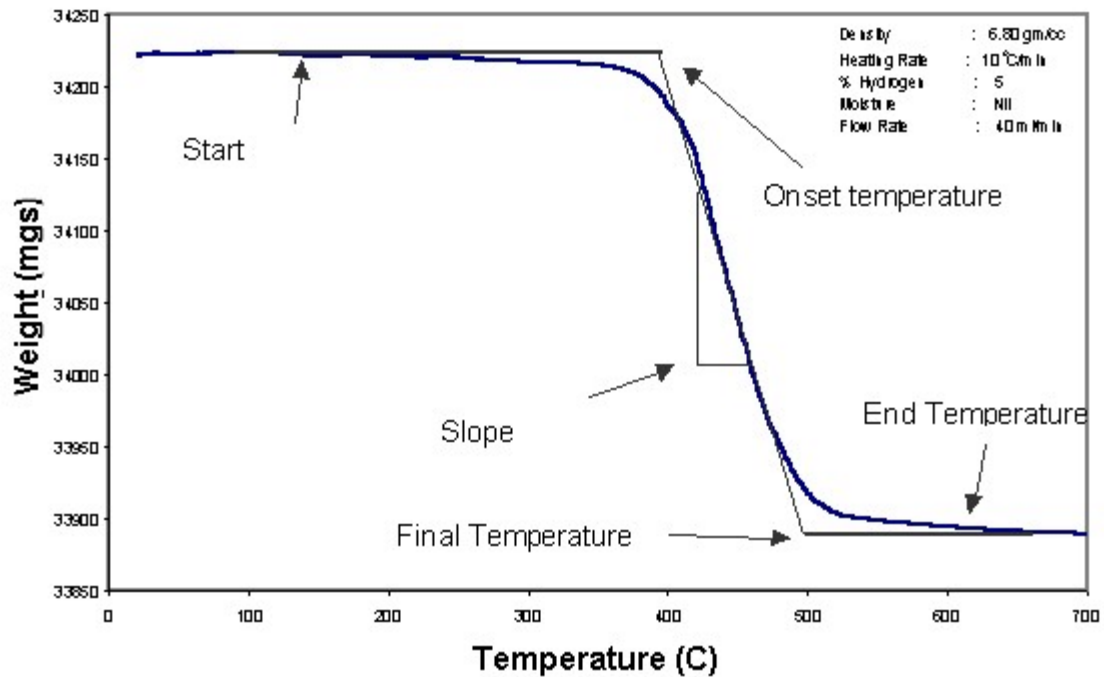

Figure 8:   Data obtained from TGA

The TGA software identifies these points and prints a report in the form of filename.rpt. Table V shows the values found by the TGA software for trial run 4 of the taguchi matrix for green density 6.80 gm/cc.

Table V. Report generated by TGA for a sample of green density 6.80 gm/cc and trial run 4 (Taguchi L9 matrix)

```
Filename     :   C:\468080.tgd
Start Temp  :  150 deg C    End Temp  :   689 deg C
Onset Temp :  457 deg C    Final Temp : 538 deg C
dW/dt          :   -88.610 mgs/min
```

In this analysis, an assumption has been made that the reduction of FeO by hydrogen would not affect the slope of the curve. This was verified by evaluating a control sample of green density 6.95 gm/cc in an atmosphere of 30 % hydrogen and 70 % nitrogen without any lubricant in the sample.
The slopes were determined using the software of the TGA. The results are shown in Table VI. It can be seen from this result that our assumption is valid.

Table VI. Report generated by TGA for a sample of green density 6.95 gm/cc in 30% hydrogen with no lubricant in the sample

```
Filename     :   C:\nl.tgd
Start Temp  :  23 deg C     End Temp:   694 deg C
Onset Temp :  308 deg C     Final Temp: 614 deg C
dW/dt          :   -0.639 mgs/min
```

The values calculated from the analysis are shown in a tabular form in Table VII - Table IX for each of the densities respectively.

Table VII.   Experimental data (6.80 gm/cc)

Trial Run	Rate of heating (^{0}C/min)	% H2	Moisture	Gas Flow (ml/min)	Slope (mgs/min)	Onset De-Lube (^{0}C)	Final De-Lube (^{0}C)
1	10	5	-	40	-38.3	400	490
2	10	15	Low	60	-46.4	408	480
3	10	30	High	80	-51	408	475
4	20	5	Low	80	-88.6	457	538
5	20	15	High	40	-91.2	465	550
6	20	30	-	60	-60.2	446	557
7	30	5	High	60	-121.8	500	550
8	30	15	-	80	-72.1	471	615
9	30	30	Low	40	-119.9	476	560

Table VIII.   Experimental data (6.95 gm/cc)

Trial Run	Rate of heating (^{0}C/min)	% H2	Moisture	Gas Flow (ml/min)	Slope (mgs/min)	Onset De-Lube (^{0}C)	Final De-Lube (^{0}C)
1	10	5	-	40	-39.1	403	491
2	10	15	Low	60	-46.7	412	480
3	10	30	High	80	-49	408	470
4	20	5	Low	80	-93.9	467	543
5	20	15	High	40	-93	471	548
6	20	30	-	60	-64.1	450	560
7	30	5	High	60	-126.9	519	580
8	30	15	-	80	-73.5	468	607
9	30	30	Low	40	-121.6	488	575

Table IX.   Experimental data (7.04 gm/cc)

Trial Run	Rate of heating (^{0}C/min)	% H2	Moisture	Gas Flow (ml/min)	Slope (mgs/min)	Onset De-Lube (^{0}C)	Final De-Lube (^{0}C)
1	10	5	-	40	-46.3	454	526
2	10	15	Low	60	-49.9	415	482
3	10	30	High	80	-49.3	410	479
4	20	5	Low	80	-96.17	462	540
5	20	15	High	40	-95	470	548
6	20	30	-	60	-54	436	562
7	30	5	High	60	-127.7	512	598
8	30	15	-	80	-74.43	478	619
9	30	30	Low	40	-124.4	485	574

3.2   Results

3.2.1 Quantitative Analysis

The data from the Table VII - Table IX were analyzed using ANOVA (Analysis of Variance). Percentage contribution on the variance of the slope was calculated and the results are shown in Table X - Table XII for each of the three densities evaluated.

Table X.   ANOVA (6.80 gm/cc)

Factors	Degrees of Freedom	Sum of Squares	Variance	Percentage Contribution
Rate of Heating	2	5338.28	2669.14	70.25
% Hydrogen	2	254.30	127.15	3.35
Moisture	2	1768.10	884.05	23.27
Gas Flow	2	237.91	118.95	3.13

Table XI.   ANOVA (6.95 gm/cc)

Factors	Degrees of Freedom	Sum of Squares	Variance	Percentage Contribution
Rate of Heating	2	5954.14	2977.07	71.62
% Hydrogen	2	364.24	182.12	4.38
Moisture	2	1761.78	880.89	21.19
Gas Flow	2	233.44	116.72	2.81

Table XII.   ANOVA (7.04 gm/cc)

Factors	Degrees of Freedom	Sum of Squares	Variance	Percentage Contribution
Rate of Heating	2	5480.60	2740.30	65.06
% Hydrogen	2	495.38	247.69	5.88
Moisture	2	2069.99	1035.00	24.57
Gas Flow	2	377.48	188.74	4.48

The percentage contribution of the processing parameters for each of the three densities is graphically represented in Figure 9,Figure 10, and Figure 11 respectively. The rate of heating is one parameter, which stands out as having a major effect in all three-density regimes.
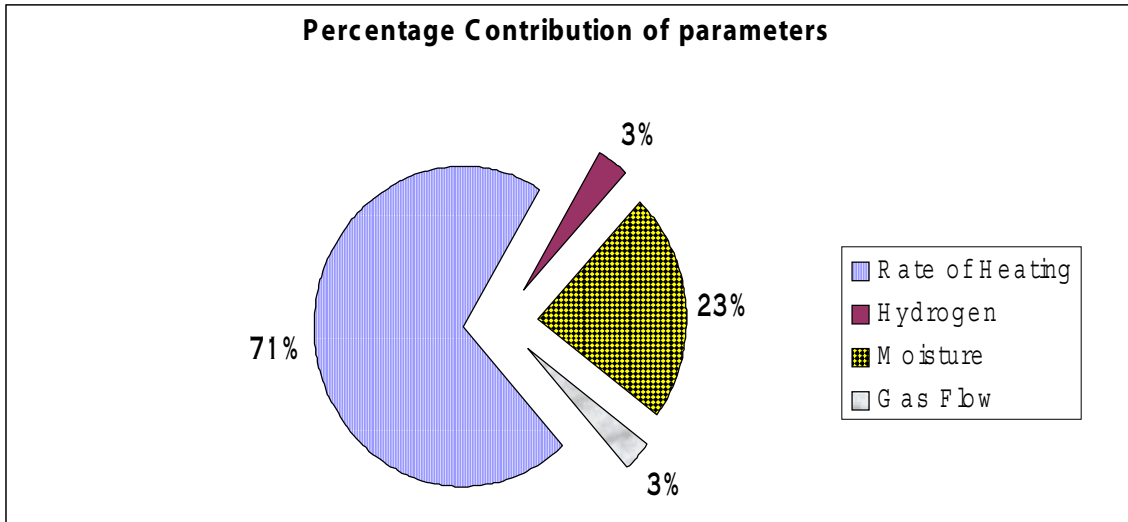

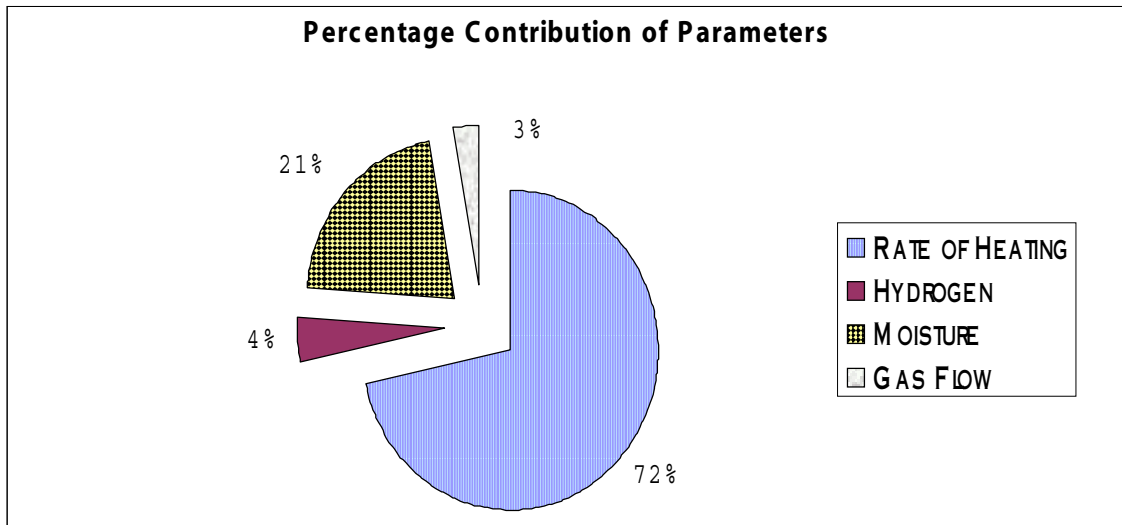**Figure 9:   Percentage contribution (green density 6.80 gm/cc)**

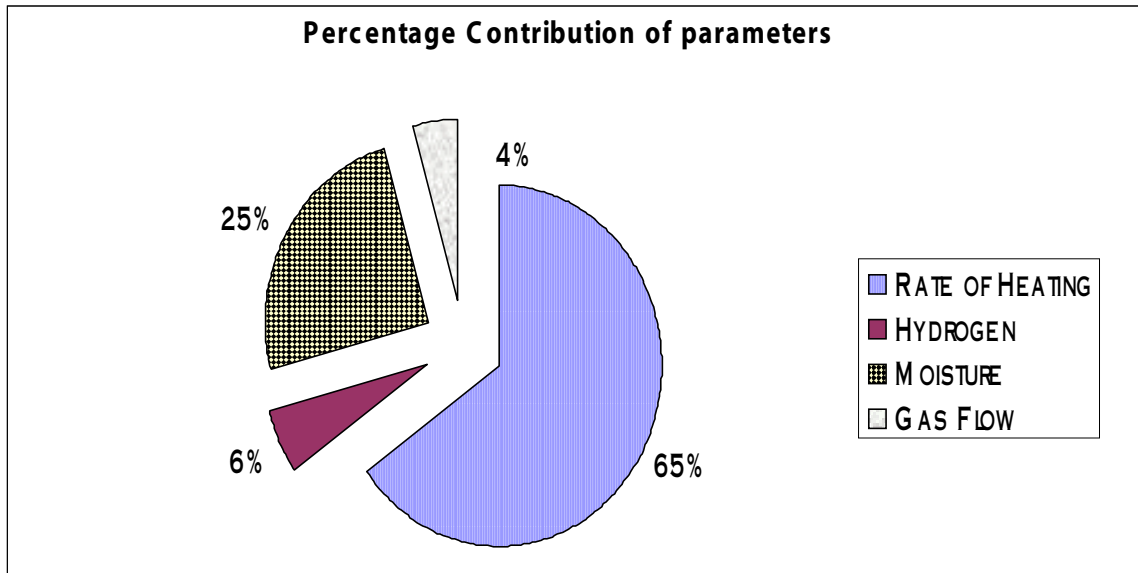**Figure 10:   Percentage contribution (green density 6.95 gm/cc)**

Figure 11: **Percentage contribution (green density 7.04 gm/cc)**

3.2.2 Qualitative Analysis

Quantitative analysis was carried out to evaluate the effect of key processing parameters on the de-lubrication process. The response of each parameter is the average of the slopes for each individual level in a given parameter. For example, for a green density of 6.80 gm/cc the data obtained (refer to Table VII) was segregated according to the levels. The rate of heating has 3 levels R1, R2 and R3. R1 representing 10 ^{0}C/Min, R2 20 ^{0}C/min, and R3 representing 30 ^{0}C/min. The corresponding slopes for heating rates of 10 ^{0}C/min were averaged (in the slopes column Table VII).

$$R1 = (-38.3 + -46.4 + -51) / 3 = -45.23$$

Similarly, the response was determined for all the levels for each parameter. Figure 12, Figure 13, and Figure 14 show the effect of de-lubrication characteristics for the three respective densities.
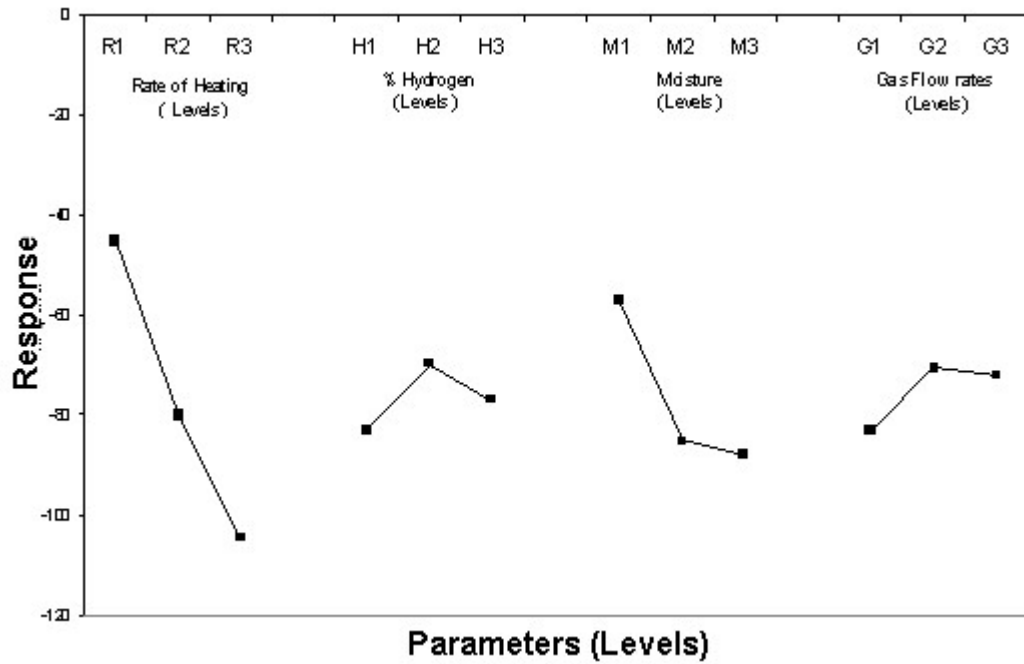
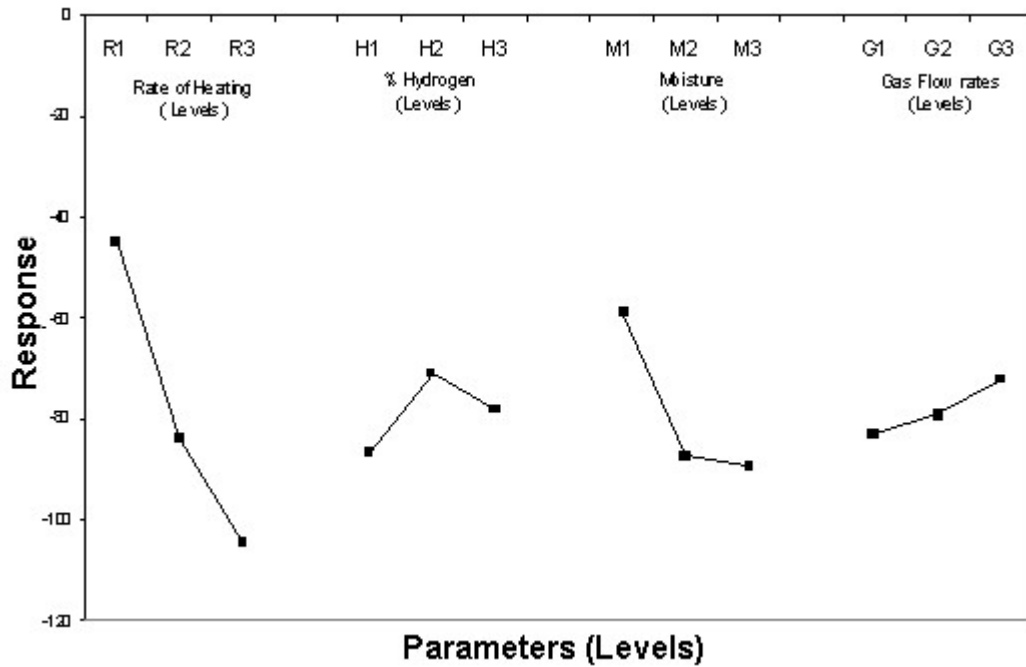**Figure 12:** Qualitative Effect of parameters (6.80 gm/cc)

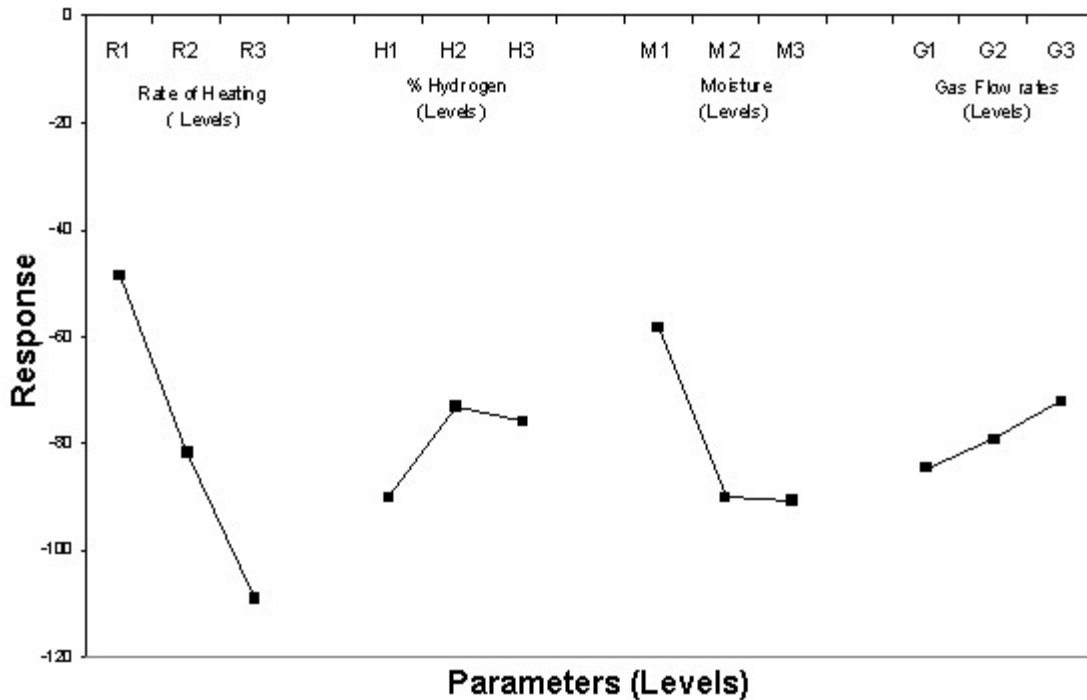**Figure 13:** Qualitative effect of parameters (6.95 gm/cc)

Figure 14:   Qualitative effect of parameters (7.04 gm/cc)

Qualitative analysis shows effect of on the slope or the kinetics of de-lubrication. If the requirement of the system is to have maximum removal in the shortest time interval, referring to Figure 12 - Figure 14, one can determine the lowest points for each individual line. For example, to have a maximum slope in Figure 14 we select the lowest points for each individual parameter line. In this case, they are R3, H1, M3 and G1, which correspond to 30 ^{0}C/min, 5% hydrogen, high moisture and low flow rate of gases. For slow removal, the highest points in the curve, i.e., R1, H2, M1 and G3 determine the optimum condition.

3.3   Discussion

Taguchi analysis has clearly shown that the kinetics of decomposition is essentially a thermal event and that the rate of heating determines the de-composition kinetics. For a control system to evolve and to ensure effective de-lubrication, the rate of heating has to be controlled. The moisture has shown to have an effect on the de-lubrication kinetics, but controlling the moisture in a control system is not desired as it oxidizes the surface of iron samples, and requires a reducing gas and hydrogen to maintain the balance. Moisture and the flow of gases may be required on the other hand to prevent sooting and the build up of a stagnant layer on the part. Though higher heating rates remove lubricants faster from the part, the "faster the better" approach might be deleterious to the

20

part. The rate of polymer breakdown to smaller hydrocarbon chains should be less or equal to the rate of removal from the part. Non-equilibrium in the rates will result in the introduction of cracks in the part.

4.0 PHASE II: <u>ANALYSIS OF GASES IN DE-LUBRICATION</u>

4.1 *<u>Motivation</u>*

One of the challenges for a sintering furnace operator is to ensure that, the lubricant in the green part is removed completely before the part enters the sintering zone. Various companies have adapted different techniques to ensure complete lubricant removal. Some manufacturers have longer de-lubrication zones while others have introduced moisture into their furnaces. Though, these "de-lube solutions" have partly solved the problems, most industries have numerous questions unanswered; what gases are released during de-lubrication? Does moisture play a role in the decomposition of lubricants? Is there the possibility to control the process? These questions were partly answered by Harb Nayar and George White **[2]** in 1995. Their study however, did not lay down the mechanism of de-lubrication and failed to conclusively identify the various gases and by-products released during de-lubrication. The effect of moisture on de-lubrication was left untouched. Understanding the fundamental reactions and identifying the gaseous by-products formed during de-lubrication is the key to sensor development. The primary motivation for this phase is to identify various gases released during de-lubrication and to identify the mechanism of de-lubrication. The results of this study will aid in the development of future sensors for de-lubrication.

4.2 *<u>Chemical Analysis By Spectroscopy</u>*

Different forms of radiant energy such as radio waves, sunlight, x-rays etc have similar properties, and are called *electromagnetic radiation*. The radiations are most commonly classified according to the frequency, ν, the number of waves that pass a particular point per unit time. In all electromagnetic waves, the following relation gives the frequency;

$$\text{Frequency } (\nu) = \frac{\text{velocity of light (cm/sec)}}{\text{wavelength (cm)}} \qquad (1)$$

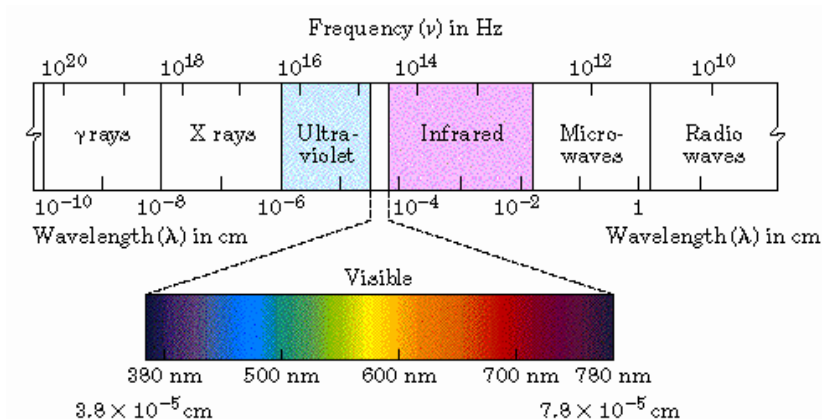Figure 15 shows the schematic diagram of the electromagnetic spectrum.

Figure 15:   Schematic of electromagnetic spectrum

4.2.1 Absorption of light

When atoms or molecules are subjected to intense heat or electric, they absorb energy and become "excited". One return to their "normal" state, they emit radiations. The energy lost in the transition is emitted in the form of light. Absorption of light by atoms or molecules is the change from a state of low energy to a one of higher energy. According to the Bohr theory, the energy changes in the atom or molecule by light absorption occur in multiples of a unit amount of energy called *quanta*. The energy changes in a molecule and the frequency of light emitted or absorbed is given by the so-called Bohr condition:

$$h\nu \quad = \quad E_f - E_i \quad\quad\quad\quad\quad (2)$$

Where,

> h   = Planks constant
> ν = Frequency
> E_f = Final energy
> E_i = Initial energy

Absorption of light leads to three types of changes in a molecule: rotation, rotation – vibration, and electronic. Electronic absorption is a combination of rotational and vibrational energy.

Rotational energy

The rotational energy of a molecule is associated with changes that occur in the rotational states of the molecules. The energies of the various rotational states differ by only a small quantity, hence the energy difference $E_f - E_i$ is a small number. From equation 2 one can conclude that the frequency of light required for this change is small. Hence, changes in pure rotational energies are observed in the far infrared and microwave regions (Figure 15).

Rotational – vibration energy

These energy changes are associated with transitions in which the vibrational states of the molecule are altered and may accompanied by a change in the rotational states. Since the energy difference is greater between the initial and the final vibrational state is greater than between rotational states, absorption occurs in at larger frequencies or shorter wavelength. Therefore the vibration – rotation transition occur in the middle infrared region (refer Figure 15).

Electronic energy

These spectra arise from the transitions from between electronic states and accompanied by simultaneous changes it the vibration and rotational states. Relatively large energy differences are involved, and hence absorption occurs at large frequencies or shorter wavelengths. All electronic transitions occur in the ultraviolet and visible region (refer Figure 15)

The various energy levels are illustrated by means of a schematic diagram, Figure 16. The dark lines represent the electronic energy levels of two electronic states. The thin lines (1,2 and, 3) represent the electronic transition when the nuclei of the atoms are held motionless i.e. no vibrational and rotational energy. The series of broken lines in the extreme right represent the various rotational levels in each electronic state. Transition from A to B is a pure rotational, from A to C is a combination of rotational vibrational and electronic (involves 1 to 2 states) transitions.
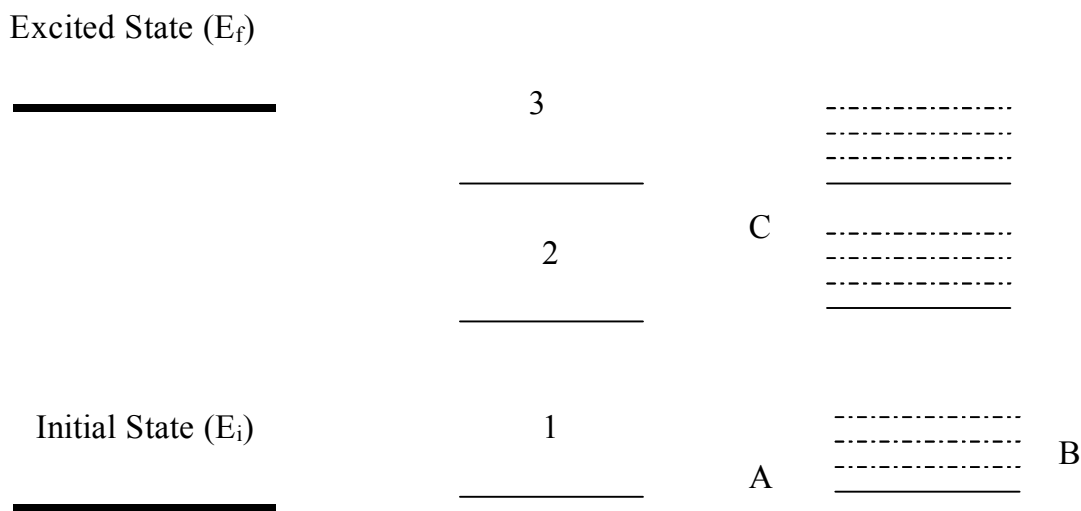
Excited State (E$_f$)

Figure 16:   Energy levels in a molecule

Each electronic state is associated with a large number (nearly infinite) of vibrational and rotational states. A large number of spectrum lines result from these transitions, and these are not widely spaced form one another. Though

these lines are of interest to find the rotational translations during absorption, practically all spectroscopy rely on the electronic transitions. Infrared spectroscopy is the study of interaction of the infrared light with matter. In spectroscopy wave number (W) is most commonly used to describe the energy transitions. Wave number is the reciprocal of wavelength.

$$\text{Wave number (cm}^{-1}) \quad = \quad \frac{1}{\text{Wavelength (cm)}} \quad\quad (3)$$

The following relation gives energy.

$$\text{Energy} \quad = \quad \frac{hc}{\lambda} \quad\quad (4)$$

Where;

h	=	Planks Constant
c	=	Speed of light
λ	=	Wavelength

Substituting equation 3 in equation 4 gives a relation where the energy is directly proportional to the wave number (W) as follows;

$$\text{Energy} \quad = \quad hcW \quad\quad (5)$$

Thus, high wave number light has a lower energy than low wave number light. When infrared radiations interact with matter it can be absorbed, causing the molecular bonds in the molecule to vibrate (4.2.1). The presence of chemical bonds is a necessary condition for infrared absorbance to occur. Chemical structural fragments within molecules, known as *functional groups*, tend to absorb infrared radiation in the same wave number regardless of the structure of the rest of the molecule. For instance, the C=O stretch occurs at 1700 cm^{-1} in ketones, aldehydes, and carboxylic acids. This correlation between the wave number and the functional group makes infrared spectroscopy a useful chemical tool.

4.2.2 Laws of light absorption

The two principle laws of light absorption are Bouguer and Lambert's law and Beer's law. Bouguer and Lambert's law states that the proportion of light absorbed by a transparent medium is independent of the intensity of the incident light. Each successive layer of the medium absorbs an equal fraction of the incident light. This is mathematically represented by the following expression.

$$I \quad = \quad I_o \; x \; e^{-\alpha b} \quad\quad (6)$$

Where,	I	=	Intensity of the light transmitted
	I_0	=	Intensity of the incident light
	α	=	Absorption coefficient of the medium

$$b \quad = \quad \text{Thickness of the layer}$$

Equation 6 can be represented as

$$\log_e \left(\frac{I}{I_0}\right) \quad = \quad \alpha bc \qquad\qquad (7)$$

When the logarithm of base 10 is used, α is converted to Bunsen and Roscoe extinction, K, and $\alpha = 2.303$ K.

The second important law, Beer's law states that the amount of light absorbed is proportional to the number of absorbing molecule through which the light passes. Light is absorbed due to the collision of photons with the molecule or atoms. The proportionality to concentration is incorporated into the Bouguer and Lambert's law to give equation 8.

$$I \quad = \quad I_0 \times 10^{-abc} \qquad\qquad (8)$$

Where,

$$
\begin{aligned}
I \,\&\, I_0 \;&=\; \text{Intensity of light transmitted and incident} \\
a \;&=\; \text{Absorptivity, a molecular property} \\
b \;&=\; \text{Cell length} \\
c \;&=\; \text{Concentration}
\end{aligned}
$$

The ratio of $\dfrac{I_0}{I}$ is usually called the transmittance, and represented by T.

$$T \quad = \quad \frac{I_0}{I} \qquad\qquad (9)$$

Substituting equation 9 to equation 8 reduces it to a form given by equation 10.

$$\log\left(\frac{1}{T}\right) \quad = \quad abc \qquad\qquad (10)$$

A typical spectrophotometer measures $\log\left(\frac{1}{T}\right)$. It is also called *absorbance*. The working principle of a FTIR is detailed in Appendix C. Spectrum obtained without the sample in the infrared beam is called a background spectrum. A typical background spectrum is shown in Figure 17.
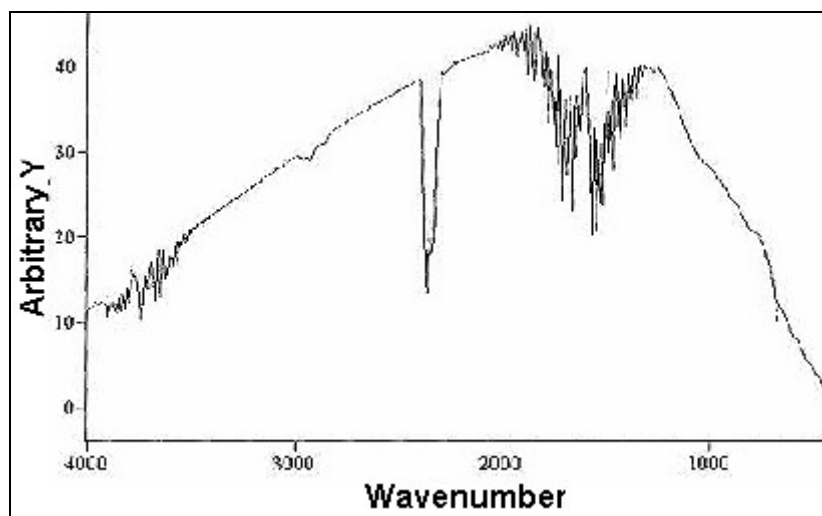
Figure 17:   Typical Background Spectrum

The background spectrum contains the instruments and the environments contribution to the infrared spectrum. Common features around 3500 and 1630 cm^{-1} are due to atmospheric water vapor, and the bands at 2350 and 667 cm^{-1} are due to carbon dioxide. When a sample is run in the FTIR, a similar spectrum is obtained except that the sample peaks are superimposed upon the instrumental and atmospheric contributions to the spectrum. The spectrum of polystyrene with the background is shown in Figure 18.
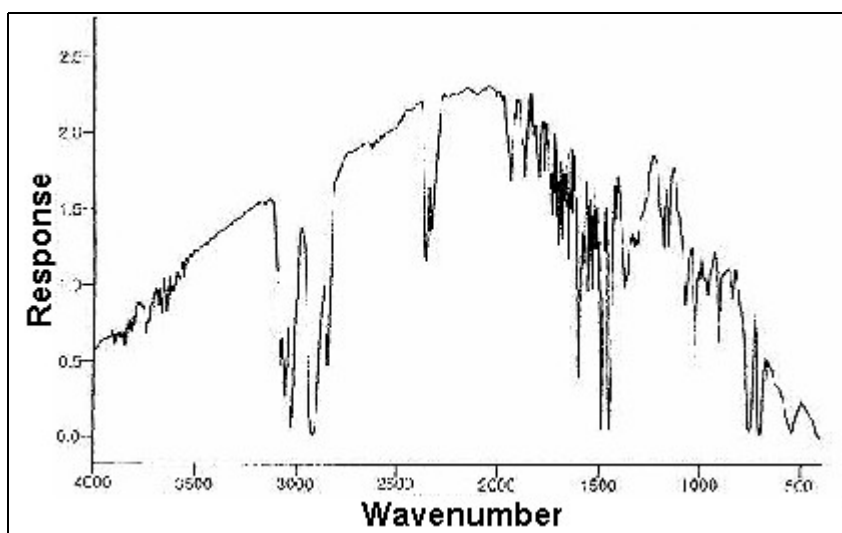
Figure 18:   Spectrum with sample

To eliminate the environment and atmospheric contribution, a ratio between the sample spectrum (Figure 17) and the background spectrum (Figure 18) is performed. This produces a transmittance spectrum as shown by Figure 19. The transmittance spectrum is represented by equation 11.

$$\% \, T \quad = \quad \frac{I}{I_0} \qquad\qquad (11)$$

Where,

$\%T$ = Transmittance
I = Intensity measured with a sample in the beam
I_0 = Intensity measured with no sample in the beam
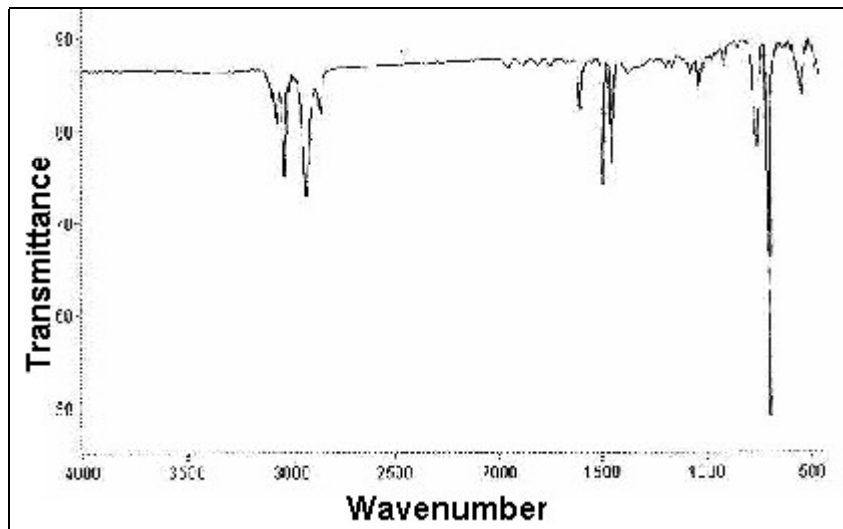
Figure 19:   The transmittance spectrum (from Figure 17 and Figure 18)

The absorbance spectrum can be obtained from the transmittance spectrum using the following equation.12

$$A \quad = \quad \log_{10}\left(\frac{1}{T}\right) \qquad\qquad (12)$$

4.3   *Experimental Setup And Design*

Samples (½" square base and height 1 ¼") containing 1% EBS ('Acrawax') as the lubricant were heated in a specially designed furnace. The schematic diagram of the furnace is shown in

Figure 20Figure 20. The slot above the sample was designed for the thermocouple. The atmosphere used in all the experiments had a composition of 95 % Nitrogen + 5% Hydrogen. To add moisture to the atmosphere, the mixture of nitrogen and hydrogen was passed through a bubbler. The flow rate of the gases was 2 liters/min. The temperature of the bubbler was maintained to the required temperature by heating coils around the bubbler. A schematic of the gas connections are shown in Figure 21.

28

Figure 20: Schematic diagram of the heating furnace
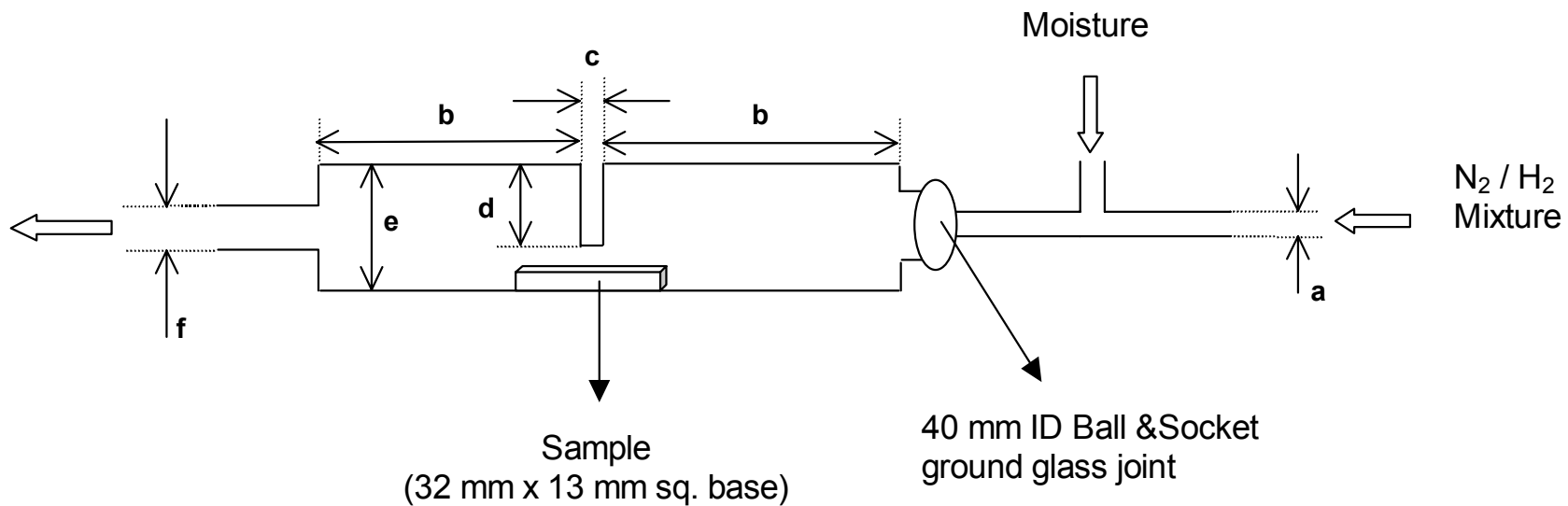
Material: Quartz
Dimesions: **a**   15 mm   **b**   150 mm   **c**   6 mm
          d   50 mm   **e**   73 mm   **f**   38 mm
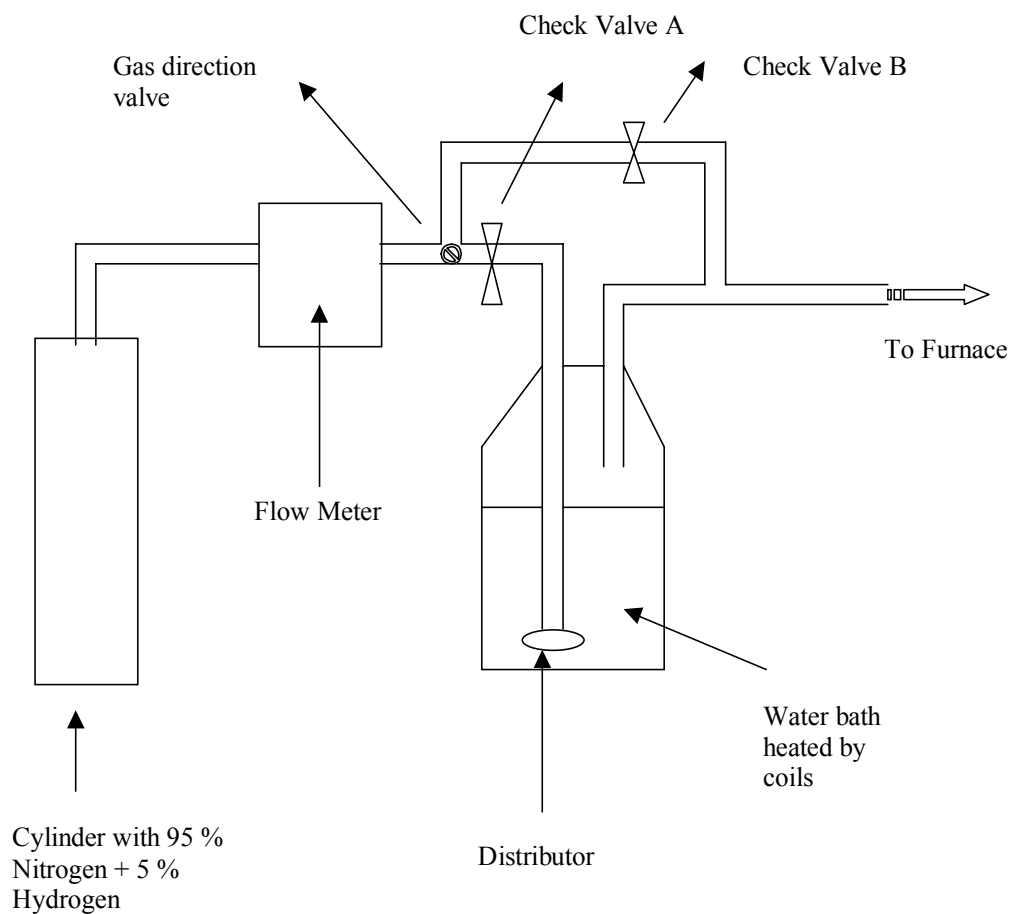
Figure 21:   Schematic diagram of gas flow direction

Check valve A and B prevented the outflow of moisture laden gas back through the flow meter in case of pressure build up. The gas direction valve ensured either moisture or no moisture into the furnace. The pipes were heated to prevent moisture condensation. The temperature was maintained buy self-heating coils. A schematic of the entire setup is shown in Figure 22.
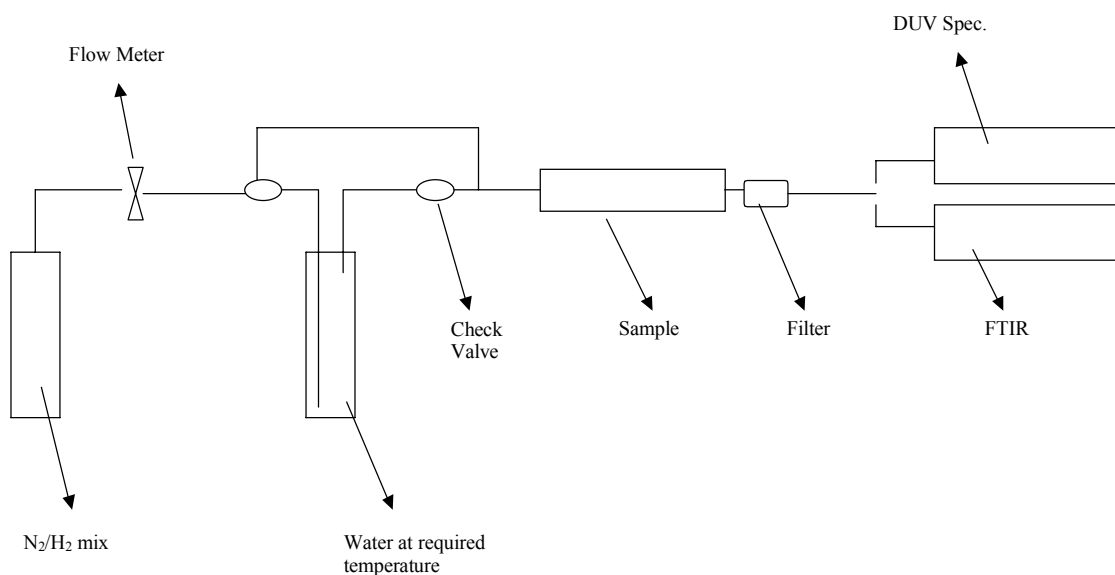
Figure 22:   Schematic diagram of the experimental setup

The actual experimental setup is shown in Figure 23. The following steps were followed in all the experiments:

- The entire system was purged with dry nitrogen for 15 minutes.
- Background spectrums were collected at random during this initial process to ensure minimum atmospheric contamination.
- The atmosphere for the experiment (N_2/H_2 mixture + moisture/no moisture) was then passed for a period of 15 min and allowed to stabilize.
- The furnace temperature with the sample was maintained and equilibrated at 100^0C during the entire process of atmospheric control.
- The temperature of the gas tubes was maintained by self-heating coils to temperature above that of the water bath (in wet conditions) to ensure that the moisture content remains constant during the collection of spectrums.
- The FTIR cell and the DUV cells were insulated and heated to 120^0C to prevent condensation of moisture on the cell windows.
- Once the background spectrums showed minimum contamination, the sample was heated at 10^0C/min to 600^0C.
- The optical path lengths (discussed in detail in Appendix C) were maintained at 5m for the FTIR and 0.5 m for the DUV.
- FTIR and DUC spectrums were collected every 2.5 minutes.
- The flow rate of the gases was maintained at 2 liters/min.

Flow Controller

Nitrogen + 4 – 5 % Hydrogen Cylinder

T – junction, for wet and dry gas.

Bubbler … for wet atmosphere

Furnace

Junction splitting the volume of by-products to DUV and FTIR cells

DUV cell

FTIR cell

Temperature controller of the furnace
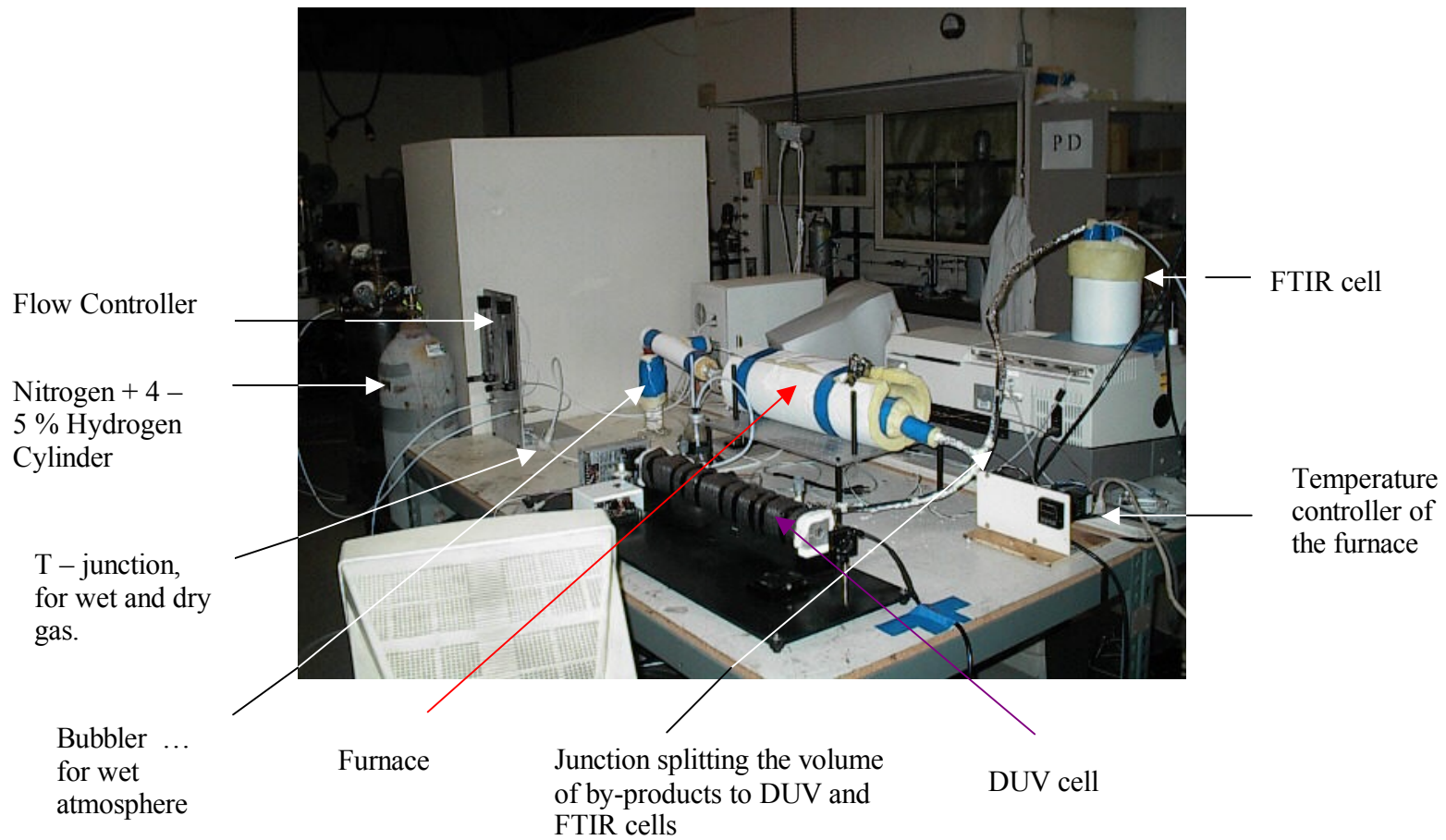
Figure 23:   Experimental Setup

4.3.1 Identification of by-products

Three experiments were performed for a wet atmosphere and three in dry conditions. The experiments were labeled as follows:

    A, C and E   -   Wet
    B, D and F   -   Dry

FTIR Spectrums

Each experiment consisted of 19 spectrums and a background spectrum. The spectrums of experiment A (page 90 – 100) and B (page 101– 110) are shown in Appendix D. All the spectrums have wave number in the X – axis and absorbance in the Y – axis. Similar spectrums were obtained for experiments C – F. The spectrums obtained were studied to identify the by-products released during the decomposition of EBS. The spectrums were analyzed for the various functional groups present in the system. Figure 24 and Figure 25 depict the characteristic wave number for the functional groups in hydrocarbon for a range of wave number (Figure 24 from 3500 – 1700 cm^{-1} and Figure 25 from 1700 – 700 cm^{-1}) [12].Figure 26 - Figure 30 show the major peaks observed during the decomposition of EBS. Figure 26- Figure 28 are enlarged from spectrum 14 of Experiment B (Appendix D, page 106). Figure 29 - Figure 30 are enlarged from spectrum 14 of Experiment A (Appendix D, page 97).
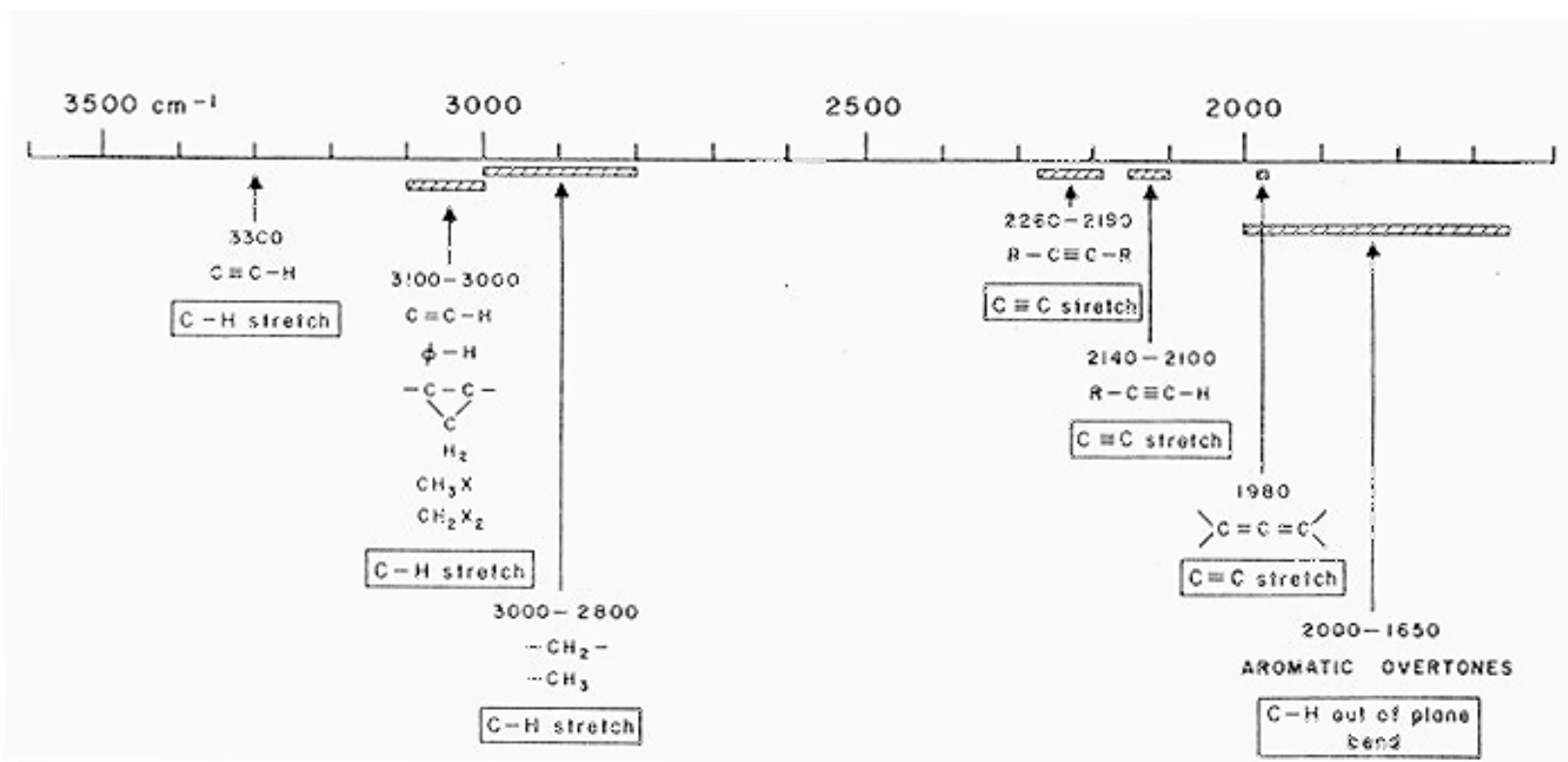
Figure 24: **Various functional group wave numbers (3500 - 1700 cm^{-1})**
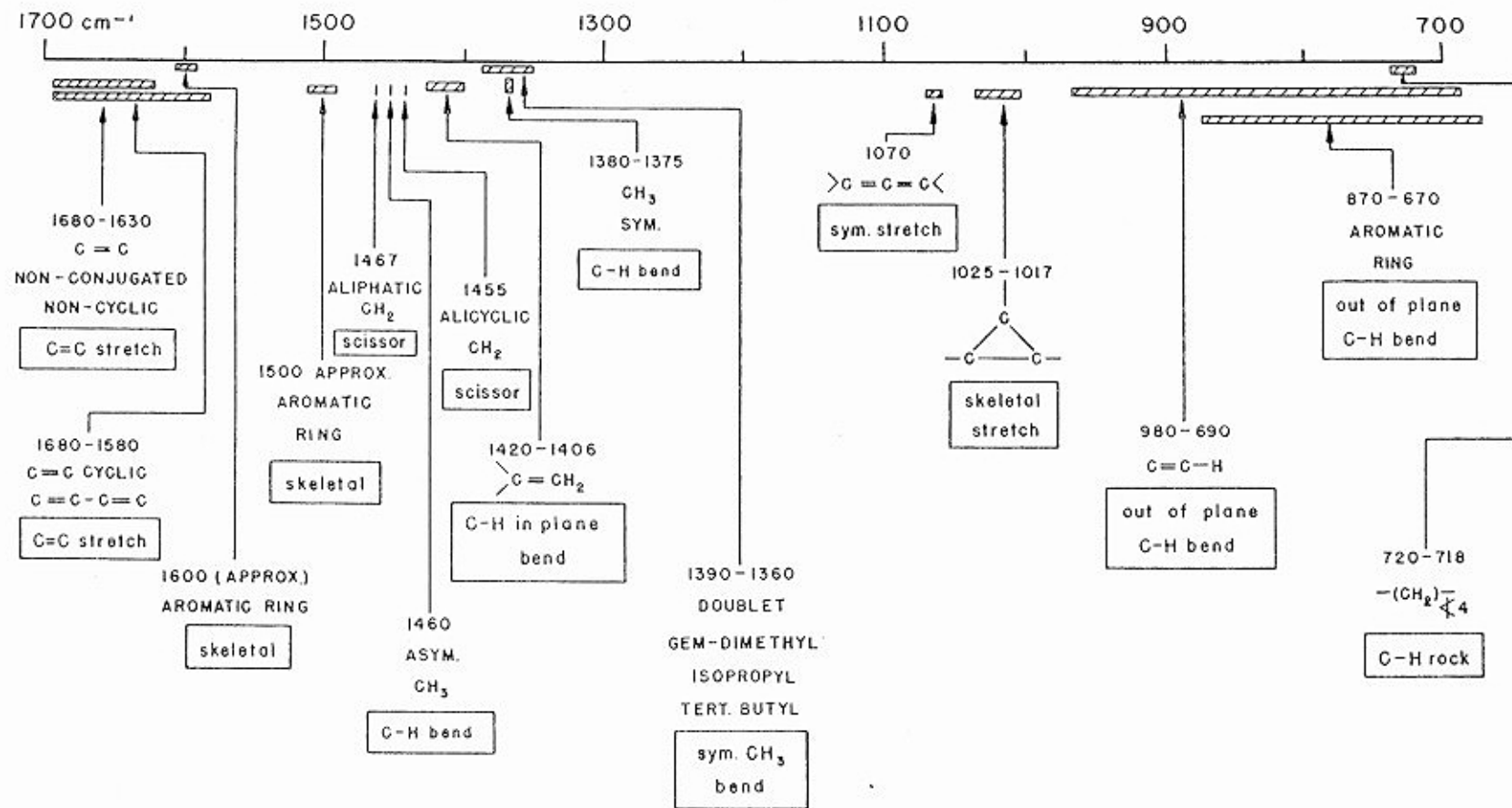
Figure 25: Functional group wave numbers (1700 – 700 cm^{-1})
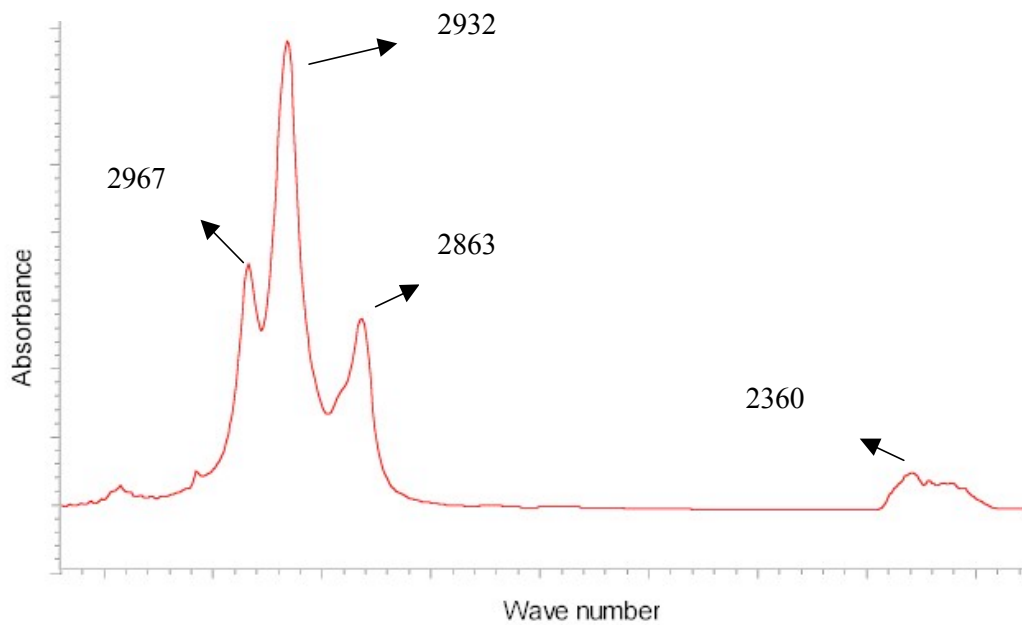
Figure 26: Observed peaks between 3000 - 2000 cm^{-1} (no moisture)
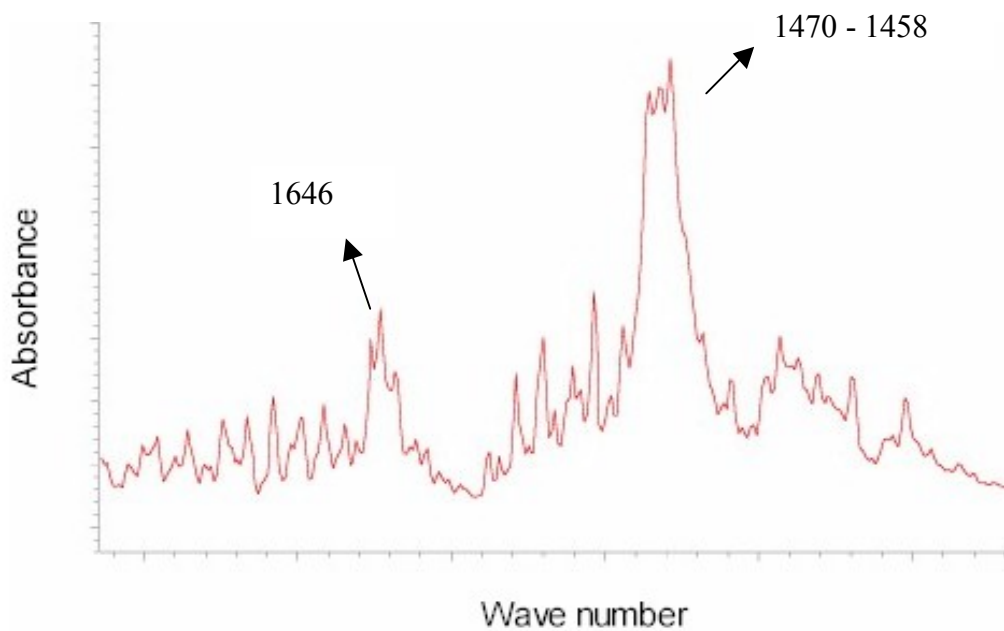
Figure 27: Observed peaks between 1800 - 1300 cm^{-1} (no moisture)
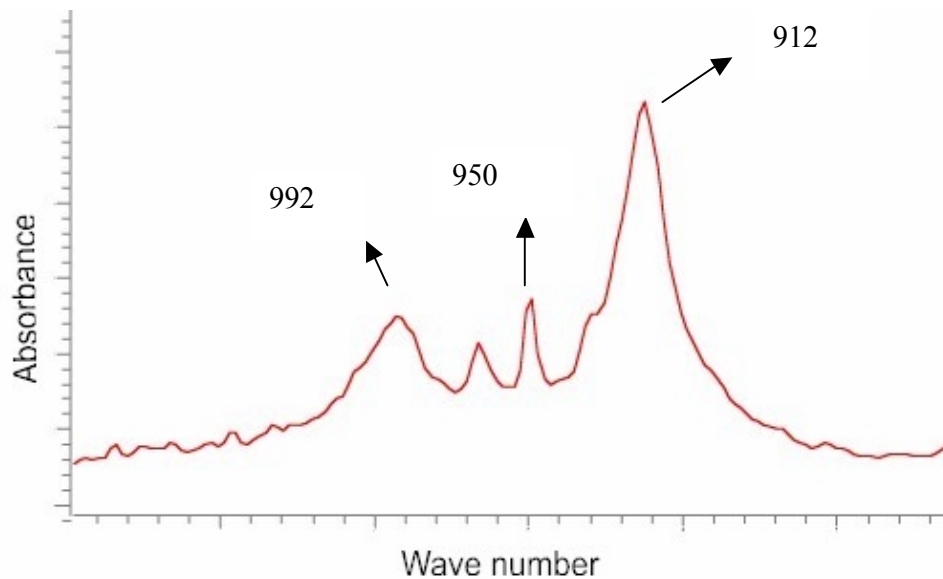
Figure 28: Observed peaks below 1000 cm^{-1} (no moisture)
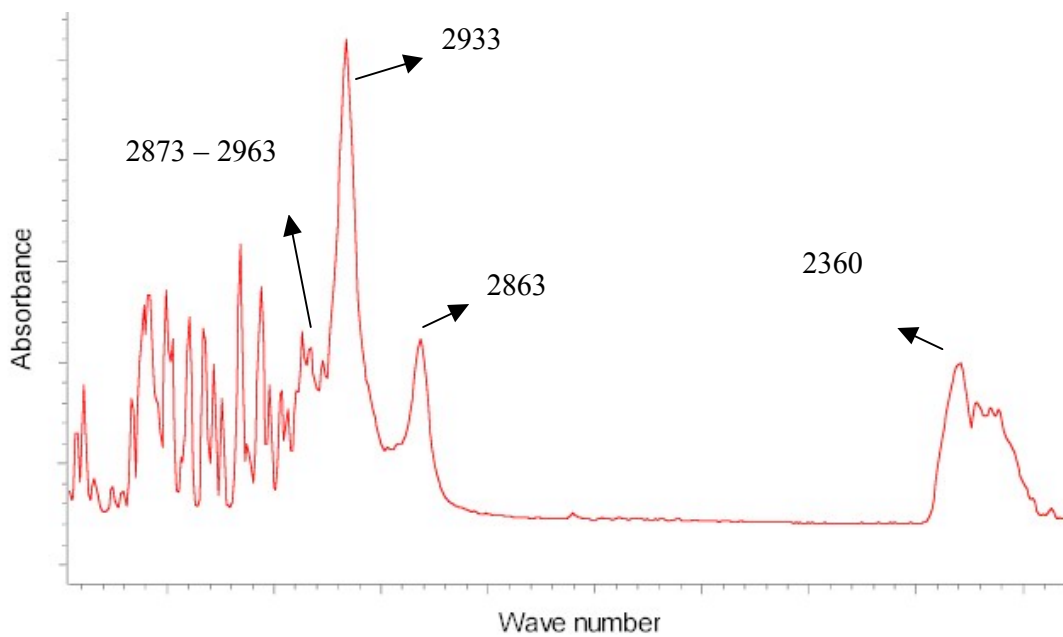
Figure 29: Observed peaks between 3000 - 2300 cm^{-1} (wet conditions)
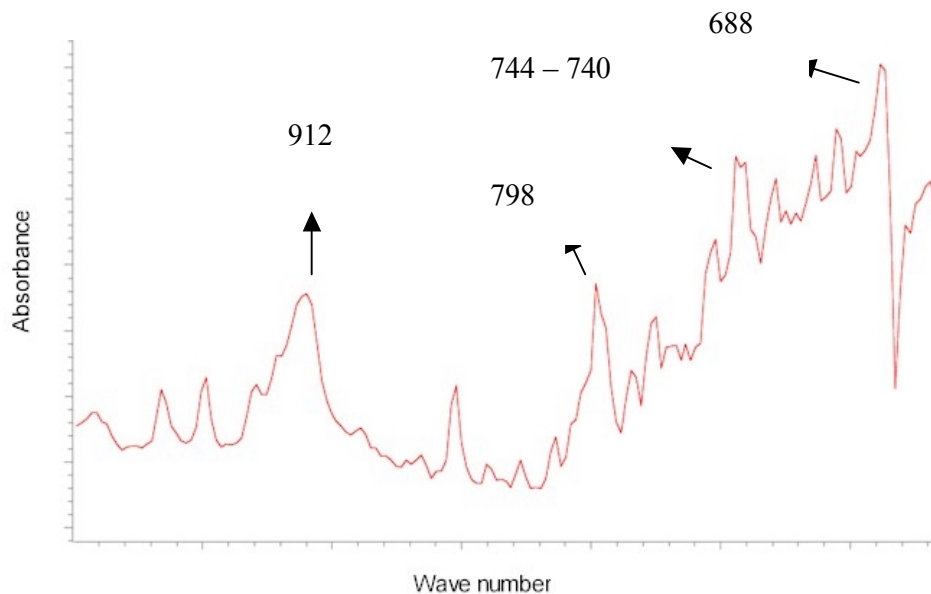
Figure 30:   Peaks below 1000 cm^{-1} (wet conditions)

DUV spectrums

Spectrums obtained in the deep ultraviolet spectroscopy are displayed in Figure 31 - Figure 32. The spectrums clearly show the presence of Ammonia as the by-product. Figure 31 is the spectrum under wet conditions. Figure 32 is the spectrum obtained for dry conditions. The spectrums shown in these figures are taken at the same time/temperatures as the FTIR spectrums.
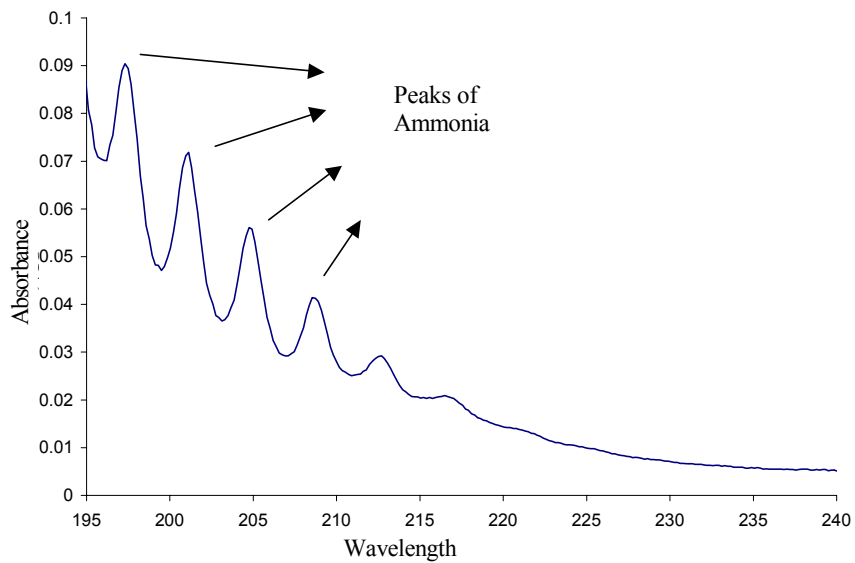
Figure 31:   Spectrum in DUV under wet conditions
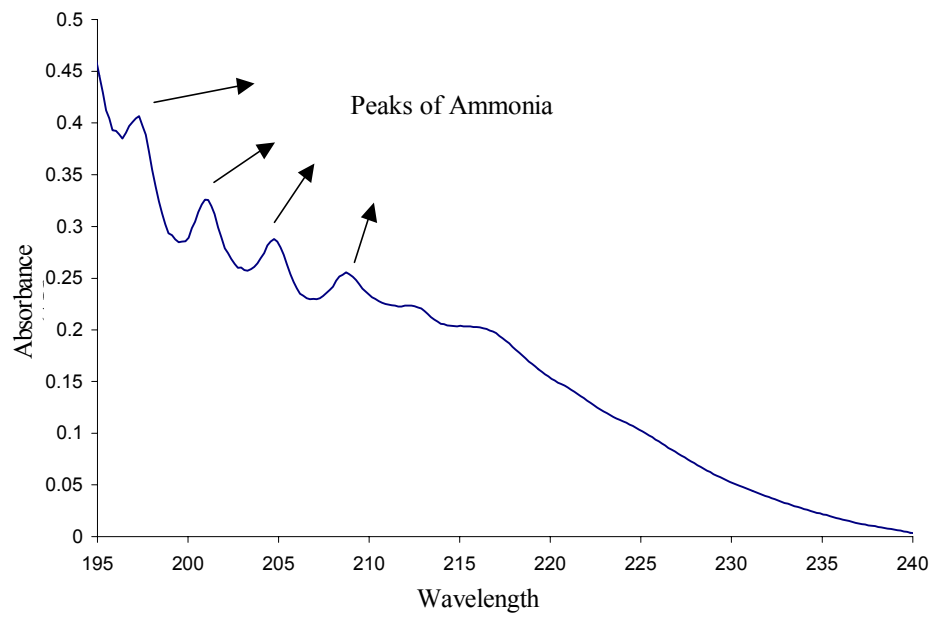
Figure 32:   Spectrum in DUV under dry conditions

Table XIII shows the various functional groups identified form the spectrums.

Table XIII.   Functional groups in the FTIR spectrums

DRY ATMOSPHERE		
Wave Number (cm^{-1})	**Functional Group**	**Theoretical Values**
3085, 3015	Stretch of unsaturated CH	3080 and 3020
2965, 2863	Stretching of Methyl (-CH$_3$)	2960 and 2870
2932, 2855	Stretching of Methylene (-CH$_2$-)	2925 and 2850
2360	O = C =O	2349
1646	C = C stretch	1640
	Terminal Methylene stretch in R/CH = CH$_2$	1645
	C = C stretch of terminal Methylene	1655
1470 - 1458	Methylene and methyl bending	1470 and 1460
992, 912	Out of plane δCH of terminal vinyl	990 and 910
966	Out of plane δCH of *trans* double bond	965
WET ATMOSPHERE		
Wave Number (cm^{-1})	**Functional Group**	**Theoretical Values**
2967, 2863	Stretching of Methyl (-CH$_3$)	2960 and 2870
2933	Stretching of Methylene (=CH$_2$)	2925 and 2850
2360	O = C =O	2349
1646	Water Interference	
1470 - 1458	Water Interference	
992, 910	Out of plane δCH of terminal vinyl	990 and 910
966	Out of plane δCH of *trans* double bond	965
798	Rocking of -CH$_3$ = CH2	780
744 - 740	Doublet of (CH$_2$)$_n$ where n > 4, Higher with lower 'n'	725 – 720

The primary by-products can be readily inferred form Table I:

- A long chain hydrocarbon (due to   - CH3, -CH2-)
- Carbon Dioxide
- Ammonia (from the DUV unit)
- Carbon Mono-oxide

To identify the hydrocarbon released during the decomposition of EBS, a sample of the solid phase was collected on a KBr disc and observed in the FTIR Figure 33 shows the spectrum obtained from the FTIR analysis.
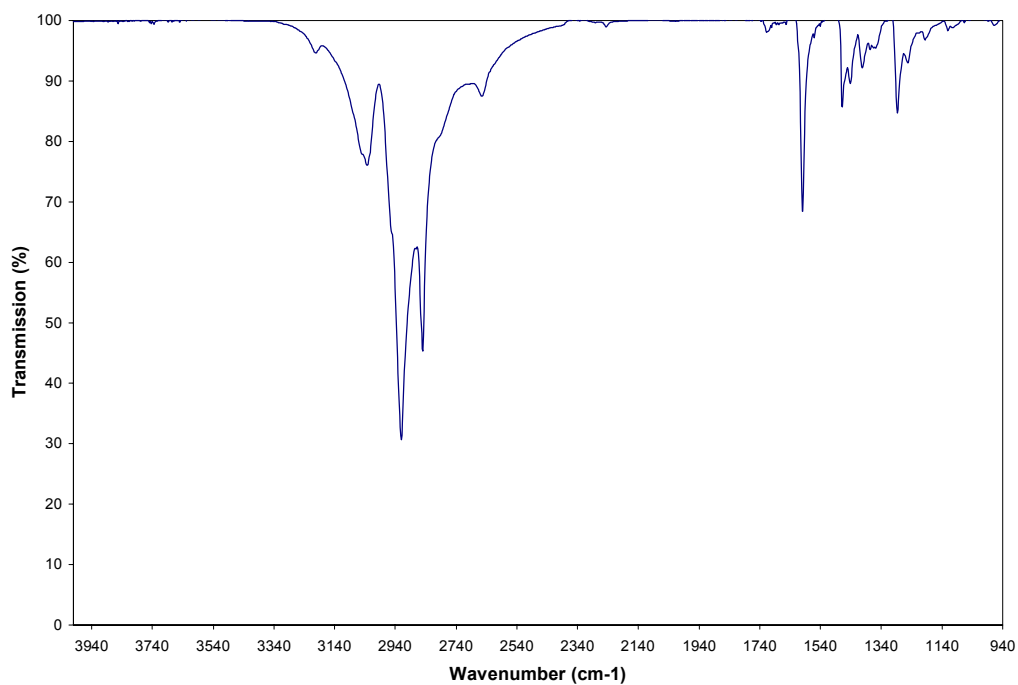
Figure 33:   Spectrum of the solid by-product (hydrocarbon)

The hydrocarbon was identified as hepta decane. Figure 34 is the spectrum of hepta-decane from NIST.
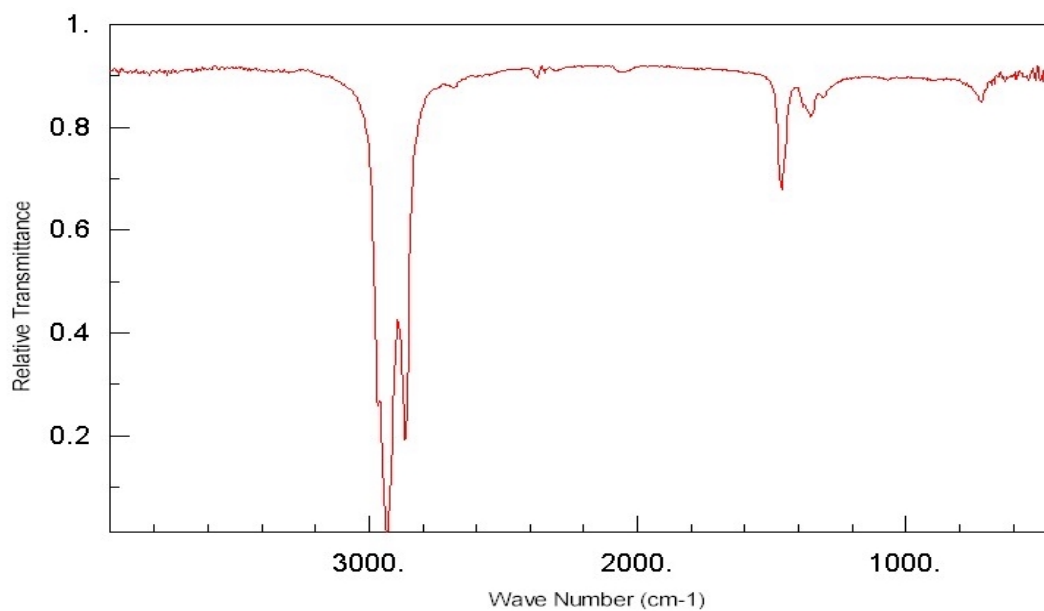
Figure 34:   Hepta-decane spectrum from NIST

4.3.2 Quantitative Analysis

As stated in section 4.2.2, the spectrum obtained from the FTIR can be used to determine the concentration of the products obtained. Theoretically, the value of 'a' in equation 10 is a unique function of the component in question (at the frequency for which it is determined). A plot of absorbance and concentration should be a straight line. However, in practice 'a' is dependent on the operating conditions, and it introduces non-linearity into the equation. This is taken care by calibrating the instrument with products of known concentration over the required range. Known concentrations of gases are passed through the instrument and the actual and observed values are compared. Figure 35 - Figure 36 show the observed and actual concentrations of CO_2 and NH_3 during calibration. All the calibrations were performed in the same operating conditions and gas flow rates as the actual experiments.

$$y = 0.000479x^2 + 1.063333x$$
$$R^2 = 0.999121$$
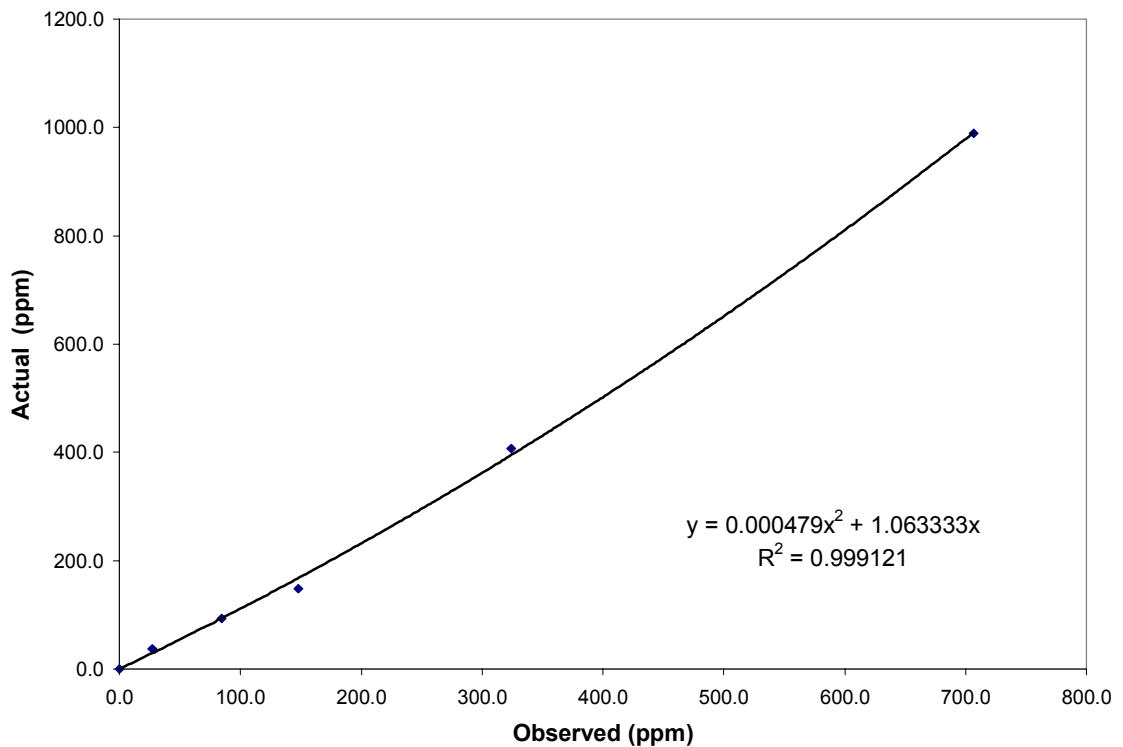
Figure 35:   Calibration curves of CO_2 (pm)
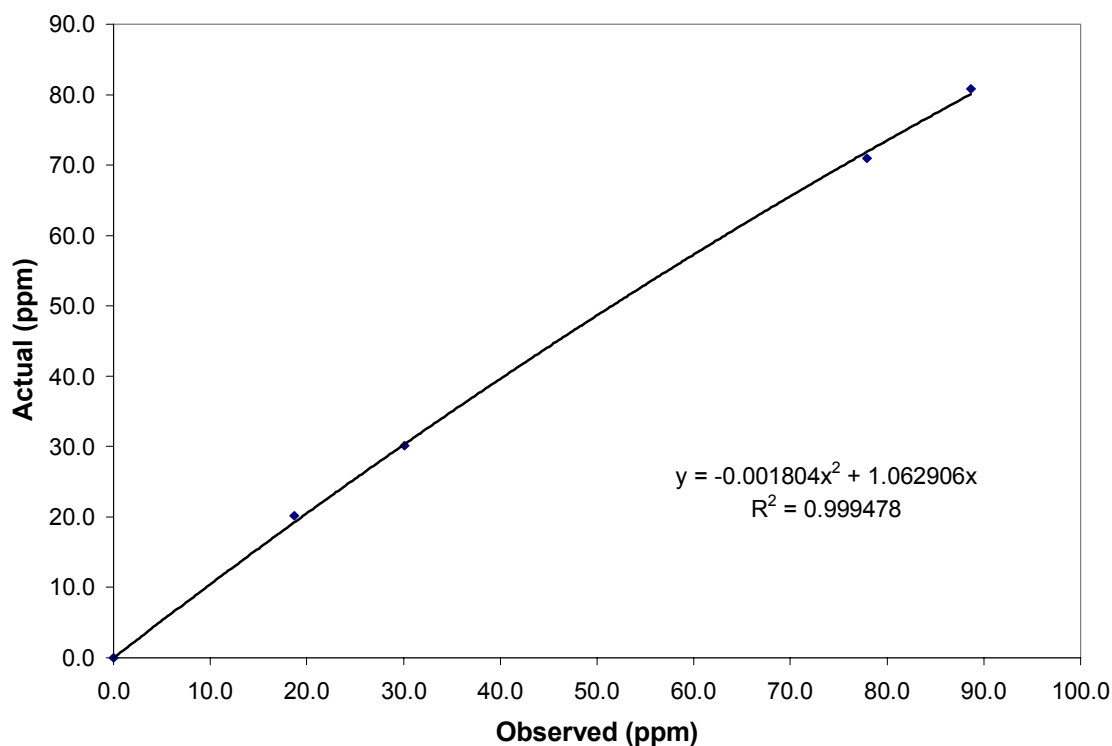
Figure 36:   Calibration curve of Ammonia

The smaller concentrations of CO involved in the experiments signify a linear relation in the range of interest. As hepta-decane cylinders of known concentrations are not manufactured, the concentration is reported as a ratio of a most readily available hydrocarbon. In this study, the concentrations of hepta-decane are compared to propane. A calibration curve of propane was obtained. Figure 37 shows the calibration curve of propane. Figure 38 shows the spectrums of the hydrocarbon and propane of known concentration. A factor was identified which would give the closest match to the hydrocarbon peaks. This factor was utilized to report the hydrocarbon concentration.

43
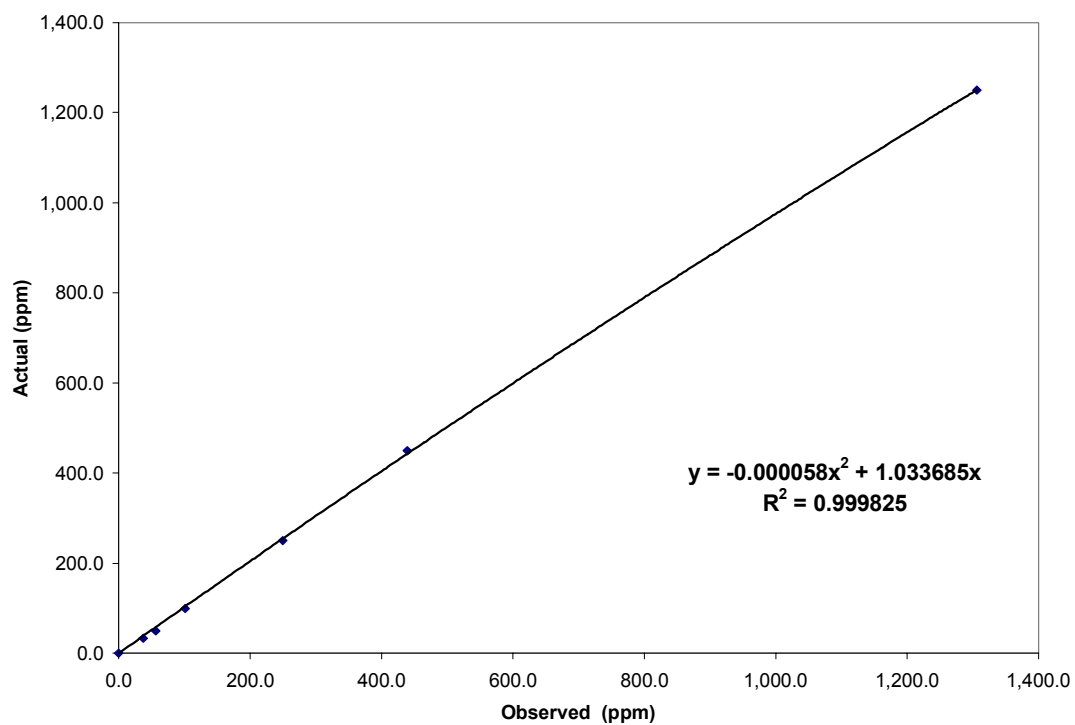
Figure 37: Calibration curve of propane
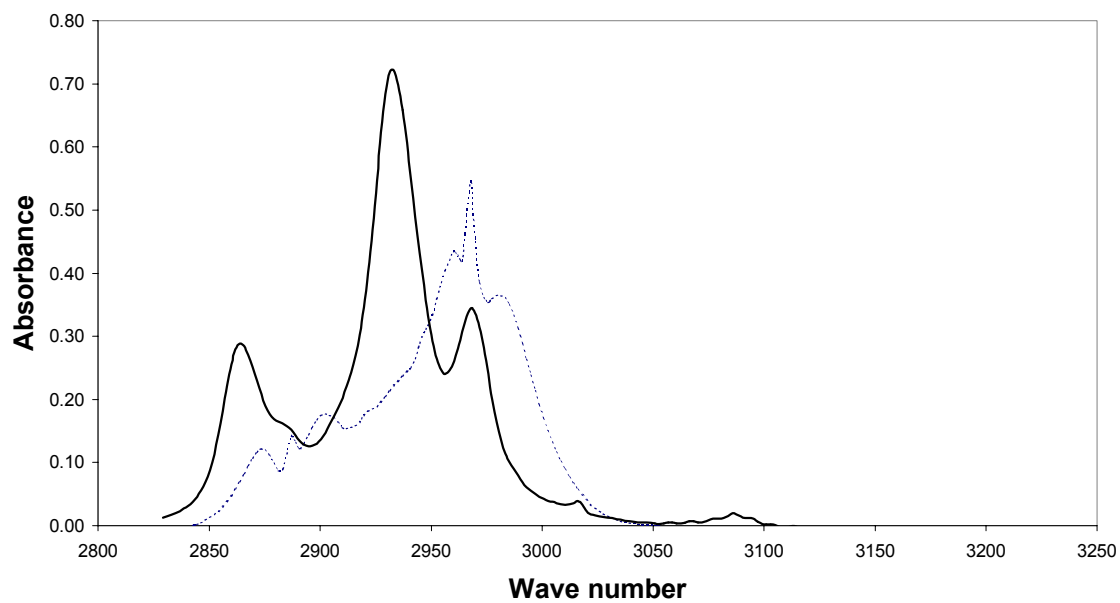
Figure 38: Hydrocarbon (dark) and propane (dotted) spectrum

The concentrations in the experiments with the experimental samples were obtained using Beer Lambert's equation (equation 10). The concentrations were then corrected using the calibrated curves shown in Figure 35 - Figure 37. For example, Table XIV shows the raw data (2nd column) obtained from the FTIR. The actual CO_2 concentrations were obtained by using the calibration equation on Figure 35. The concentration of CO_2 with time is shown in Figure 40.

Table XIV.   Raw and calibrated data for CO_2 (Experiment A)

Time (min)	Raw	Calibrated
0	13.0659	0.921099191
2.75	12.7196	0.552637149
5.5	12.9641	0.812772409
8.25	12.2746	0.079327308
11	11.461	-0.785541495
13.75	11.3022	-0.954274272
16.5	11.2312	-1.029707434
19.25	12.941	0.788192763
22	21.3628	9.783322969
24.75	47.9823	38.66179907
27.5	90.4783	86.17096836
30.25	187.323	200.9040682
33	104.637	102.3841754
35.75	33.7232	23.10822468
38.5	29.3762	18.40533574
41.25	28.5281	17.48991224
44	30.4542	19.56990363
46.75	33.8579	23.25424174
49.5	38.9001	28.7325743

Similar calculation was performed for the other identified by-products; the concentrations of CO, hydrocarbon (as propane) and NH_3 are shown in Figure 39, Figure 41,and Figure 42 respectively.
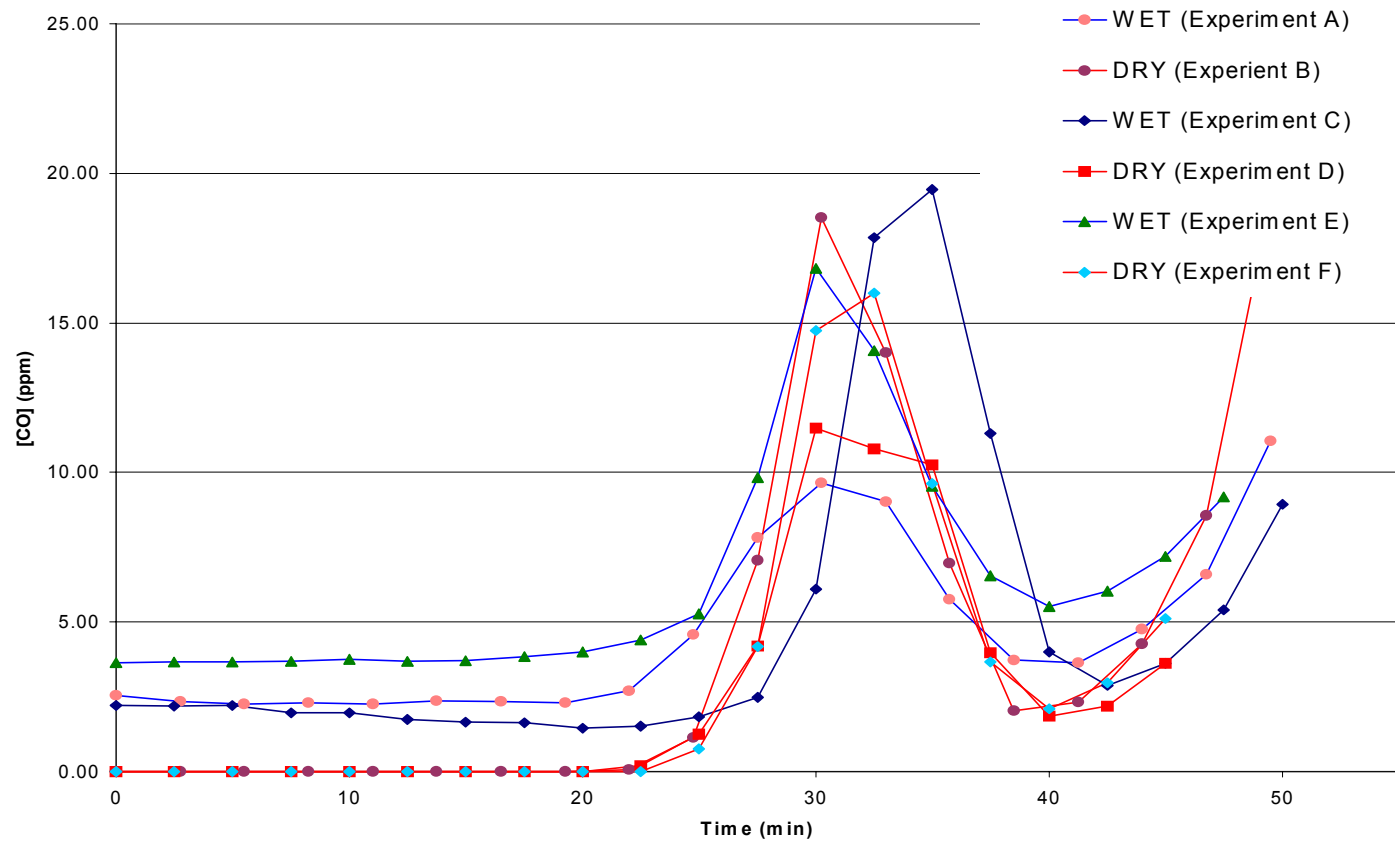
Figure 39: CO concentration with time (min)
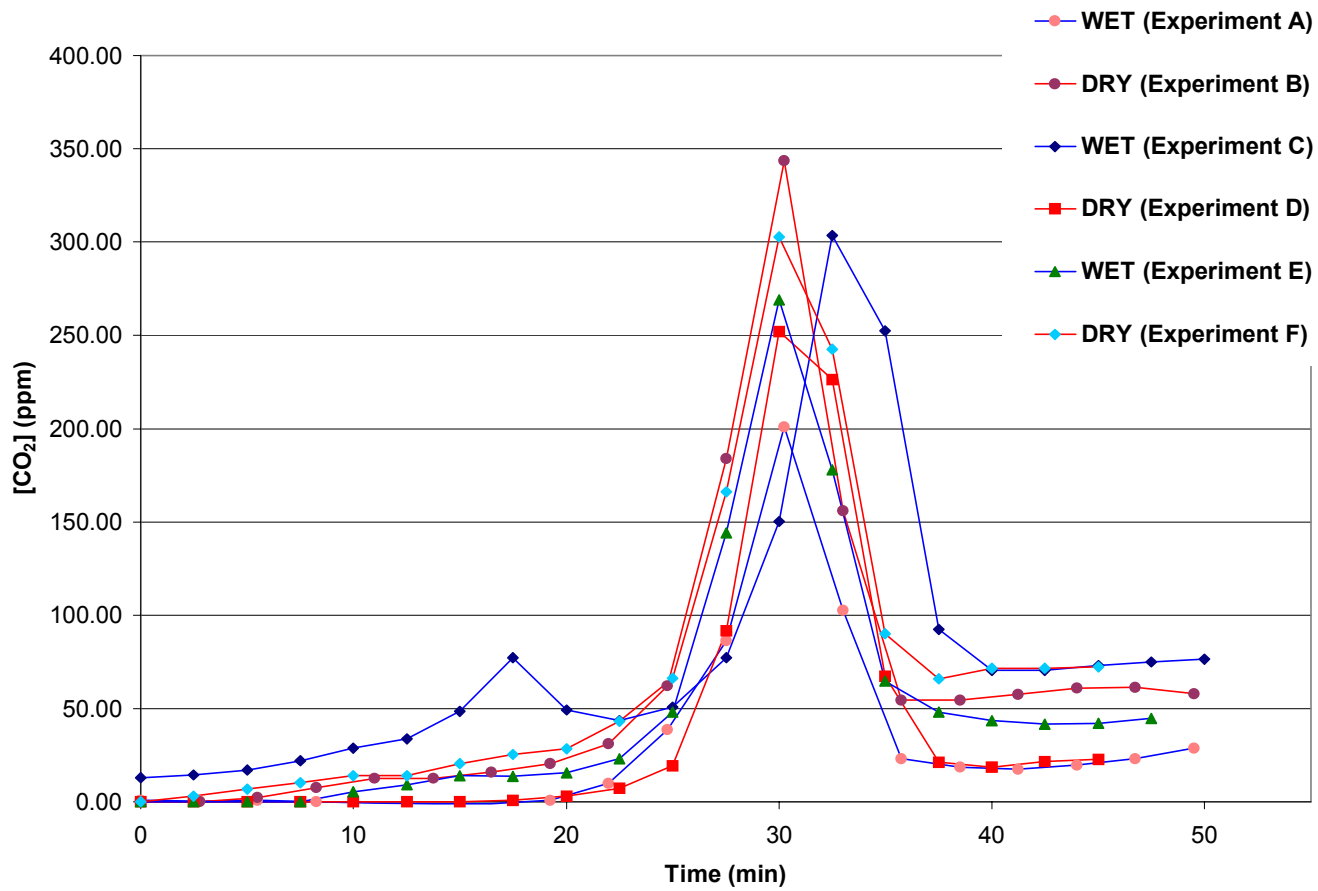
Figure 40:   CO$_2$ concentration with time (min)
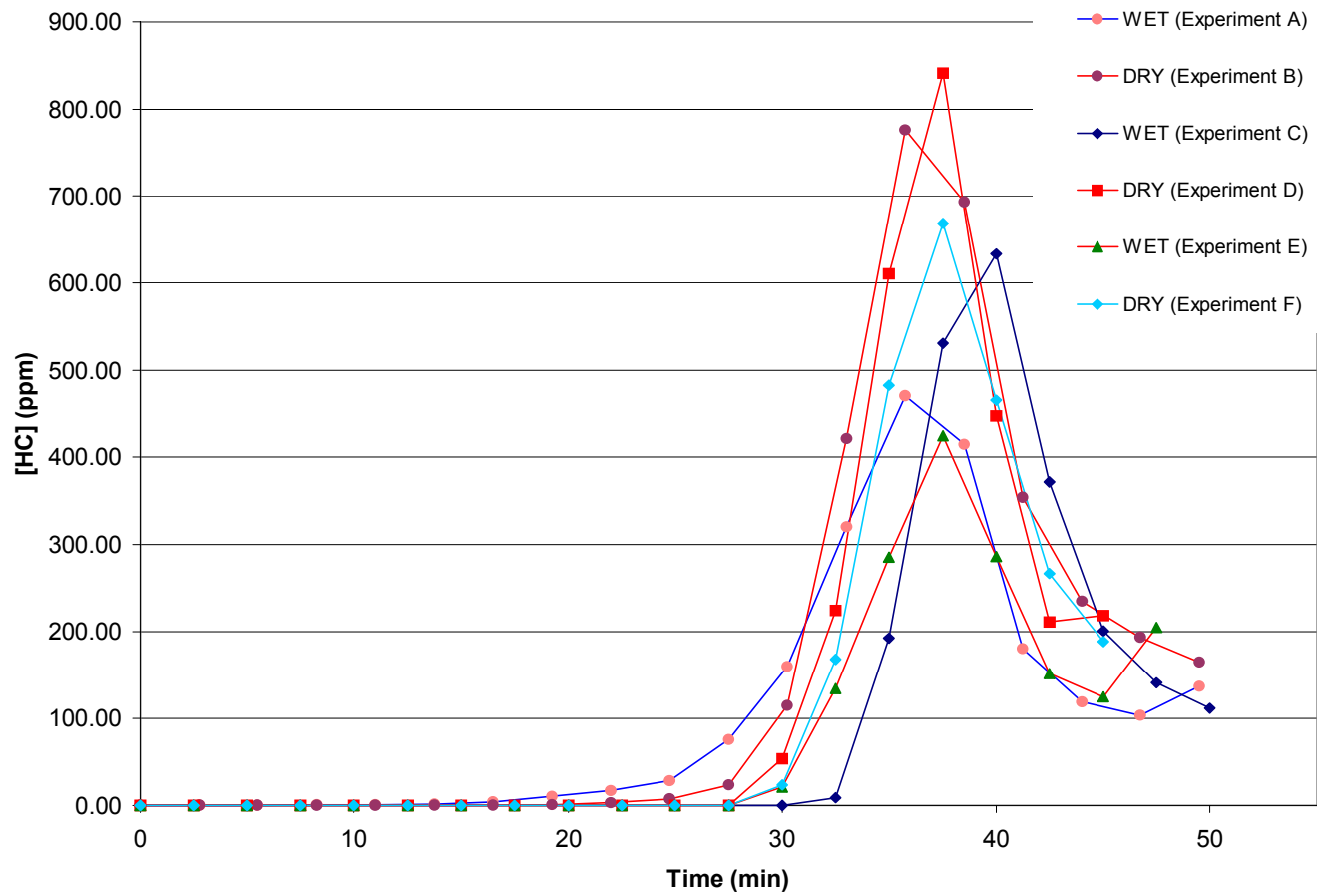
Figure 41: **Hydrocarbon concentration (as propane) vs time (min)**
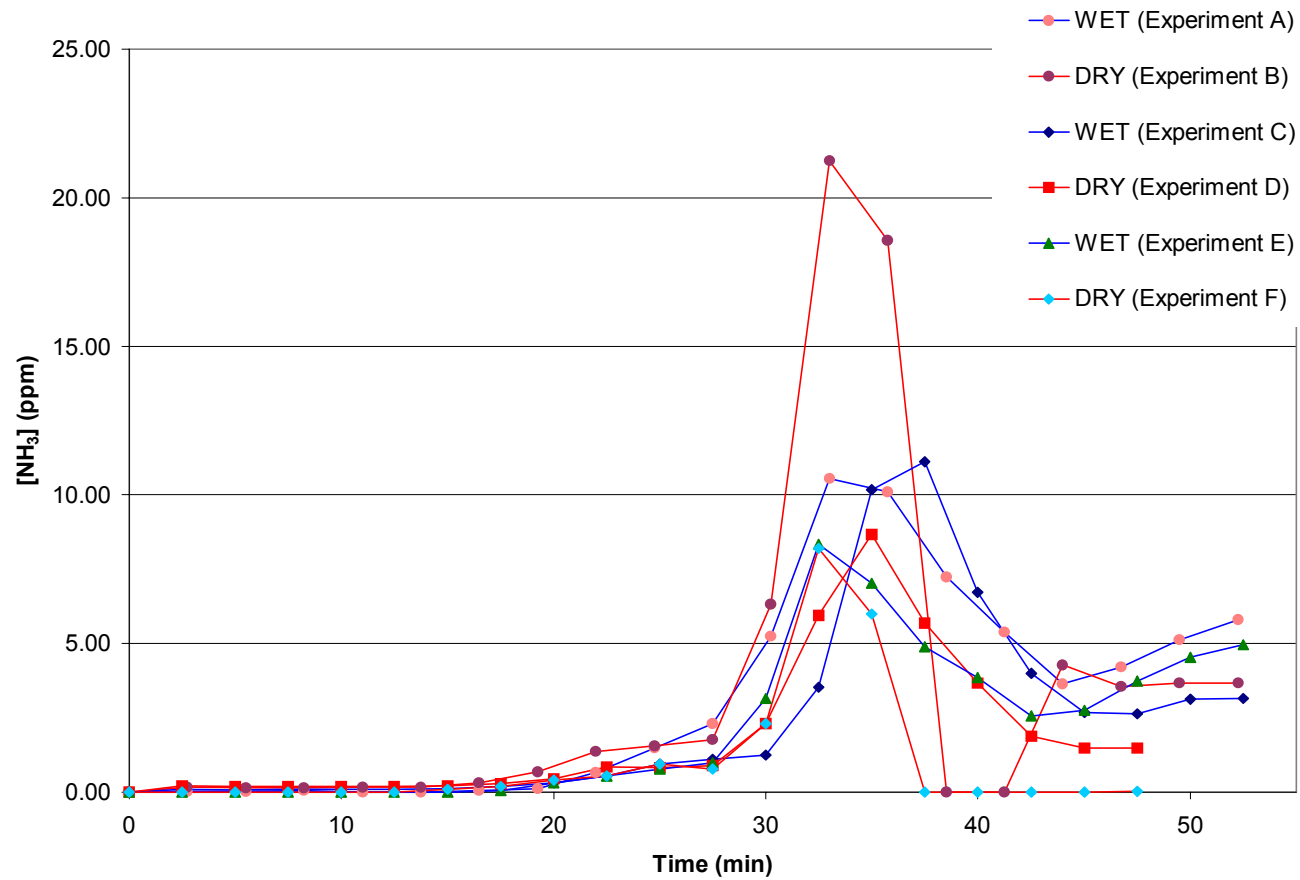
Figure 42:   Ammonia concentration with time (min)

4.4   Mechanism of decomposition

A molecule of EBS contains C-H, C-N, C=O, and C-C bonds. The bond energies are summarized in Table XV.

Table XV.   Various bond energies

Bond	Bond Energy (kcal/mol)
C-C	80
C-H	98.2
N-H	84
C-N	62
C=O	178

It can be noted from that, the decomposition of an EBS molecule will lead to the cleavage of the weakest bond in the presence of heat (in this case C-N bond). Moreover, the presence of an adjacent strongly electronegative carbonyl group (C=O), tends to bind the unshared pair to the nitrogen via an inductive effect. This is shown schematically in Figure 43. This makes the molecule amenable to attack by water. This is schematically shown in Figure 44.
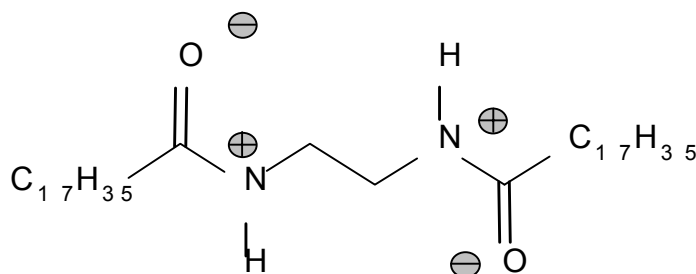
Figure 43:   Effect of C=O on C-N bond

The presence of moisture in the system leads to the hydrolysis of the molecule due to the presence of the OH⁻ radical in water. This reaction is followed by a proton transfer (H⁺) from water. The resulting reaction yields hepatadeconic acid, which in the presence of heat readily decomposes to Hepta-decane and CO_2. The schematic of the proposed mechanism of break down is shown in Figure 44. The presence of Ammonia is explained by the breakdown of the unstable NH_2-CH_2-CH_2-NH_2 in the presence of H^+.
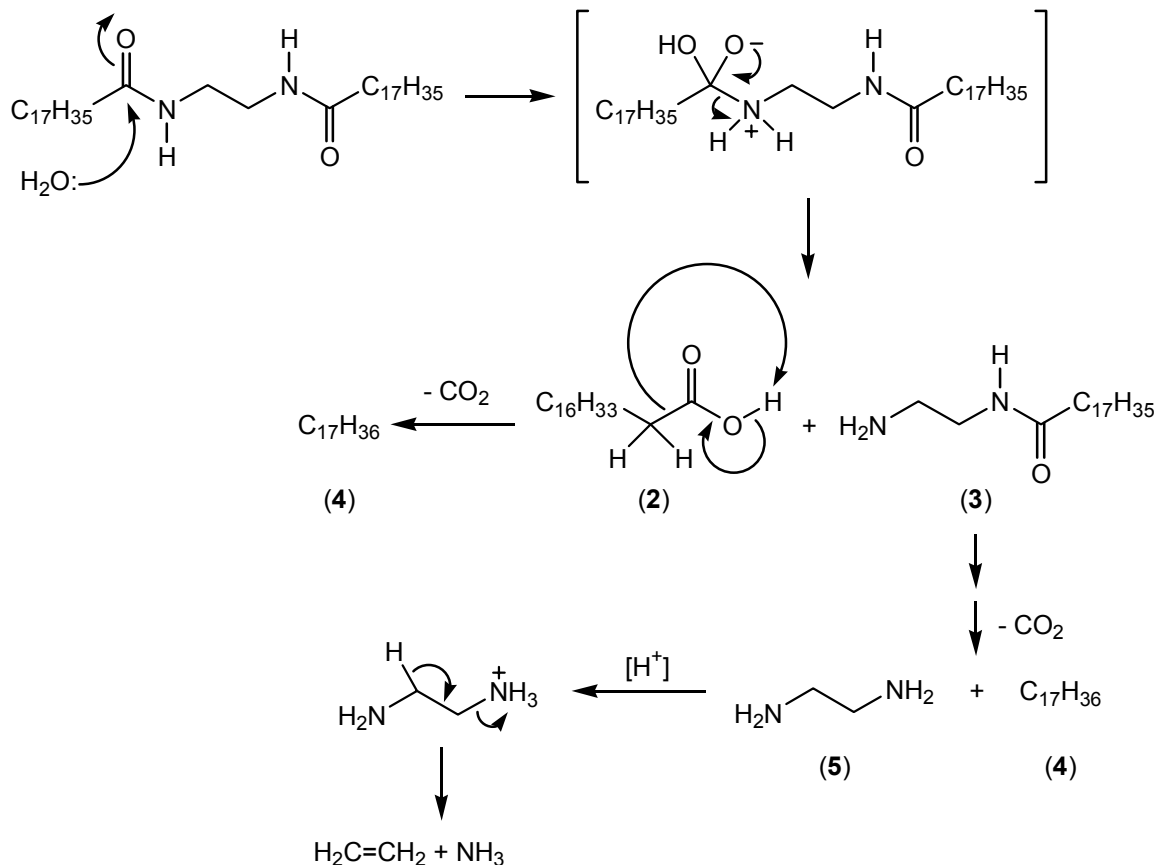
Figure 44:   **Schematic of the reactions during the decomposition of EBS**

4.5   *Conclusions*

The effect of moisture in the decomposition of EBS is a simple hydrolysis reaction. The reaction probably occurs on the P/M part surface. This explains the effect of moisture observed in the Phase I of our experiments. The primary gases identified during the decomposition of EBS are carbon dioxide, carbon monoxide, ammonia and a heavy hydrocarbon (hepta-decane). The experiments involved are from a part containing 1%lubricant (EBS) in them. The maximum concentration detected for the various identified gases are listed as follows:

Carbon Monoxide	-	19	ppm
Carbon dioxide	-	350	ppm
Ammonia	-	22	ppm
Hepta-decane	-	850	ppm

Development of sensor to detect the changes in concentration would require the detection of CO_2 and hepta-decane. A typical furnace has a load varying from

150 lb/hr – 1000 lb/hr. The concentrations listed above are for a single part of weight 35 gm. The concentration of gases under industrial conditions should be an order of magnitude higher.

5.0 PHASE III: <u>MATHEMATICAL MODEL FOR DE-LUBRICATION</u>

5.1 Introduction

De-lubrication is the first stage in a typical sintering operation where, the lubricant in a compacted part is removed by controlled heating and atmospheric conditions. Previous researchers have shown the effect of various parameters on the kinetics of de-lubrication **[13,14,15,16]**. The important parameters, which need to be considered, are heating rate, moisture content, hydrogen and the flow rate of the gases. However, an understanding of this process is complete only when the process is well described by a mathematical function, which incorporates in it, all the parameters involved. To control the de-lubrication process a quantitative (not qualitative) understanding and a functional relationship of the process parameters. Such knowledge enables are to predict and control the process on-line. De-lubrication is a combination of two processes:

1. The thermal degradation of the polymer to smaller hydrocarbons.
2. The transfer of the polymer/degraded molecules from the part to the atmosphere.

The kinetics of degradation of any polymer is given by the following equation:

$$\frac{d\alpha}{dt} = A(1-\alpha)^n \exp(\frac{-E}{RT}) \qquad \textbf{(13)}$$

Where;

α = Weight fraction of polymer
A = Pre-exponential factor (1/min)
E = Activation energy (J/mol)
R = Gas Constant (8.314 J/mol K)
T = Temperature (K)
n = reaction order

The values of 'n', 'A' and 'E' vary with the amount of energy supplied. The energy supplied is directly dependent on the applicable heating rate. If the constants 'n', 'A' and 'E' are known for a heating rate, the process is fully described. However, the additional variables in powder metallurgical applications such as green density, % hydrogen and moisture, make the exact mapping of n, A and E with temperature quite complex. To describe the process mathematically with the objective of having a workable model for de-lubrication, we have taken two parallel approaches:

1. Evaluate the average activation energies (E), A and n as described in equation or various conditions during de-lubrication.
2. Formulate an empirical predictive model for the process of de-lubrication, which is empirically based.

5.2   Theoretical Model Of De-Lubrication

Experiments on polymers are performed on a Thermo-gravimetric analysis machine (TGA), which determines the weight loss of the lubricant as a function of time / temperature. Thermo-gravimetric analysis can be used to provide information regarding the activation energy and the overall reaction order **[17 - 20]**. A typical TGA curve is shown in Figure 45. However, deducing precise information on the kinetics of polymer breakdown cannot be obtained from TGA data because the reaction order (n) is not known. Most researchers assumed a first order reaction (n = 1), which remains a good approximation **[21]**.
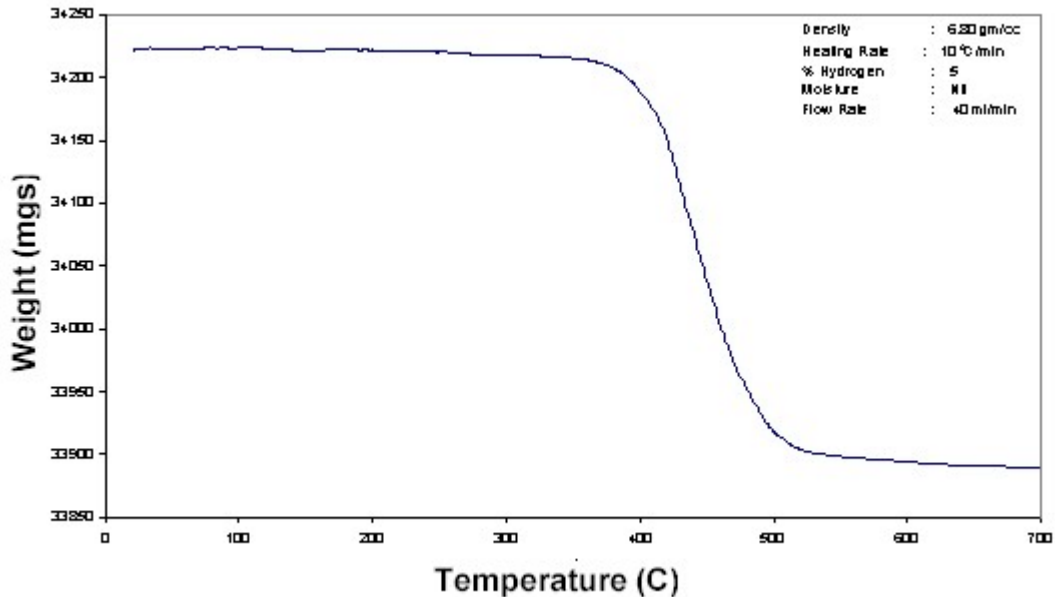
Figure 45:   Typical weight loss curve

Mathematical analysis of equation (14) performed by Kyong Ok Yoo et al **[22]** has shown that the plot of Ln(Rate of heating) and $1/T_{max}$ should be a straight line. T_{max} is the temperature on the curve where the rate of weight loss is the maximum (point of inflection on the TG-curve / $\frac{\partial^2 \alpha}{\partial t^2} = 0$). Figure 46 illustrates the inflection point. The following data can be inferred form the curve of 1/Tmax and Ln(Rate of Heating):

Slope   =   –E/R

54

$$\text{Intercept} = \ln(A_0) + \left(\frac{3}{2}\right)*\ln(T_{max}) - \ln\left(\frac{E}{RT} + \frac{1}{2}\right)$$
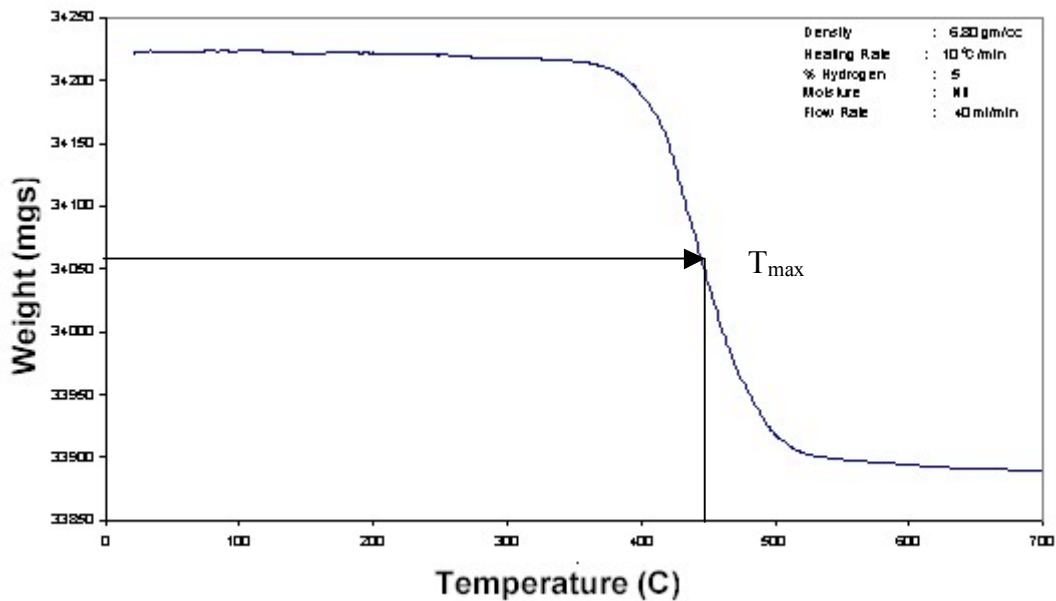
Figure 46:   Point of inflection

5.2.1 *Experimental Work*

To determine the kinetic parameters of de-lubrication during the process of sintering, TGA was performed with samples containing 1% acrawax (EBS). All the samples were compacted to densities ranging from 6.80 – 7.04 gm/cc. Only Fe-0.8%C compacted powders were considered for analysis. Historically, equation (1) has been used in the study for the degradation of pure polymers. The activation energies would vary in a compacted part, compared to that of a pure lubricant, as the presence of metal can alter the reaction kinetics. To have a model, that predicts the breakdown of lubricant in a furnace, necessitates the use of metallic compacts. The compacts had the following dimensions: 1/2" square base and 11/4" height. Experiments were conducted in the presence and absence of moisture. Figure 47 - Figure 48 show the plot of Ln (Rate of Heating) and $1/T_{max}$ for the two conditions, without moisture and with moisture.
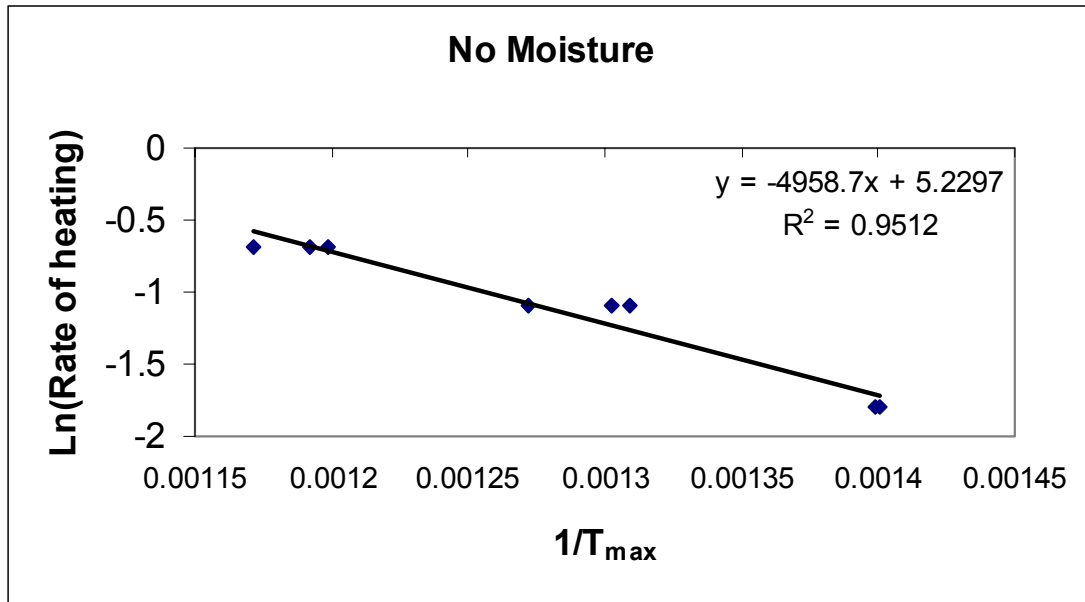
Figure 47: In(heating rate) Vs $1/T_{max}$ in dry conditions
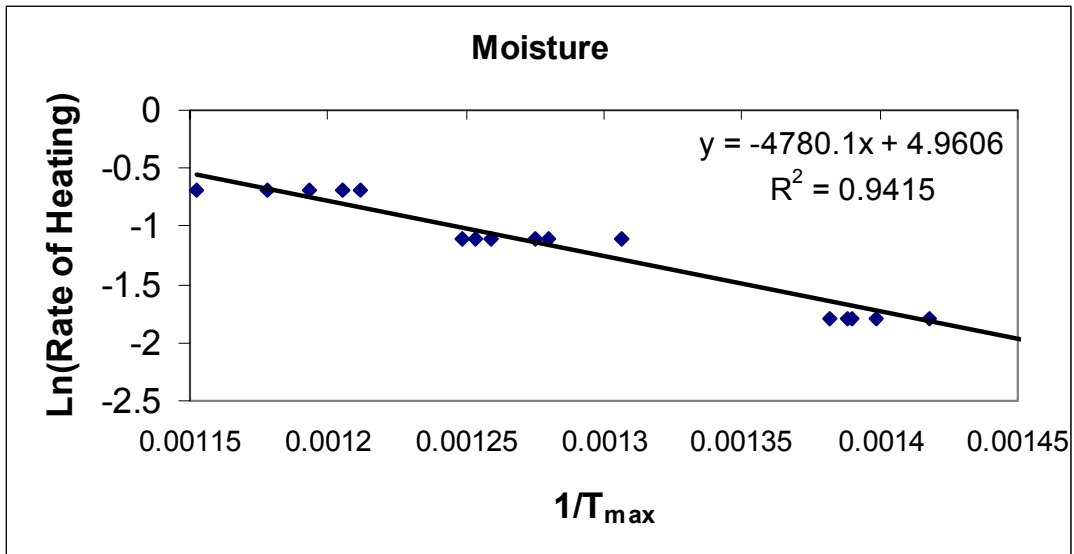
Figure 48: In(heating rate) Vs $1/T_{max}$ in wet conditions

5.2.2 Results

The values of A_0 and E calculated from the data of Figure 47 - Figure 48 are shown in Table XVI.

Table XVI.   'A0' and 'E' for EBS at the point of inflection

Rate of Heating (°C/min)	No Moisture (Nitrogen)		Moisture	
	A_0 (1/min)	E (kJ/mol)	A_0 (1/min)	E (kJ/mol)
10	1.0067		0.9138	
20	1.0577	41.229	0.9610	39.743
30	1.0929		0.9938	

Table XVI clearly shows that there is a slight decrease in the activation energy of de-lubrication when moisture is added to the system. However, these values of E and A are at the point of inflection ($\frac{\partial^2 \alpha}{\partial t^2} = 0$). The order of reaction (n) varies over the entire range of decomposition. According to Denq et al [20], thermal degradation by zero-order reaction order indicates that the molecular chain breaks by monomer scission at the chain end. Thermal degradation by first-order reaction indicates weight loss by the random scission of the main chain [19]. A second order reaction order would indicate intermolecular transfer and random scission. FTIR (Fourier Transform Spectrometer) analysis performed by Harb Nayar and George White [2] shows the presence of monomer units (-CH_3, -CH_2-) in the by-product during the initial period of de-lubrication followed by the presence of large hydrocarbon molecules at higher temperatures. EBS molecule (shown in Figure 49) shows that the –CH3 group is positioned at the ends of the polymer chain. This indicates that the decomposition of EBS proceeds by the scission at the polymeric ends (-CH_3) and at the center (-CH_2-). This implies a first order reaction order.
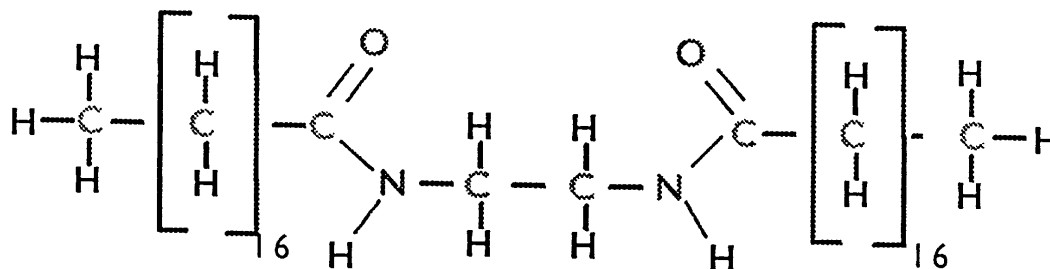
Figure 49:   Molecular structure of EBS

5.2.3 Conclusions

The kinetic model shows that moisture reduces the activation energy required for thermal degradation. The decrease in energy is however negligible (ΔE = 1.484 KJ/mol). The same model can be used to determine the affect of alloying elements (Ni, Cu, etc in the compact) on de-lubrication. The drawback of this analysis is the determination of 'n' during degradation. Though the average value of 'n' can be considered equal to unity, the value of 'n' changes as the decomposition changes from the scission of $-CH_3$ / $-CH_2-$ monomer units to other random units. Moreover, the activation energy determined from this model is the energy at the point of inflection. Realistically, the value of E changes as the mode of scission changes from one monomer unit to another. The change in the values of n and E with time only complicates the mathematical model, as more approximations are made to mathematically solve the problem.

5.3   *Empirical Model For De-Lubrication*

The kinetic model explained in the earlier section clearly explains the underlying thermal kinetics. In this section we determine an empirical model for de-lubrication by curve fitting techniques. De-lubrication curves obtained from the experiments in the previous section were analyzed to determine a mathematical function. The de-lubrication curve can be described as shown in equation 14.

$$\alpha = \frac{1}{1 + (\frac{t}{t_{max}})^b} \quad\quad (14)$$

Where,

α = $\frac{W_t}{W_0}$ (Weight fraction at any time 't')

W_0 = Initial weight of the lubricant

W_t = Weight of the lubricant at any time 't'

t = Time

t_{max} = Time at the point of inflection (Max. slope of the curve)

b = Constant depending on the conditions

The boundary conditions governing the equation are: t = 0, α =1 and t = infinite, α = 0. Appendix E shows the actual Vs the predicted data (-Pr). The values of 'b' and t_{max} ('c' in the graphs) appear at the right hand top corner. Table XVII summarizes the values of 'b' and t_{max} for all the experiments.

Table XVII. 'b' and 'tmax' for the predicted curves

Rate of Heating (^{0}C/min)	No Moisture		Moisture (Low)		Moisture(High)	
	b	t_{max} (secs)	b	t_{max}(secs)	b	t_{max} (secs)
10	20.4	2647	23.6	2678	22.57	2651
	20.4	2652	22.2	2593	21.2	2489
			23.5	2705	23	2684
20	18.2	1484	29.7	1477	35.3	1583
	18.7	1540	31.7	1533	31.3	1525
	15.1	1473	32.7	1563	33.37	1575
30	18.5	1132	32.8	1113	33.3	1104
	18.6	1123	34.8	1130	37.8	1190
	18.7	1161	30.9	1073	36	1152

Plots of Ln (rate of heating) and $1/t_{max}$ are shown in Figure 50 and Figure 51. Figure 50 shows a plot for the in the absence of moisture, Figure 51 is a similar plot in the presence of moisture.
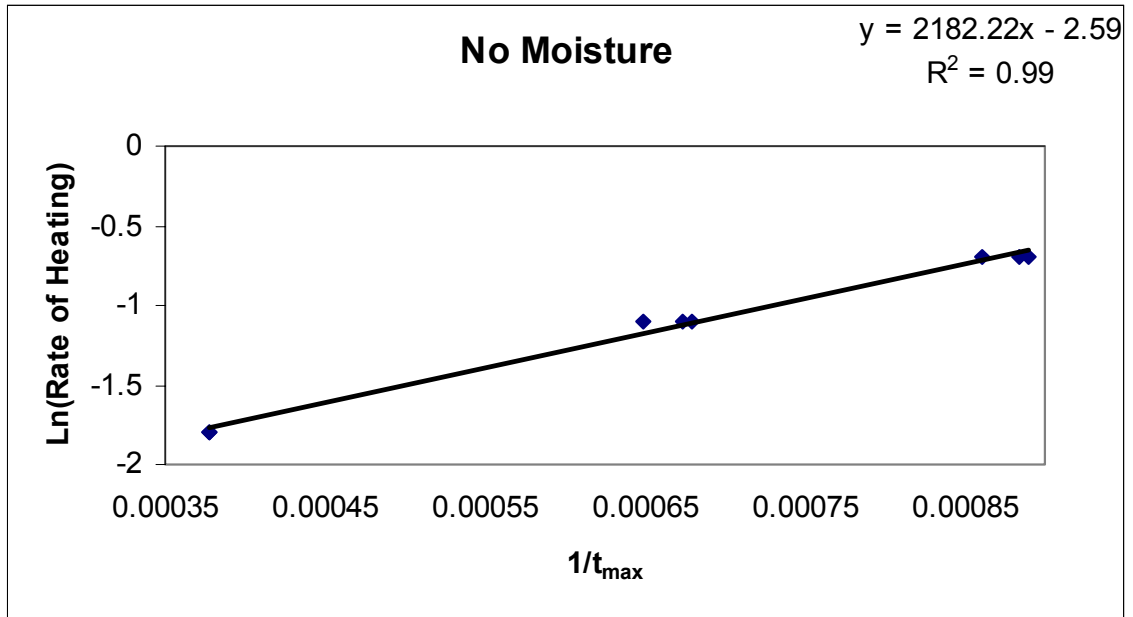
Figure 50: ln(rate of heating Vs 1/tmax (dry condition)
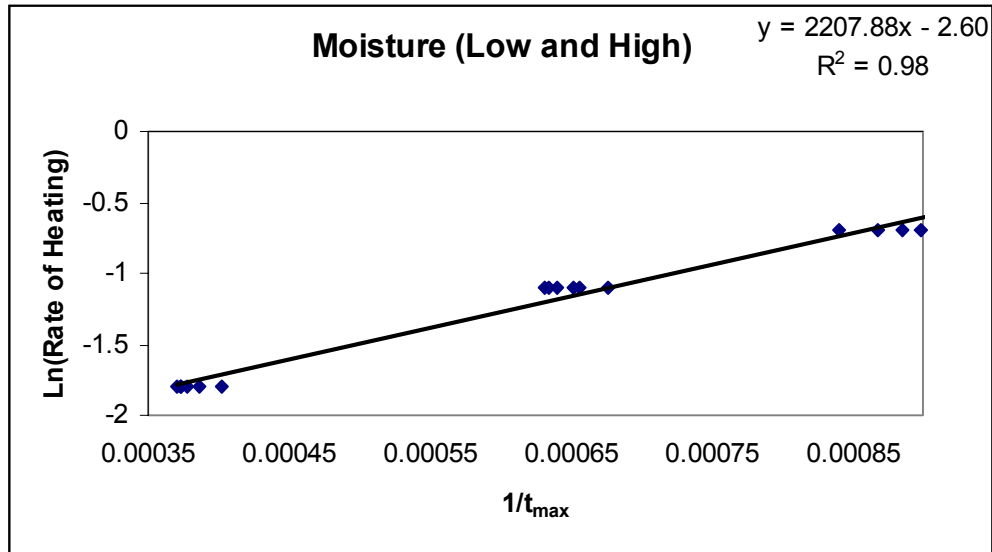
Figure 51:   ln(rate of heating) Vs 1/tmax (wet conditions)

Figure 52 shows the plot of 'b' for various atmospheric conditions and the rate of heating.
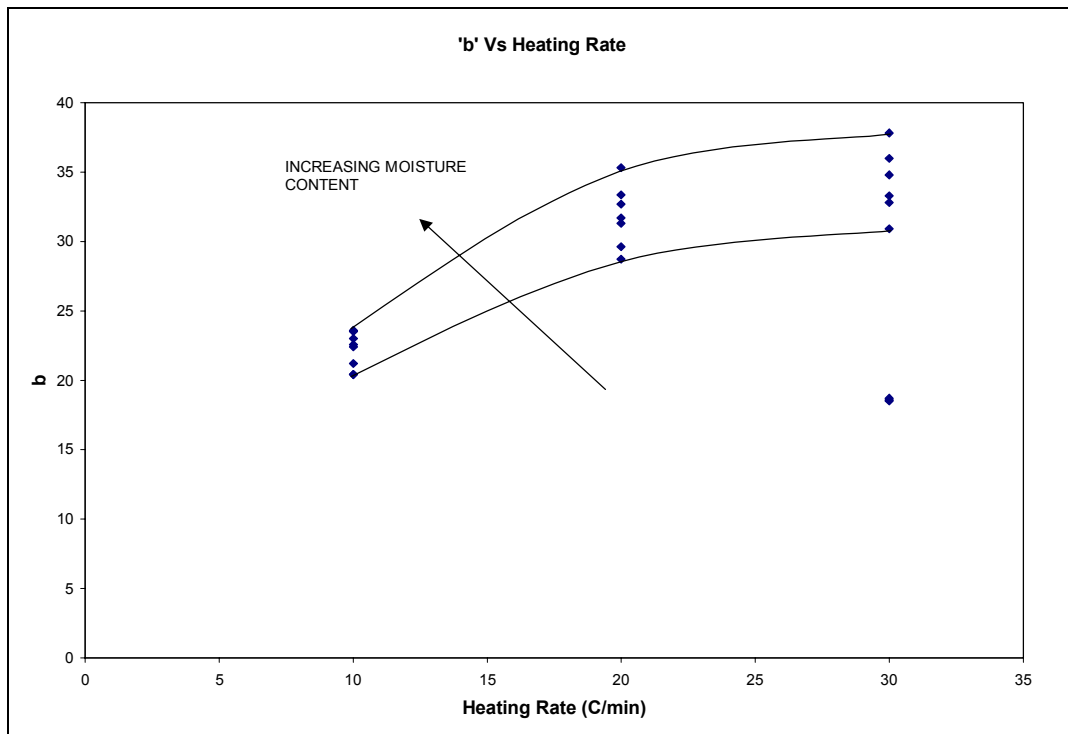
Figure 52:   'b' Vs rate of heating

5.4 Industrial Validation of the Mathematical Model

The proposed mathematical model was applied in furnace to see if there was an anomaly in the model. Ten compacts (Figure 53) of different weights were put in a furnace. All the compacts had 0.5 % lubricant in them. The largest of the sample had a weight of 35 gm and the smallest 24 gm. The furnace conditions are tabulated in Table XVIII.

Figure 53: Compacts used for the validation of model

Table XVIII. Sintering furnace condition

	TEMP. SET POINT (^{O}F)	FLOW RATE OF GASES (SCFH)			Length (ft)
		Nitrogen	Moisture	Hydrogen	
PREHEAT ZONE					
Zone 1	950	300	COLD	70	16
HIGH HEAT ZONE					
Zone 2	1250				
Zone 3	1675	800	-	80	60
Zone 4	2020				
Zone 5	2020				
COOLING ZONE	Room temp.	350			na

The following calculations were performed to estimate the time required for de-lubrication the sample.

Rate of Heating (from the slope of the thermal profile) = 0.30 ^{O}F/sec

t_{max} =   2731.7 sec (From Figure 51)

b   =   22 (From Figure 52 for nitrogen through water at room temp.)

61

Part1 =   24 gm (0.5 % lubricant (EBS))
Part2 =   36 gm (0.5 % lubricant (EBS))

W_t as a function of time was plotted (Figure 54) using equation 15. Ideally the value of $W_t = 0$ at infinite time (t); the value is however, negligible after 3500 sec.
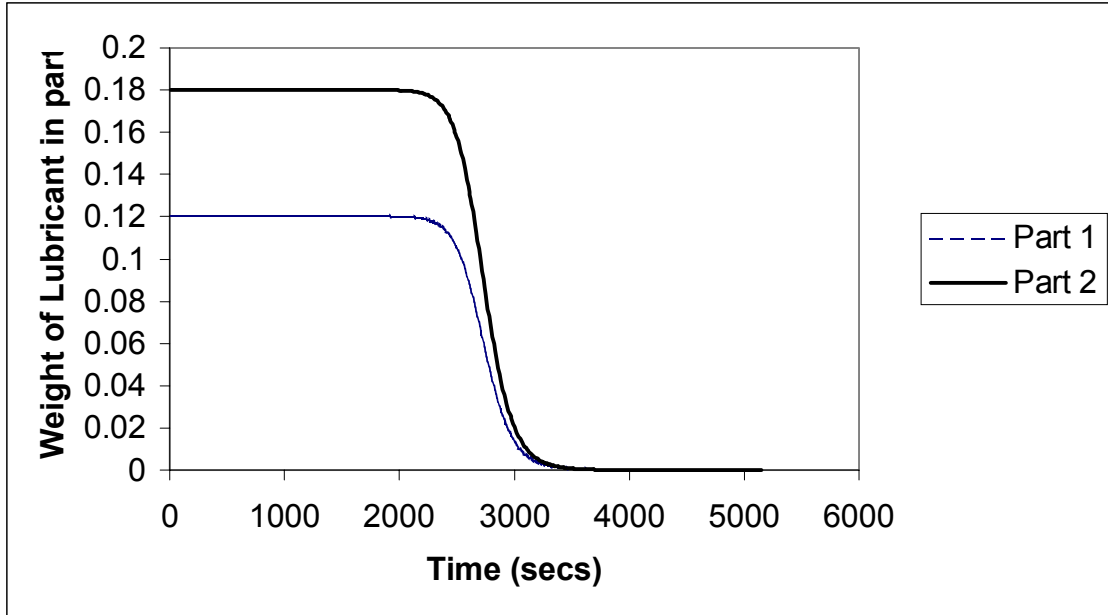
Figure 54:   Predicted weight of the lubricant Vs time

The model predicted that the parts be put in the furnace for 3500 sec (58.33 min) for complete de-lubrication. The belt speed was determined using the following calculations:

    Length of the Pre-heat zone   =   16 ft
    Time required for de-lubrication   =   58 min
    Belt speed   =   0.27 ft/min   =   3.24 inch/min

The parts were put on a plate and heated in the furnace at the required belt speed for a period of 53 min. 5 min were taken to pull the parts from the furnace and for them to cool down. The samples were then re-heated to 600 ^{O}C in a TGA machine to study the amount of residual lubricant.

5.4.1 Results

The samples from the furnace were put in a TGA machine and reheated at 10 ^{O}C/min to 600 ^{O}C. The atmosphere was 100 % Nitrogen. Figure 55 shows a close up of the parts. The parts have no stains on them; implying clean burnout.
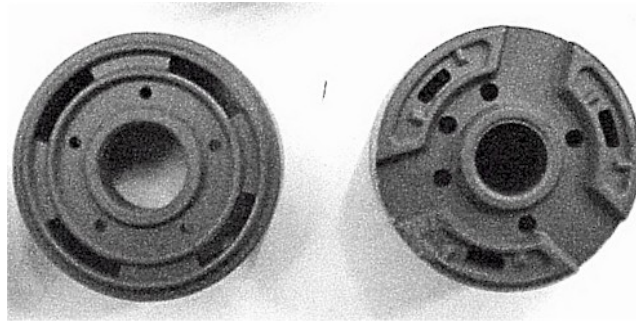
Figure 55:   Absence of 'C' stains

Figure 56 and Figure 57 are the representative curves for parts with weight 24 gram and 34 gram respectively. The curves clearly show the absence of remnant lubricant in the part.
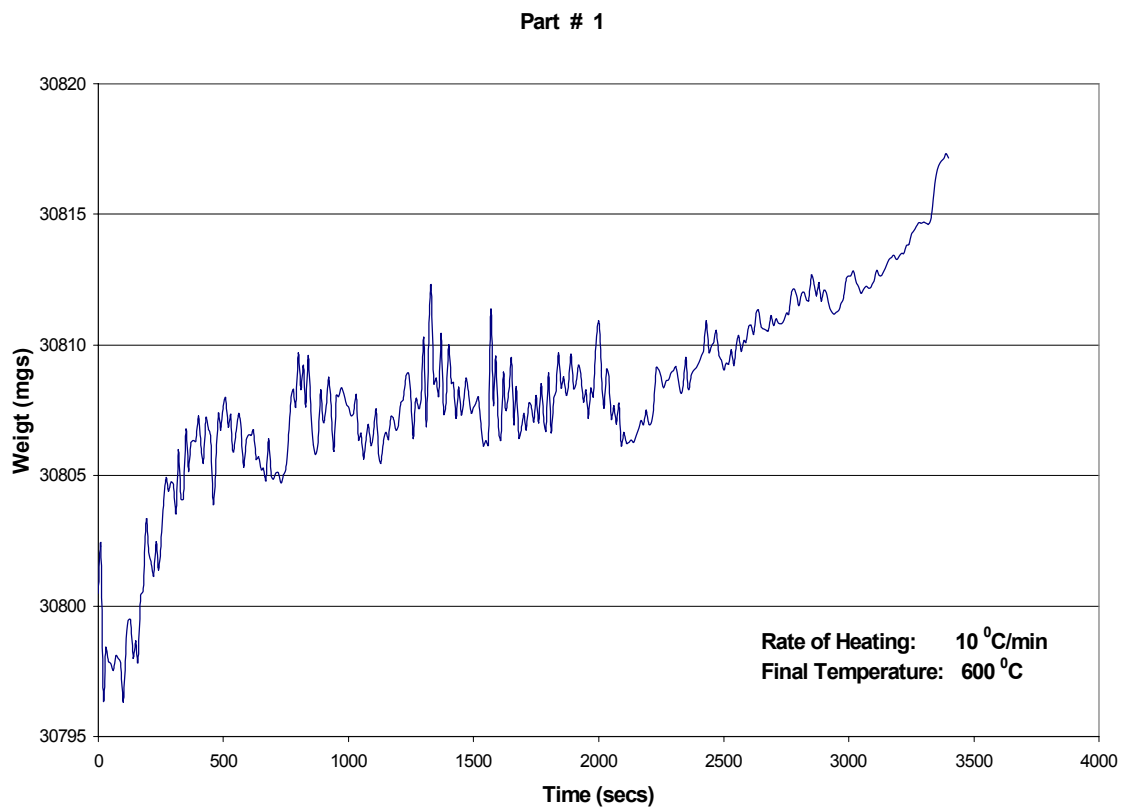
Figure 56:   Larger parts re-heated to 600 ^{0}C
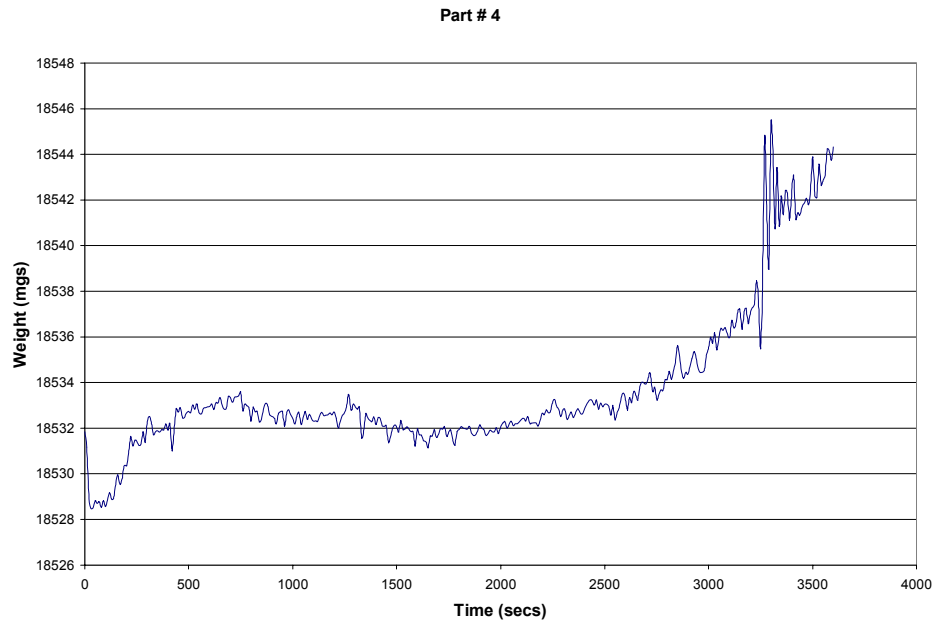
Figure 57:   Smaller parts re-heated to 600 ^{0}C

5.4.2 Conclusions

The empirical model has only two parameters ('b' and 't$_{max}$') and it completely describes the process of de-lubrication. Unlike the theoretical model, where the values of E and n are the average values of the entire process, the parameters in the empirical model can be classified as follows:

-   't$_{max}$' is an intrinsic property of a polymer (equal to the point of inflection in a TGA curve) and is independent on external conditions.
-   'b' is an extrinsic property, which varies on external conditions (Moisture, Gas flow rate, Hydrogen, rate of heating etc).

This model can be utilized directly in the development of control systems for its simplicity. Once the system conditions are gauged and the value of 'b' determined, the model easily predicts the time required for complete de-lubrication. Figure 58 shows the mathematical model in relation to the FTIR analysis performed in section 4.0. The top graph is a concentration plot with time for all the identified gases; the bottom graph is a weight loss plot of a similar sample (weight and %EBS) predicted by the mathematical model. The value of 'b' used in the model is an average of the all the 'b' values in Table XVII. The Figure 58 clearly shows that the point of inflection predicted by the model (in this case $\frac{\partial^2 \alpha}{\partial t^2} = 0$ is at 2637 sec = 712.5 K). Referring to the FTIR graph, the

64

decomposition of the hydrocarbon (which is the heavier molecule in the system) is maximum at 748 K. The error calculated between predicted and actual observed maxima is 36.
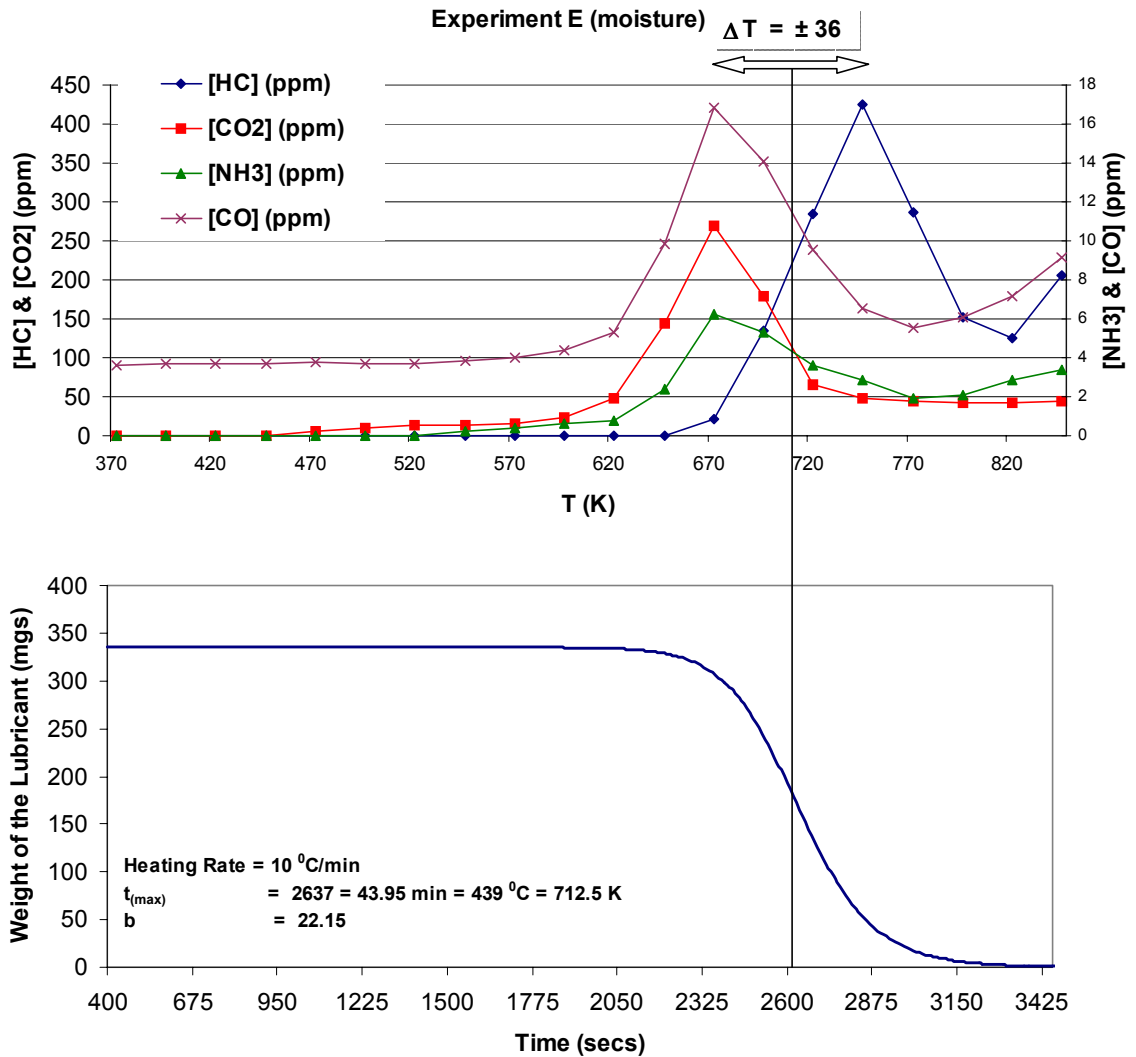
Figure 58:   Comparison of the FTIR data and the mathematical model

6.0 <u>CONCLUSIONS</u>

The main conclusions from the all of the project are as follows:

- The decomposition of EBS is essentially a thermal event. The rate of heating has shown to have the largest contribution in the decomposition kinetics of EBS (65 – 71 % on the variance)

- Analysis of variance in the Phase I of our experiments also illustrated, that moisture plays a significant role in the decomposition of EBS (23 – 25 % on the variance). This was confirmed in the Phase II of our experiments, wherein it was shown that moisture aids in the decomposition if EBS via a simple hydrolysis reaction

- FTIR and DUV analysis in the Phase II of our experiments identified the gases released during the decomposition of EBS. The primary gases released are hepta-decane ($C_{17}H_{35}$) and carbon dioxide (CO_2). The trace gases consisted of carbon monoxide and ammonia. The identification of gases maps out the direction for the development of future sensors, specifically, a sensor which can measure the concentration of CO_2 - $C_{17}H_{35}$ will enable the control f process of de-lubrication

- A mathematical model, has been developed, verified and validated to predict de-lubrication. The model was verified in industrial conditions and has shown a strong correlation when compared to the experiments of Phase II. The proposed model has only been verified and correlates well with compacts having a density up to 7.04 gm/cc. Further work is underway at PMRC to validate the model for densities up to 7.5 gm/cc.

7.0   FUTURE WORK

This section deals with the various suggestions and recommendations resulting from this work.

- Phase 2 of our study clearly shows that the breakdown of EBS results in the release of gases such as CO_2, CO, NH_3 and hepta-decane which can be detected using a sensor. Development of sensors, which would detect the concentration of CO_2 and hepta-decane, is a real possibility. The concentrations of CO and NH_3 are however, too low (< 60 ppm) to be economically viable. The sensor would need a non-dispersive IR absorption spectroscopy as its *modus operandi.*

- As hepta-decane has a sublimation of 302^0C, the problem of 'sooting' can be related to the condensation of this high molecular weight hydrocarbon in the cooler parts of the furnace (front) onto the parts. As the part gets heated in the de-lubrication zone, the hydrocarbon decomposes by thermal pyrolysis to carbon or 'soot' on the furnace. Preheating the parts or increasing the furnace temperature in the front zone of the furnace to above the sublimation of hepta-decane might solve the problem of 'sooting'. This might explain the increased incidence of 'sooting' during the sintering of high Ni parts. It is well known that Ni is a very good catalyst (commonly used in the hydrogenation of oils), presence of hydrogen, a heavy weight hydrocarbon and Ni can lead to the rapid breakdown of the lubricant / hepta-decane to free carbon. This hypothesis however, needs to investigated and studied in detail.

- Phase III of our research clearly shows that the mathematical model can be used an algorithm in the 'control system'. The values of 'b' reported in phase II, are values determined for a Fe – 0.8 C compacted system. In reality, 'b' incorporates into it, the thermal properties of the alloy used. For the model to be applicable to industrial furnaces, the database of 'b' for

various alloy system should be determined. This would make the control system 'Alloy independent'.

- The value of t_{max} in our experiments is for the decomposition of EBS. However, industrially, various lubricants are used during the compaction. Determination of t_{max} for other lubricants will be a boon to the industry.

8.0   <u>REFERENCES</u>

1. "<u>Powder Metallurgy Science</u>", Randall M. German

2. Harb Nayar & George White, "Indication of complete delubing", *Advances in Powder Metallurgy and Particulate Materials*, 1995, Part 3, Page 3-11 to 3-18.

3. Y.Kankava, K.Saitou, T.Kida, K.Ono and Y. Kaneko, "Injection Molding of SUS3 Powder with polyacetal", *J. Japan Soc. Powder Met*. 40,1993,379- 383.

4. Joseph N. Auborn and Joon .S.Choo, "Effect of Chemistry and Compact Density on the Decomposition of P/M Lubricants*", Advances in Powder Metallurgy and Particulate Materials*,Vol 3,1994,pp 103-106.

5. J.Woodthorpe, M.J.Edirsinghe and J.R.G.Evans, " Properties of Ceramic Injection Molding Formulations. Part 3, Polymer Removal", *J.Material Science*, 24,1989, pp 1038-1048.

6. Collen F. Legzdins, Indira Samarasekera and tom Troczynski, "Experimental Studies of Zinc Sterate De-Lubrication in High Temperature Sintering of Ferrous Compacts", *PM Tech, 1999*, Vancouvar, BC.

7. C.F.Cullis & M.M.Hirschler, "The combustion of Organic Polymers", *Oxford university press*, NewYork, 1981.

8. George White and Harb Nayar, " Monitoring of the De-Lubrication Process Under production Conditions", *Advances in Powder Metallurgy and Particulate Materials*, 1996, Vol. 3, pp 10.27 – 10.40.

9. M. Renowden and P. Pourtalet, " Experimental Studies on Lubricant Removal", *Advances in powder Metallurgy*, 1990, Vol. 1, pp 261-278.

10. George R. White, Anthony Griffo and Harb Nayar, " Effects of Atmosphere additions on Increasing Efficiency on Fe-2Cu-0.8C", *Advances in Powder Metallurgy and Particulate Materials*, 1994, Vol. 3.

11. Joseph N. Auborn and Joon .S.Choo, "Effect of Chemistry and Compact Density on the Decomposition of P/M Lubricants", *Advances in Powder Metallurgy and Particulate Materials*,Vol 3,1994,pp 103-106.

12. Collen F. Legzdins, Indira Samarasekera and tom Troczynski, "Experimental Studies of Zinc Sterate De-Lubrication in High Temperature Sintering of Ferrous Compacts", *PM Tech*, 1999, Vancouvar, BC.

13. George R. White, Anthony Griffo and Harb Nayar, " Effects of Atmosphere additions on Increasing Efficiency on Fe-2Cu-0.8C", *Advances in Powder Metallurgy and Particulate Materials*, 1994, Vol. 3.

14. C.F.Cullis & M.M.Hirschler, "The combustion of Organic Polymers", *Oxford university press*, NewYork, 1981.

15. Petrovic Z.S, Zavargo Z.Z, *Journal of Polymer Science* 1986, Vol. 32, 4353

16. Nam J.D, Seferis J.C, *Journal of Polymer Science* 1991, Vol. 29, 601.

17. Jimenez A. Berenguer V, Lopez .J, Sanchez A., *Journal of Polymer Science* 1993, Vol 50, 1565.

18. Salin J.M, Seferis J.C*, Journal of Applied Polymer Science* 1993, Vol 47, 847

19. J.E.J. Staggs, "Modelling thermal degradation of polymers using single-step first-order kinetics", *Fire Safety Journal*, 1999, Vol. 32, 17-34.

20. J.W.Park, S.C. Oh, H.P. Lee, H.T. Kim, K.O. Yoo, "A Kinetic Analysis of Thermal Degradation of polymers using a Dynamic Method", *Polymer Degradation and Stability* 2000, Vol. 67,535 – 540.

APPENDIX A: THE THERMO-GRAVIMETRIC ANALYZER (TGA)

TGA is an acronym for Thermo-gravimetric Analysis. The TGA is a useful tool in the determination of minute weight changes (as low as 1 micro-gram) with temperature. The set-up consists of a furnace, which holds a crucible that is hung from one side of a weighing balance. The crucible contains a sample to be analyzed. This may be a metallic sample or otherwise. The sample to be analyzed is progressively heated to desired temperatures and the balance as it is being heated, measures the change in weight of the sample. Normally, an organic compound losses weight as it is heated to higher temperatures as it decomposes. The loss in weight is normalized to the weight of the sample and is an indicator of the rate of decomposition. The machine has an on-line data collection system, which collects data. Typically the system generates a plot between the absolute weight, temperature and time. The software in the machine can generate the first / second derivatives and other mathematical functions depending on the requirement. A schematic of the apparatus is shown in Figure A-1.

The apparatus has several features, which make it possible to conduct a variety of tests. The most important feature is the controllability of the furnace atmosphere. The furnace is sealed from the atmosphere and one can introduce a specific gas in the furnace for a specific period of time during a single test. The electrically initiated solenoid valves in the furnace do this. One can pass a particular gas at a particular temperature and switch to another gas at another

pre-determined temperature. Helium gas flushes out all the emission gases from the system.
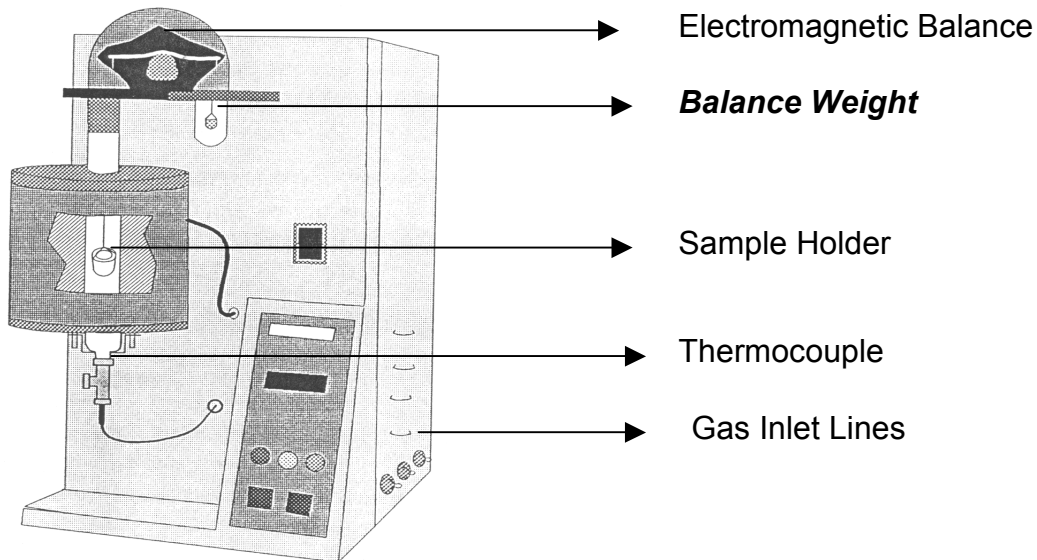
Figure A-1:   Schematic of a TGA machine

The heating system is also monitored using the system software. The heating process may be customized at a single test procedure or can be broken down to several ramping/cooling cycles.

To start a test the following procedure is adhered to:

- The TGA apparatus and the computer are both turned ON.

- The TSR (Program which runs the controls in the TGA machine) is loaded.

- A method is selected using the ones currently prevailing, or a fresh one is created.

- On the method screen (see Figure A-2) time, temperatures and ramp rates for all segments are completed correctly.

- Appropriate gas settings are selected.
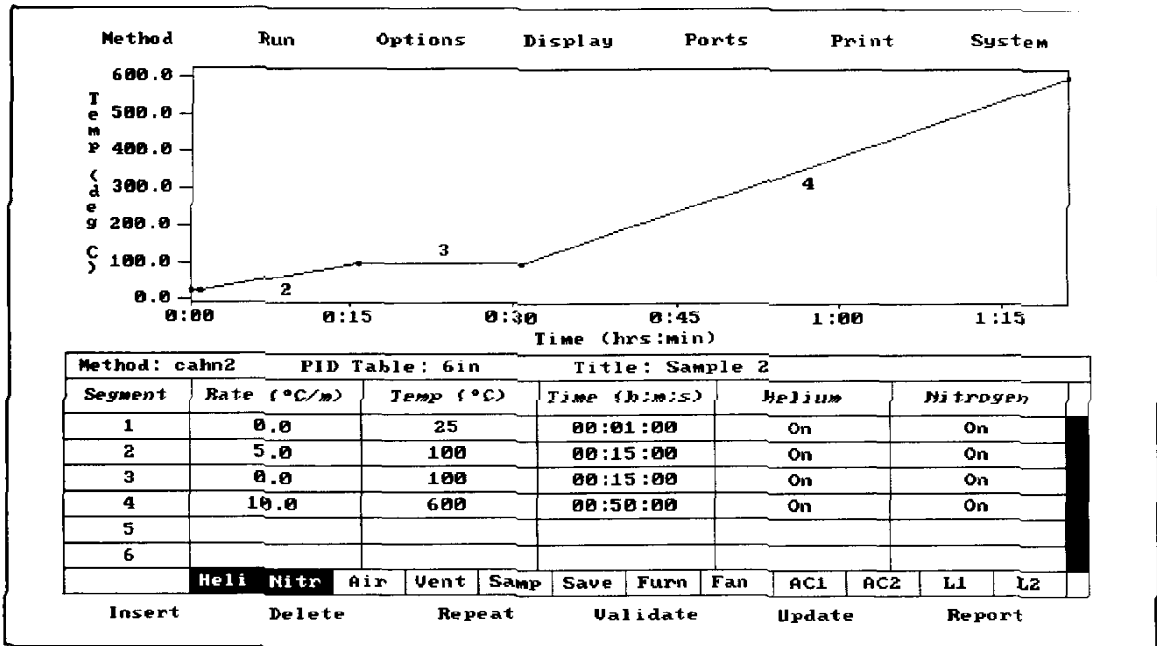
Figure A-2: Typical method screen

- The balance is calibrated each time the unit is turned on. This is performed by placing a known weight on the tare side of the balance.

- The balance is electro-magnetically tared such that the scale reads zero. This done with no sample on the crucible. The user-friendly TGA software permits these steps very easily.

- The sample is loaded by lowering the furnace. Once the furnace is lowered, the crucible is removed from the wire basket, which hangs from side of the balance. The sample is placed in the crucible and the crucible is placed back into the hanging wore basket. Thereafter, the furnace is moved upwards until the sample lies approximately within the center of the furnace.

73

- The weight of the sample, as measured by the balance, is recorded on the computer screen after allowing it to stabilize. This is the initial weight of the sample.

- Clicking RUN at the menu starts the experiment.

- During the run, the gases are switched automatically as specified in the method.

- The test stops automatically after the duration (specified earlier in the test method) has elapsed.

- The results may be viewed using the TGA software or the data file may be exported to other applications.

APPENDIX B: TGA GRAPHS GENERATED FOR THE TAGUCHI RUNS

Weight loss Vs Temperature

Density   : 6.80 gm/cc
Heating Rate : 10 °C/min
% Hydrogen   : 5
Moisture   : Nil
Flow Rate   : 40 ml/min
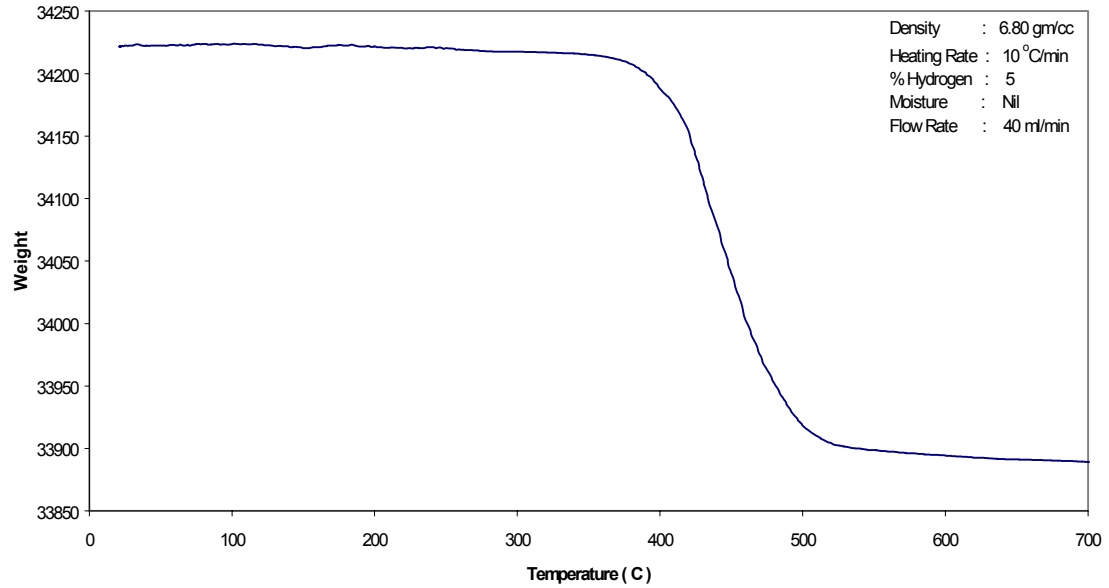
1. *Taguchi Trial No: 1; Density 6.80 gm/cc*

Weight Loss Vs Temperature

Density   : 6.80 gm/cc
Heating Rate: 10 °C/min
% Hydrogen : 15
Moisture   : Low
Flow Rate   : 60 ml/min
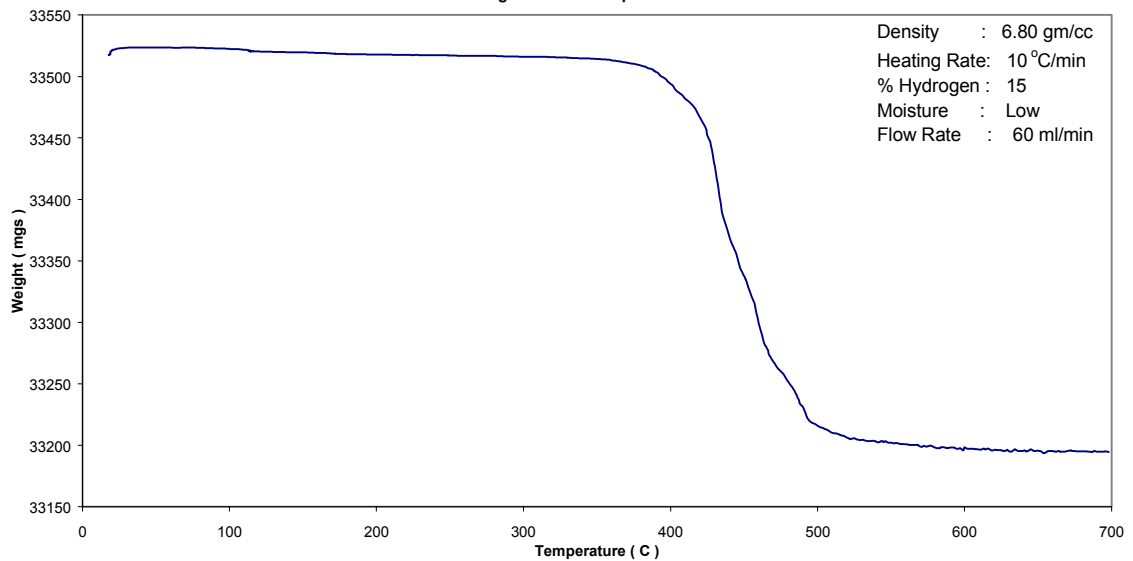
2. *Taguchi Trial No: 1; Density 6.95 gm/cc*

Weight Loss Vs Temperature

Density : 7.04 gm/cc
Heating Rate : 10 ^{o}C/min
% Hydrogen : 5
Moisture : Nil
Flow Rate : 40 ml/min
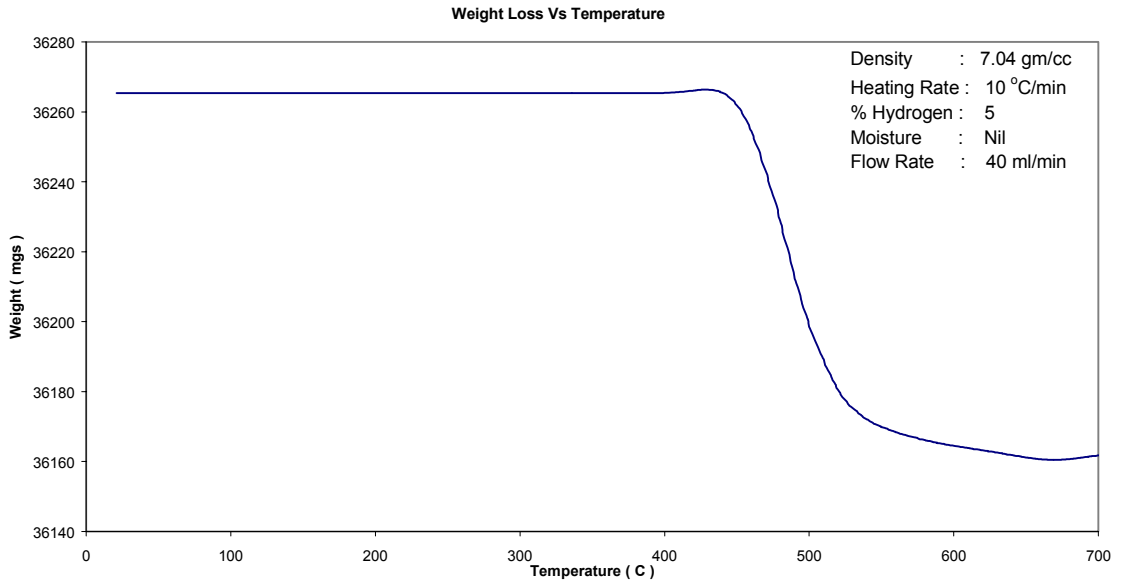
3. *Taguchi Trial No: 1; Density 7.04 gm/cc*

Weight Loss Vs Temperature

Density : 6.80 gm/cc
Heating Rate: 10 ^{o}C/min
% Hydrogen : 15
Moisture : Low
Flow Rate : 60 ml/min
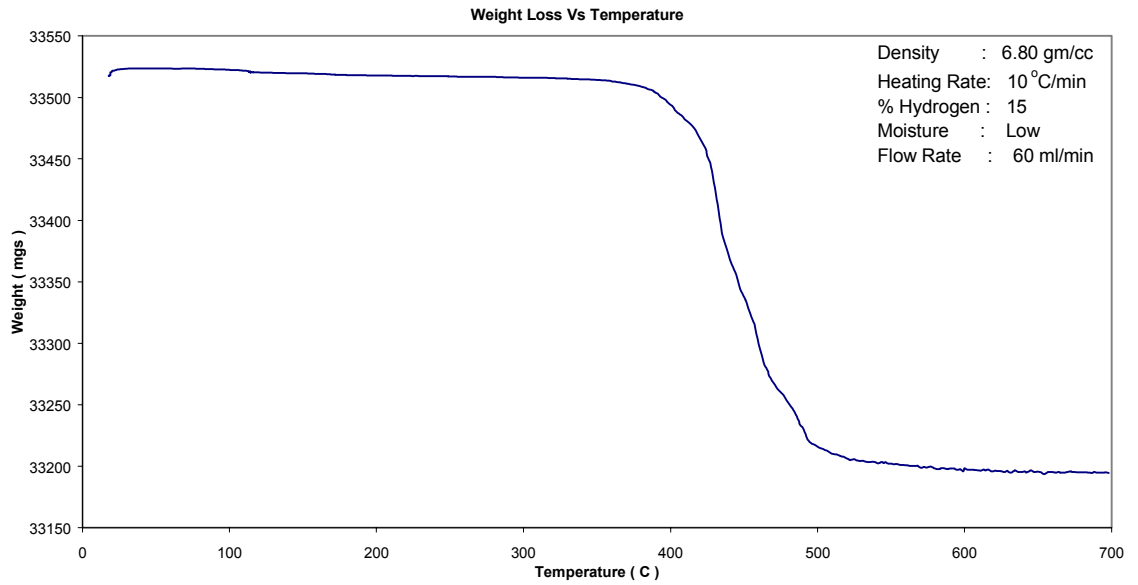
4. *Taguchi Trial No: 2; Density 6.80 gm/cc*

76

Weight Loss Vs Temperature

Density : 6.95 gm/cc
Heating Rate : 10 ^{o}C/min
% Hydrogen : 15
Moisture : Low

Y-axis: Weight (mgs)
X-axis: Temperature (C)
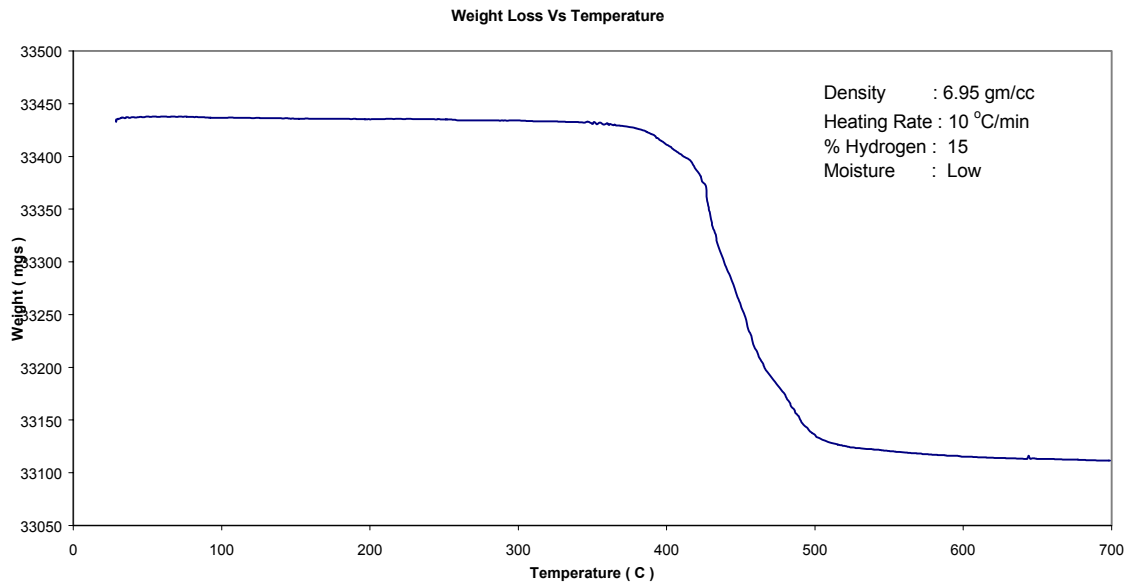
5. _Taguchi Trial No: 2; Density 6.95 gm/cc_

Weight Loss Vs Temperature

Density : 7.04 gm/cc
Heating Rate: 10 ^{o}C/min
% Hydrogen : 15
Moisture : Low
Flow Rate : 60 ml/min

Y-axis: Weight (mgs)
X-axis: Temperature (C)
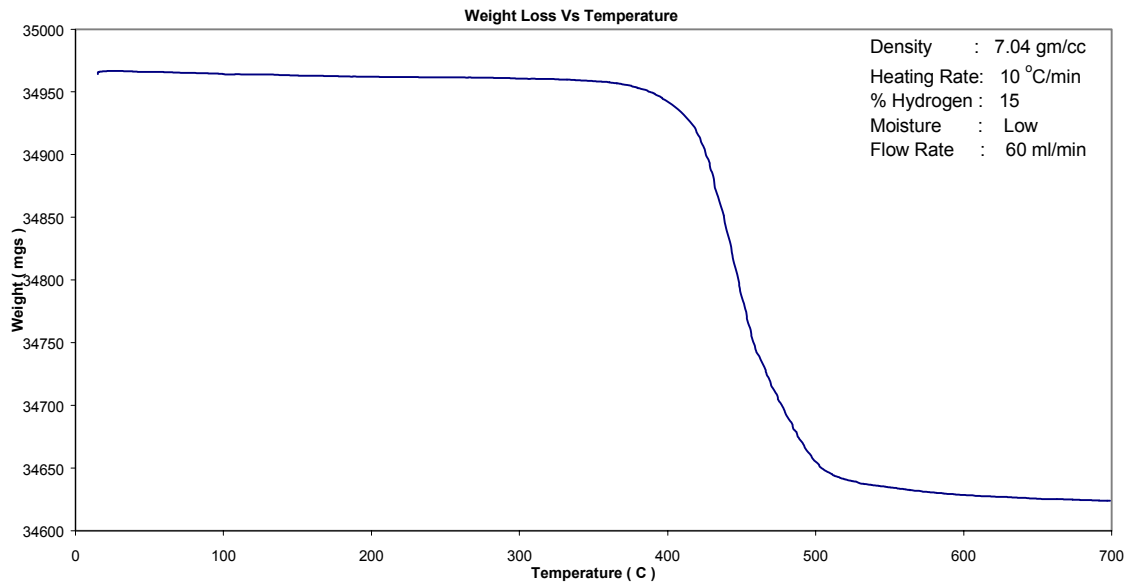
6. _Taguchi Trial No: 2; Density 7.04 gm/cc_

77

Weight Loss Vs Temperature

Density   : 6.95 gm/cc
Heating Rate   : 10 $^{\circ}$C/min
% Hydrogen   : 30
Moisture   :   High
Flow Rate   : 80 ml/min
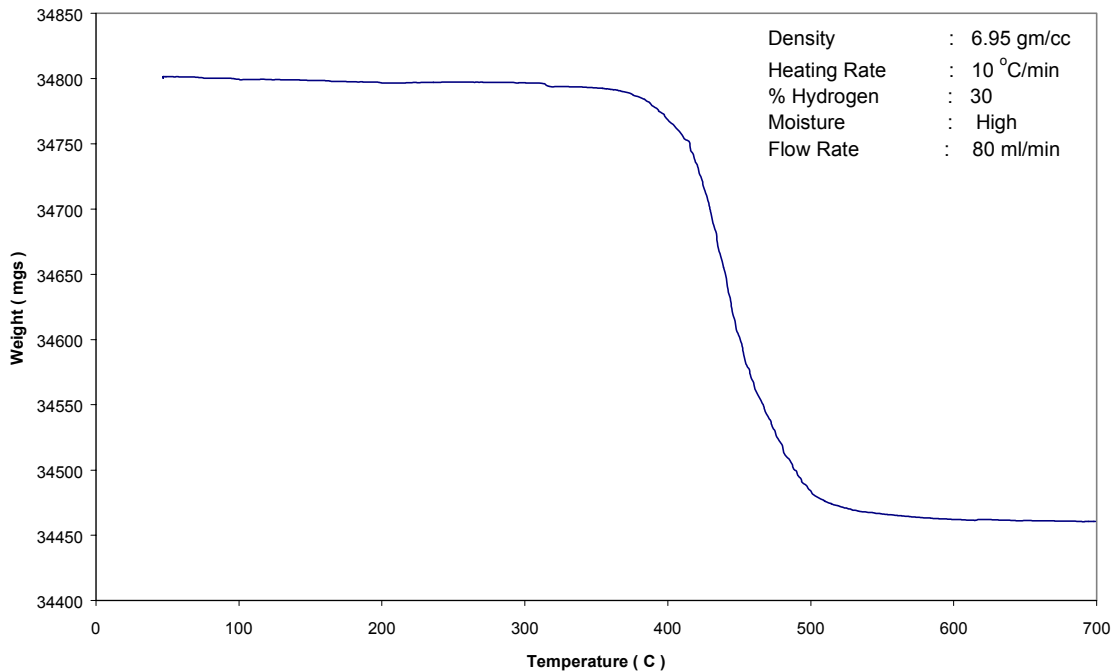
7. Taguchi Trial No: 3; Density 6.80 gm/cc

Weight Loss Vs Temperature

Density   : 6.80 gm/cc
Heating Rate   : 10 $^{\circ}$C/min
% Hydrogen   : 30
Moisture   :   High
Flow Rate   :   80 ml/min
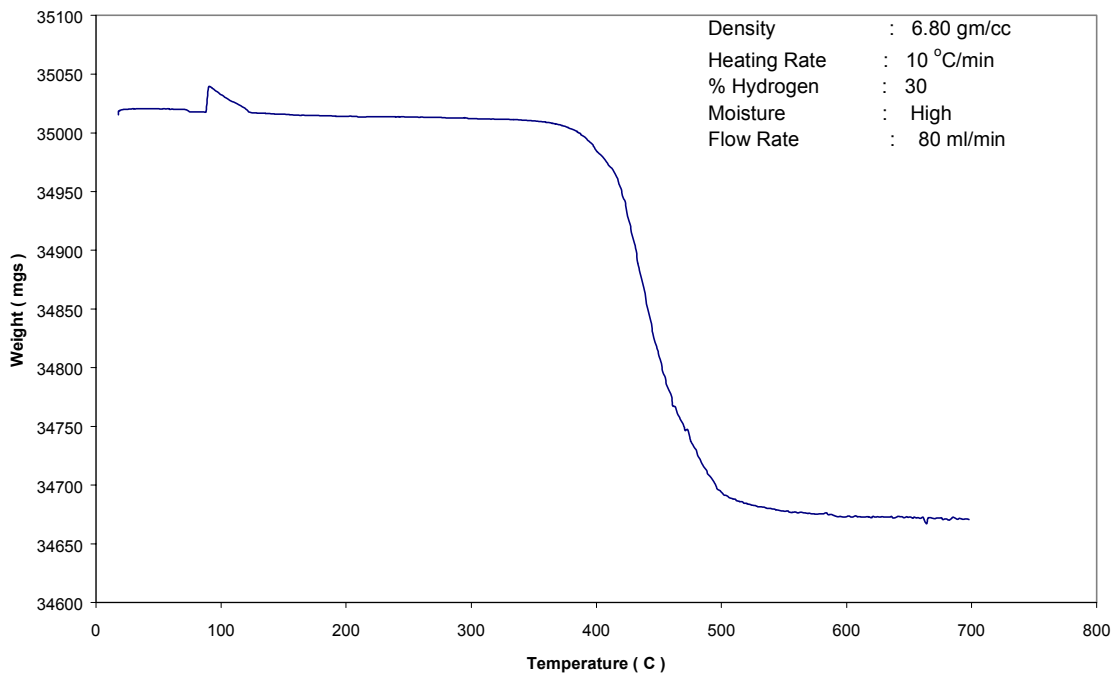
8. Taguchi Trial No: 3; Density 6.95 gm/cc

Weight Loss Vs Temperature

Density	: 6.80 gm/cc
Heating Rate	: 20 °C/min
% Hydrogen	: 5
Moisture	: Low
Flow Rate	: 80 ml/min
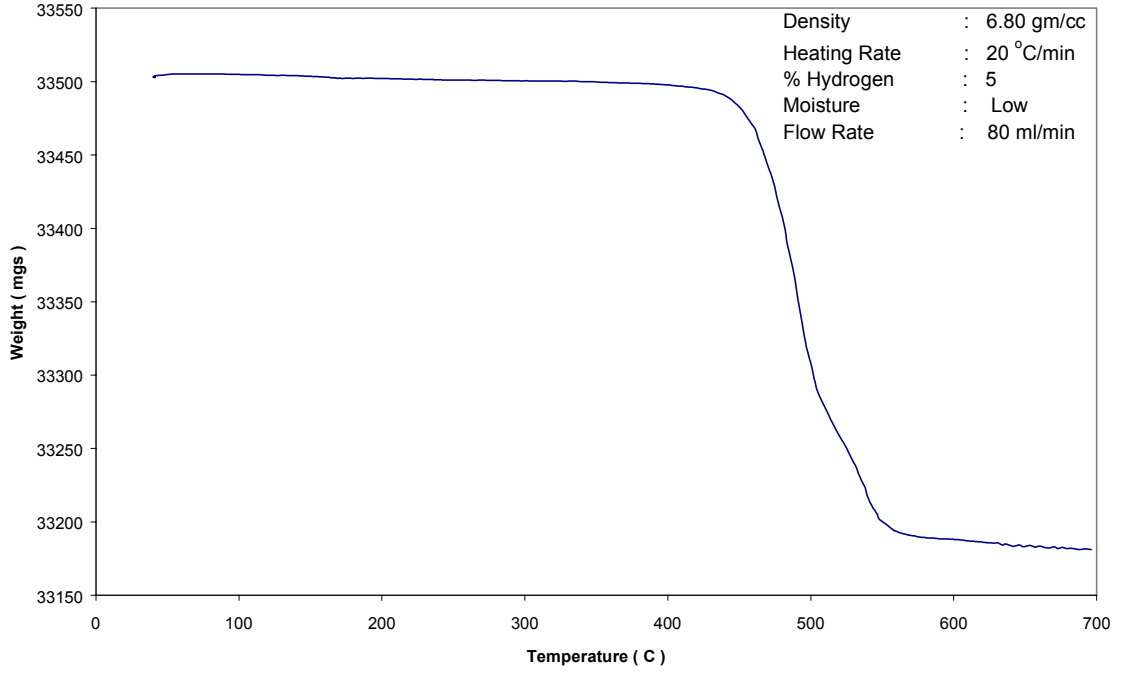
9. _Taguchi Trial No: 3; Density 7.04 gm/cc_

Weight Loss Vs Temperature

Density	: 7.04 gm/cc
Heating Rate	: 10 °C/min
% Hydrogen	: 30
Moisture	: High
Flow Rate	: 80 ml/min
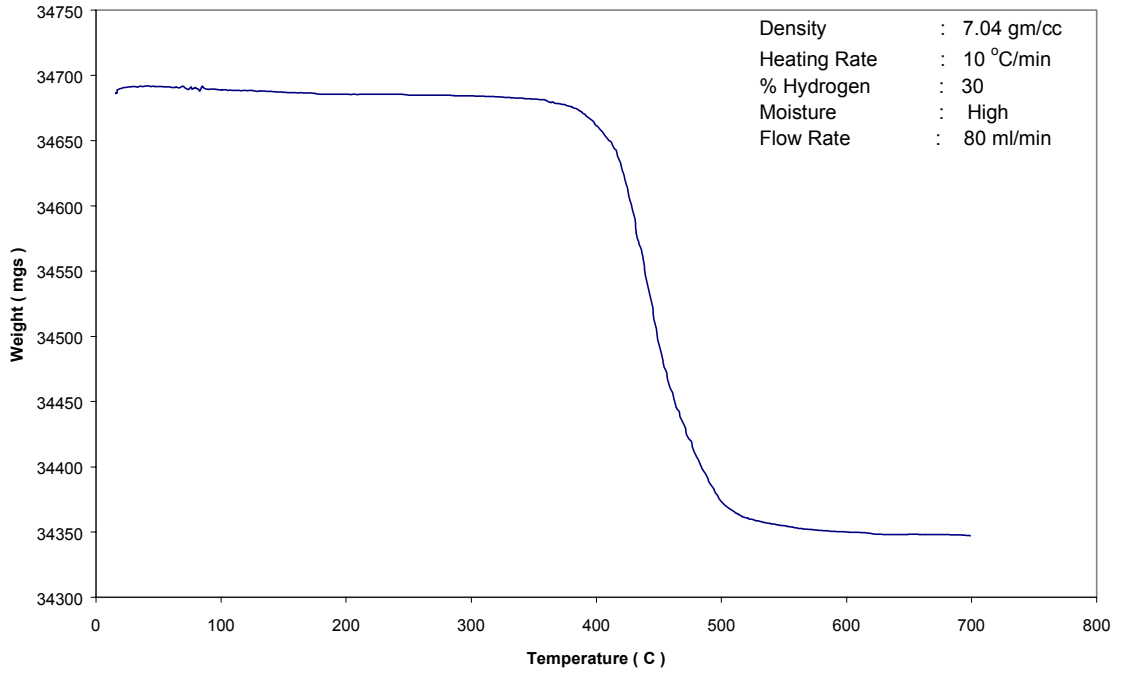
10. _Taguchi Trial No: 4; Density 6.80 gm/cc_

Weight Loss Vs Temperature

Density : 6.95 gm/cc
Heating Rate : 20 °C/min
% Hydrogen : 5
Moisture : Low
Flow Rate : 80 ml/min
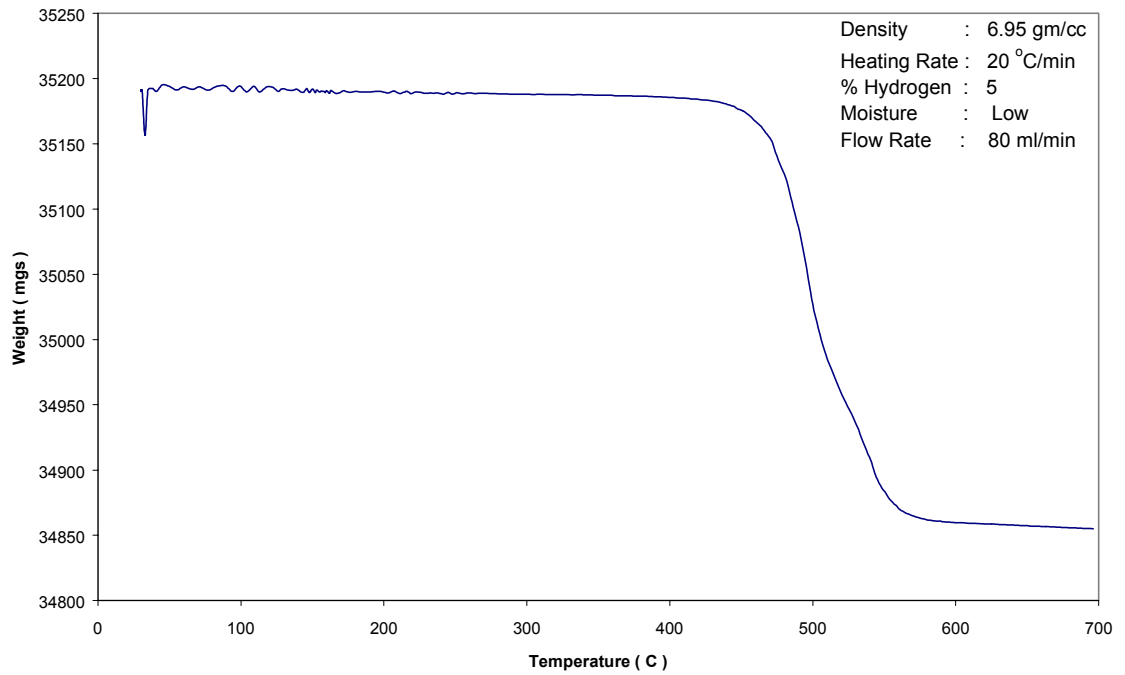
11. *Taguchi Trial No: 4; Density 6.95 gm/cc*

Weight Loss Vs Temperature

Density : 7.04 gm/cc
Heating Rate: 20 °C/min
% Hydrogen : 5
Moisture : Low
Flow Rate : 80 ml/min
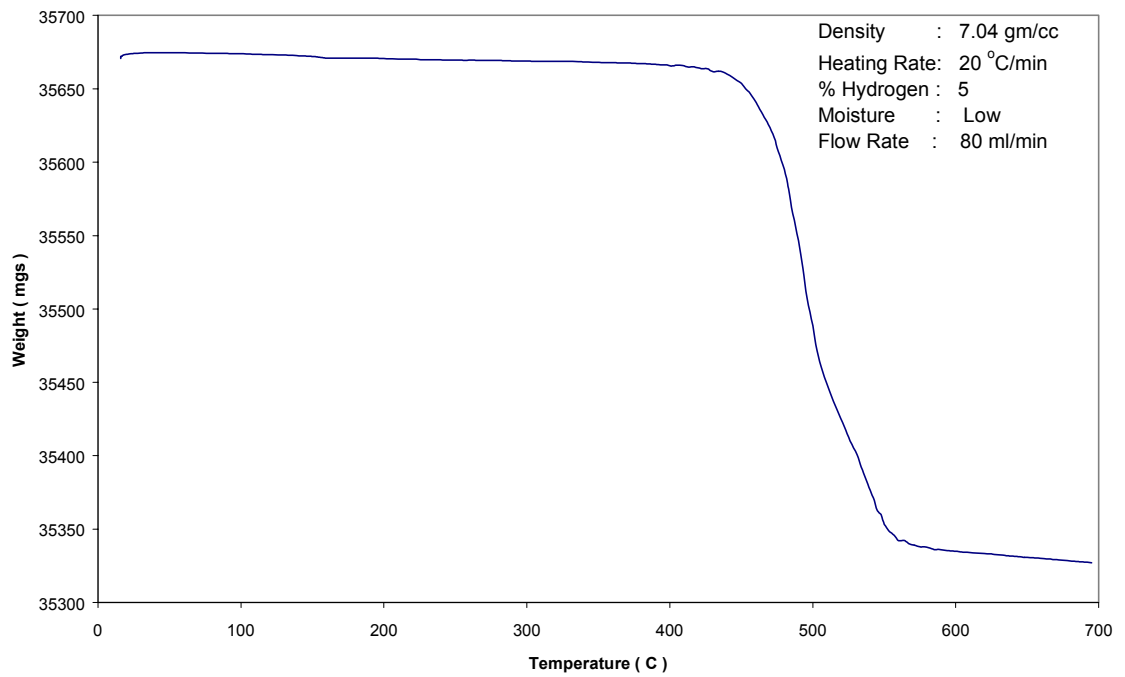
12. *Taguchi Trial No: 4; Density 7.04 gm/cc*

Weight Loss Vs Temperature

Density   : 6.80 gm/cc
Heating Rate: 20 ^{o}C/min
% Hydrogen : 15
Moisture   :   High
Flow Rate   :   40 ml/min
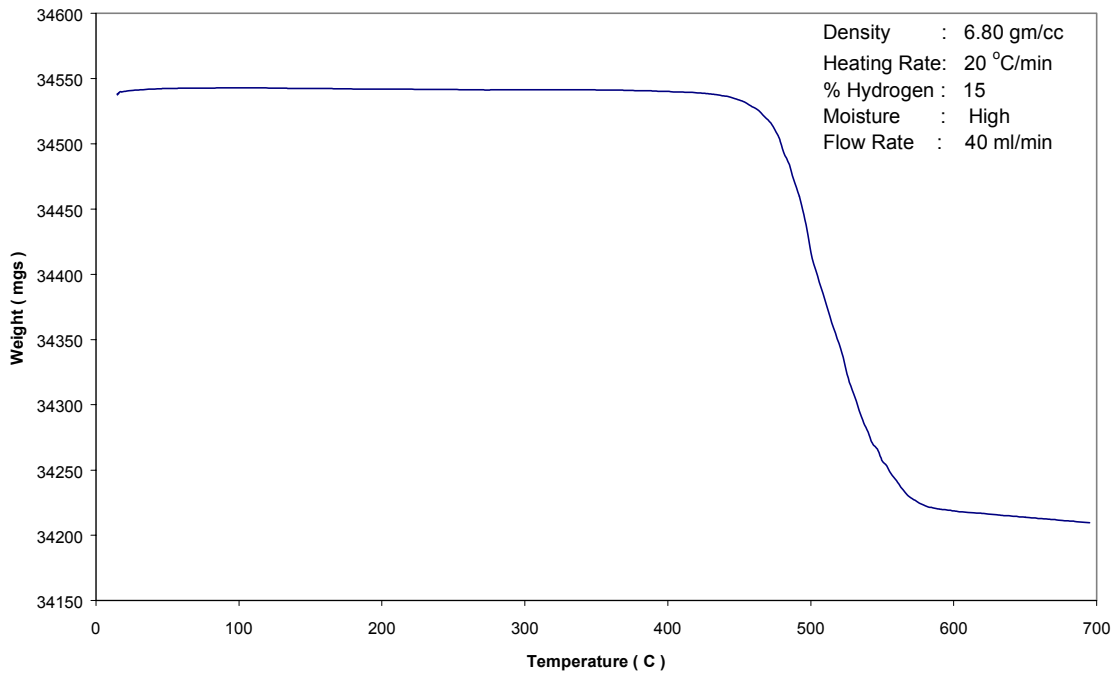
13. Taguchi Trial No: 5; Density 6.80 gm/cc

Weight Loss Vs Temperature

Density   : 6.95 gm/cc
Heating Rate: 20 ^{o}C/min
% Hydrogen : 15
Moisture   :   High
Flow Rate   :   40 ml/min
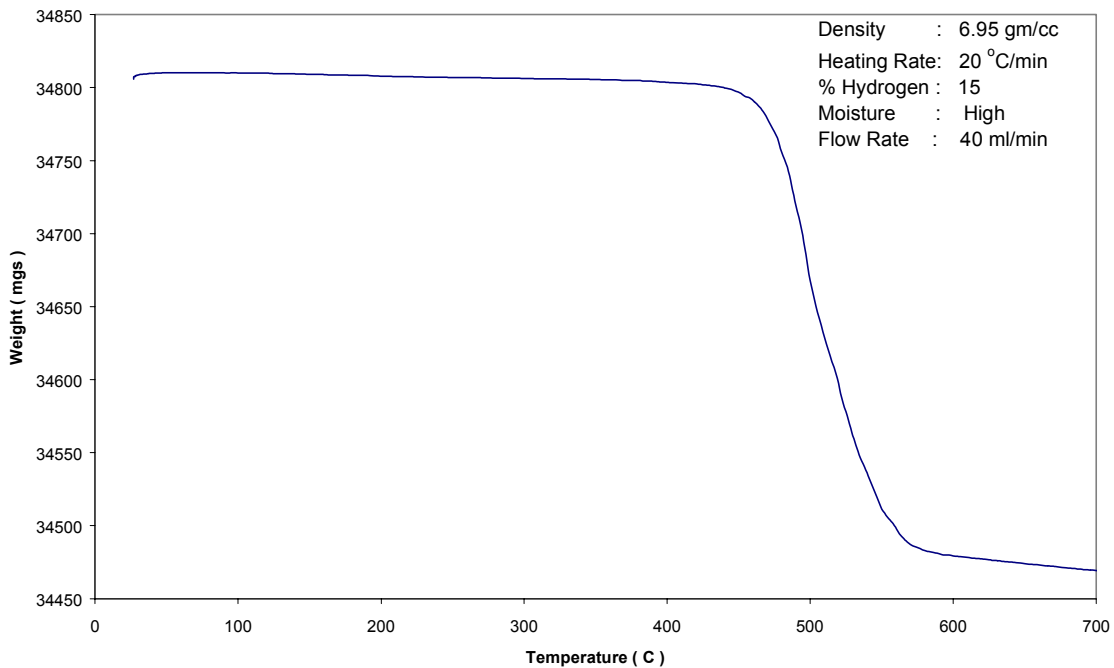
14. Taguchi Trial No: 5; Density 6.95 gm/cc

Weight Loss Vs Temperature

Density : 7.04 gm/cc
Heating Rate : 20 °C/min
% Hydrogen : 15
Moisture : High
Flow Rate : 40 ml/min
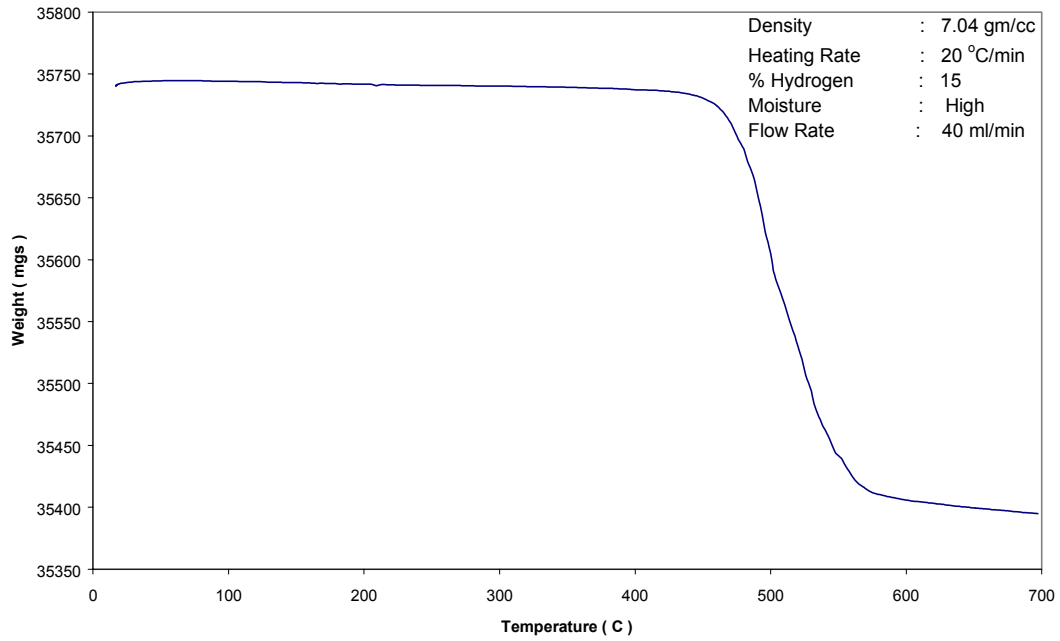
15. *Taguchi Trial No: 5; Density 7.04 gm/cc*

Weight Loss Vs Temperature

Density : 6.80 gm/cc
Heating Rate : 20 °C/min
% Hydrogen : 30
Moisture : Nil
Flow Rate : 60 ml/min
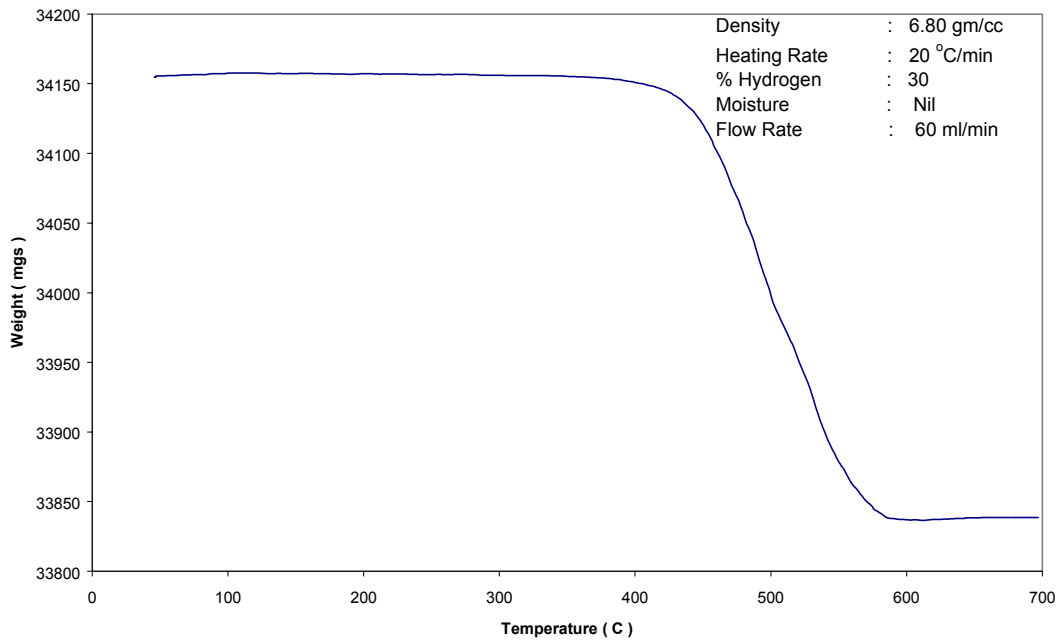
16. *Taguchi Trial No:6; Density 6.80 gm/cc*

Weight Loss Vs Temperature

Density	:	6.95 gm/cc
Heating Rate:		20 °C/min
% Hydrogen :		30
Moisture	:	Nil
Flow Rate	:	60 ml/min
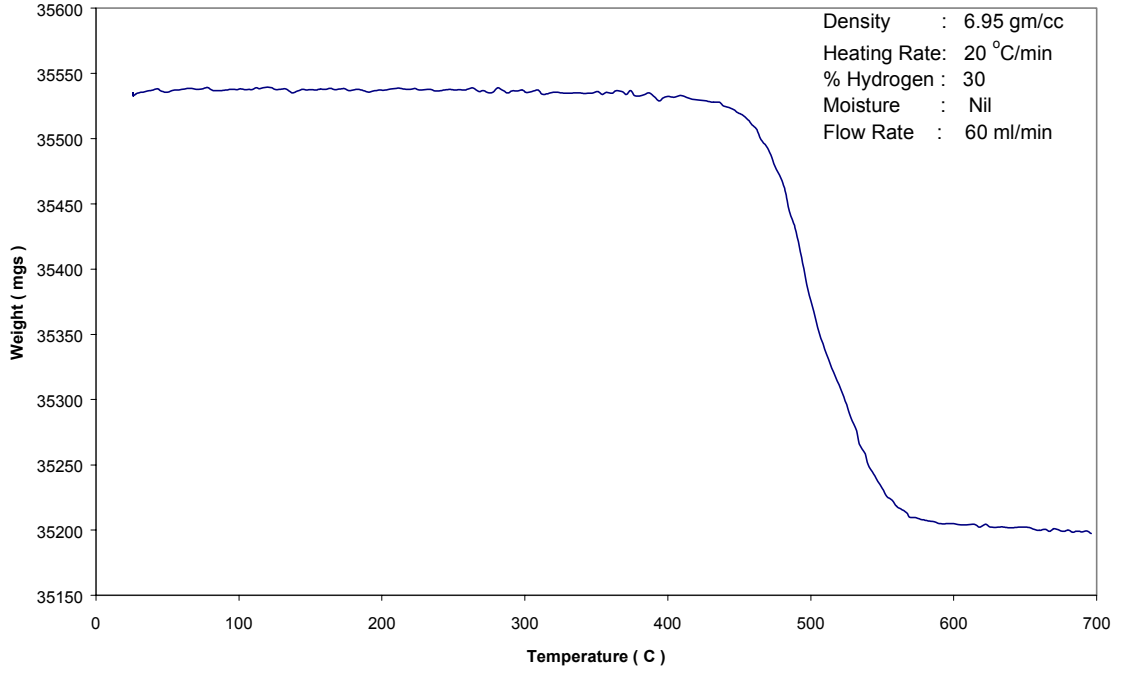
17. *Taguchi Trial No: 6; Density 6.95 gm/cc*

Weight Loss Vs Temperature

Density	:	7.04 gm/cc
Heating Rate	:	20 °C/min
% Hydrogen	:	30
Moisture	:	Nil
Flow Rate	:	60 ml/min
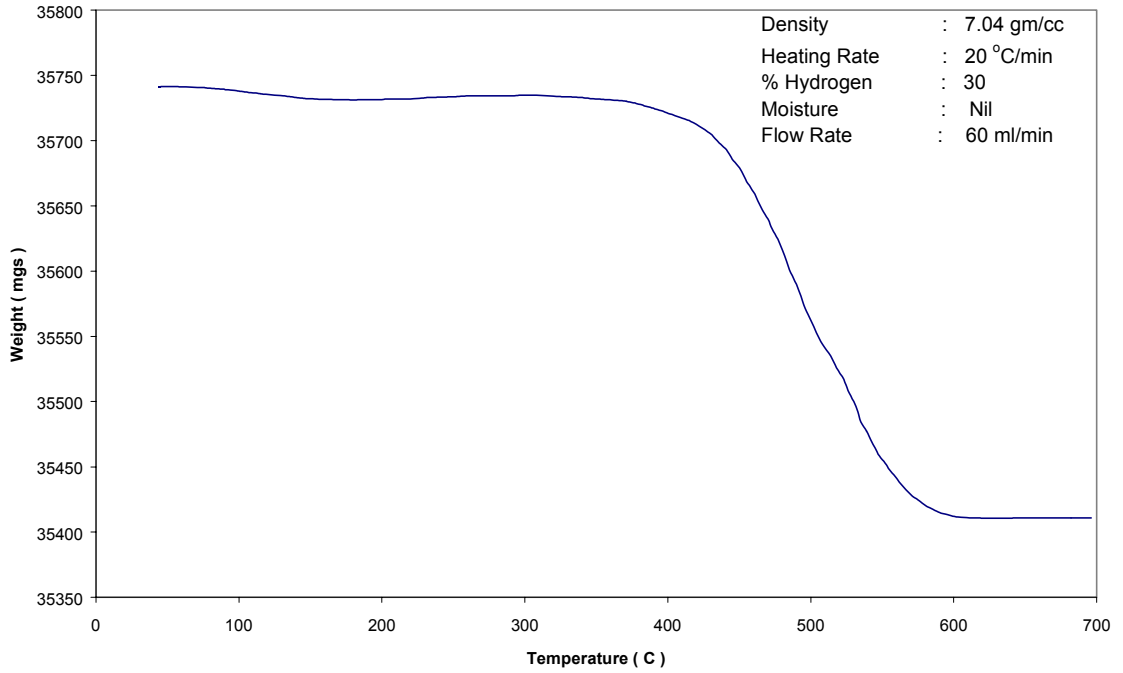
18. *Taguchi Trial No: 6; Density 7.04 gm/cc*

Weight Loss Vs Temperature

Density   :   6.95 gm/cc
Heating Rate: 30 °C/min
% Hydrogen : 5
Moisture   :   High
Flow Rate   :   60 ml/min
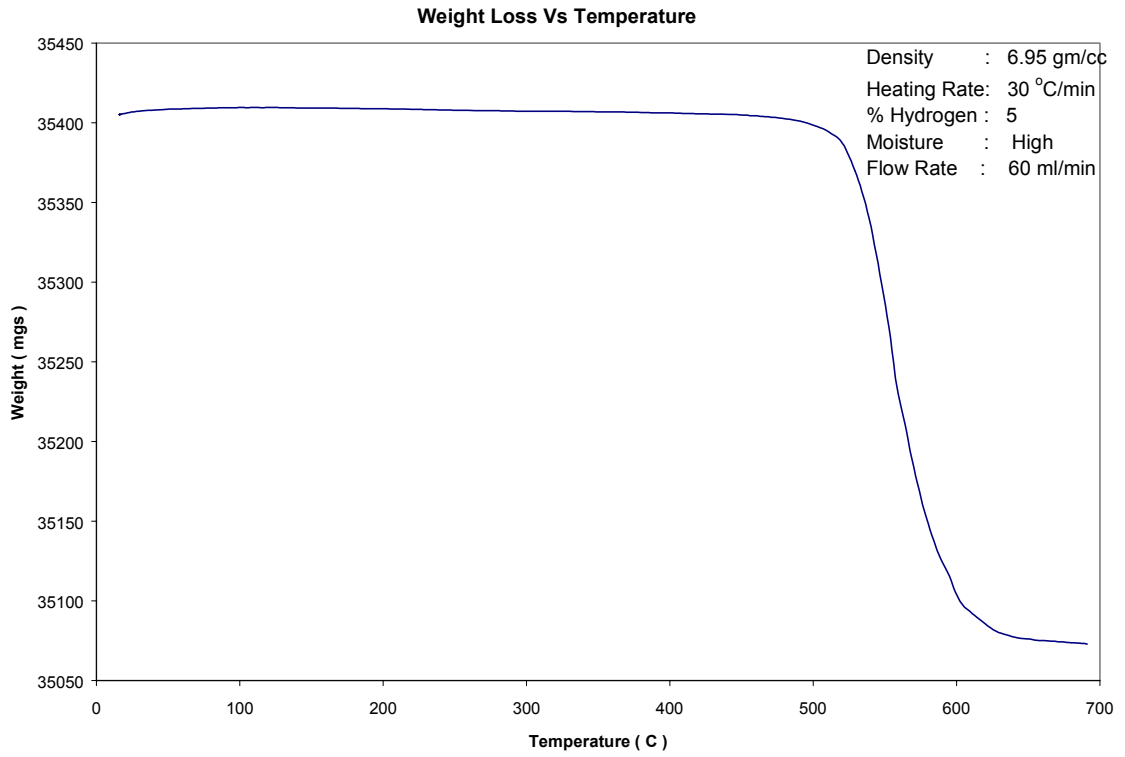
19. *Taguchi Trial No: 7; Density 6.80 gm/cc*

Weight Loss Vs Temperature

Density   :   6.80 gm/cc
Heating Rate: 30 °C/min
% Hydrogen : 5
Moisture   :   High
Flow Rate   :   60 ml/min
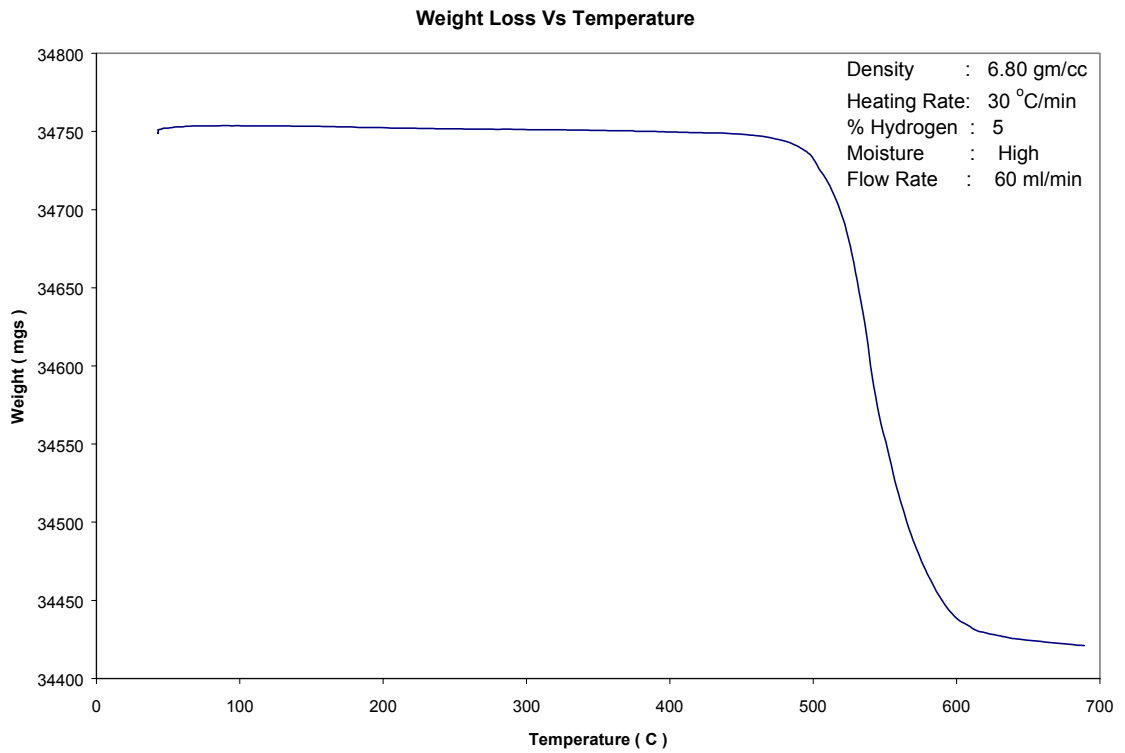
20. *Taguchi Trial No: 7; Density 6.95 gm/cc*

Weight Loss Vs Temperature

Density : 7.04 gm/cc
Heating Rate : 30 ^{o}C/min
% Hydrogen : 5
Moisture : High
Flow Rate : 60 ml/min
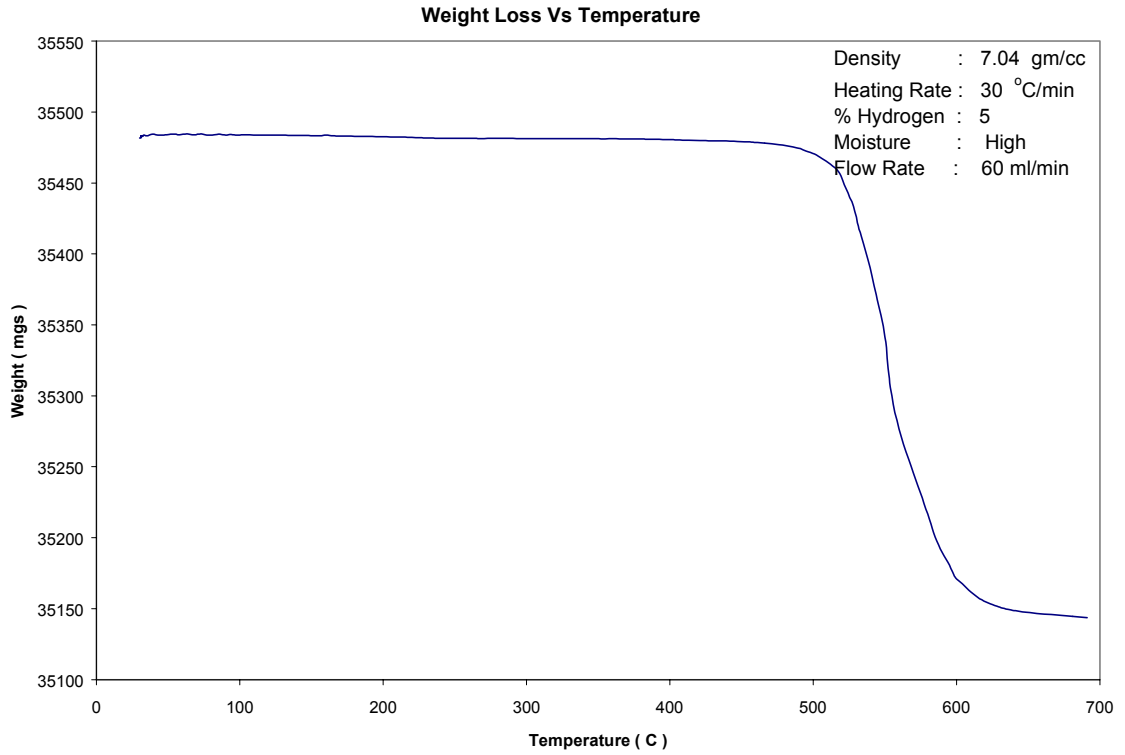
21. *Taguchi Trial No: 7; Density 7.04 gm/cc*

Weight Loss Vs Temperature

Density : 6.80 gm/cc
Heating Rate: 30 ^{o}C/min
% Hydrogen : 15
Moisture : Nil
Flow Rate : 80 ml/min
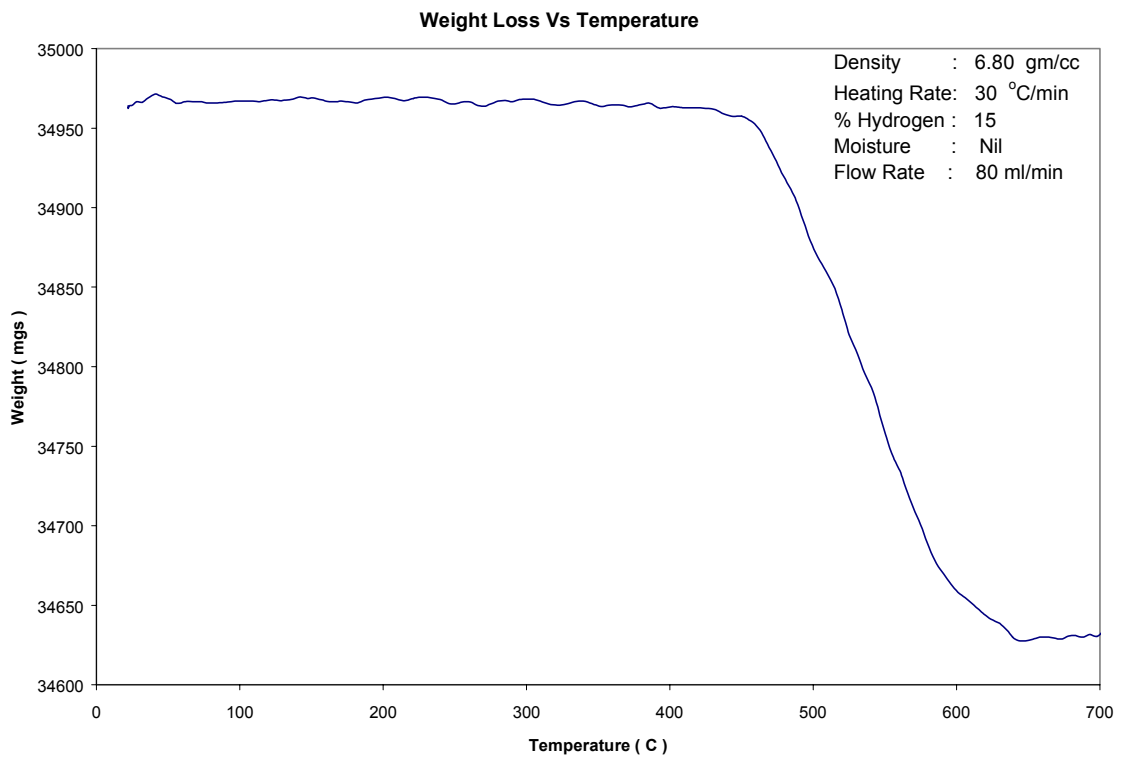
22. *Taguchi Trial No: 8; Density 6.80 gm/cc*

Weight Loss Vs Temperature

Density	: 6.95 gm/cc
Heating Rate	: 30 °C/min
% Hydrogen	: 15
Moisture	: Nil
Flow Rate	: 80 ml/min
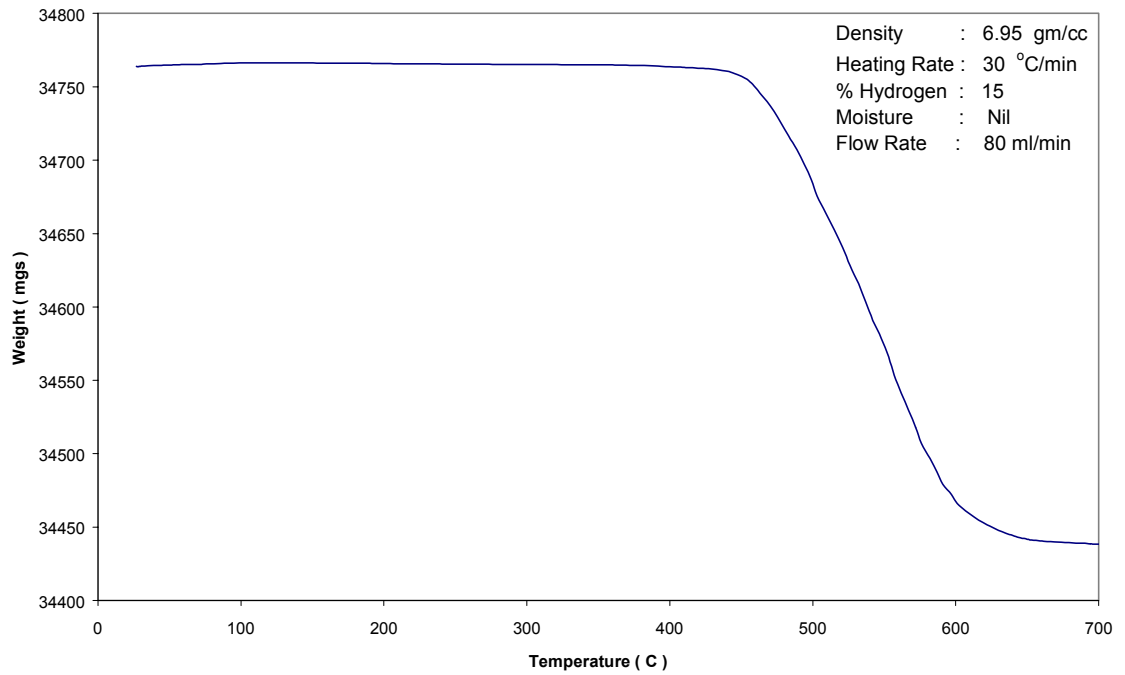
23. *Taguchi Trial No: 8; Density 6.95 gm/cc*

Weight Loss Vs Temperature

Density	: 7.04 gm/cc
Heating Rate	: 30 °C/min
% Hydrogen	: 15
Moisture	: Nil
Flow Rate	: 80 ml/min
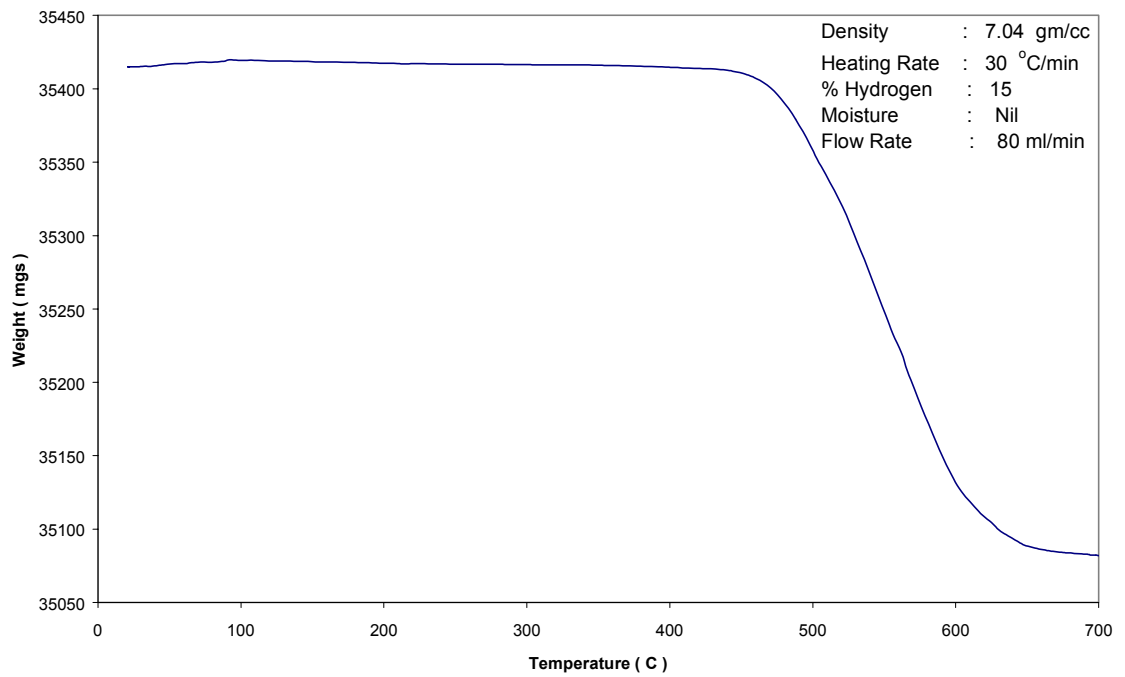
24. *Taguchi Trial No: 8; Density 7.04 gm/cc*

Weight Loss Vs Temperature

Density   : 6.80 gm/cc
Heating Rate : 30 °C/min
% Hydrogen   : 30
Moisture   : Low
Flow Rate   : 40 ml/min
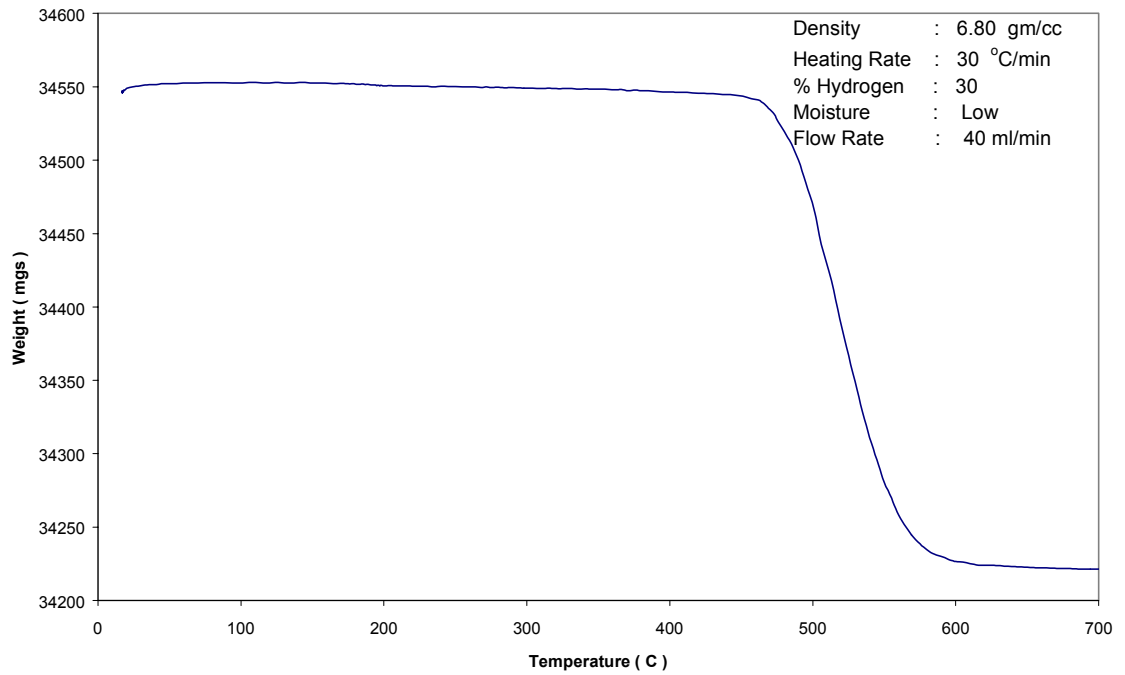
25.Taghuchi trial No 9; Density 6.95 gm/cc

Weight Loss Vs Temperature

Density   : 6.95 gm/cc
Heating Rate : 30 °C/min
% Hydrogen   : 30
Moisture   : Low
Flow Rate   : 40 ml/min

26. Taguchi Trial No:9; Density 6.95 gm/cc

Weight Loss Vs Temperature
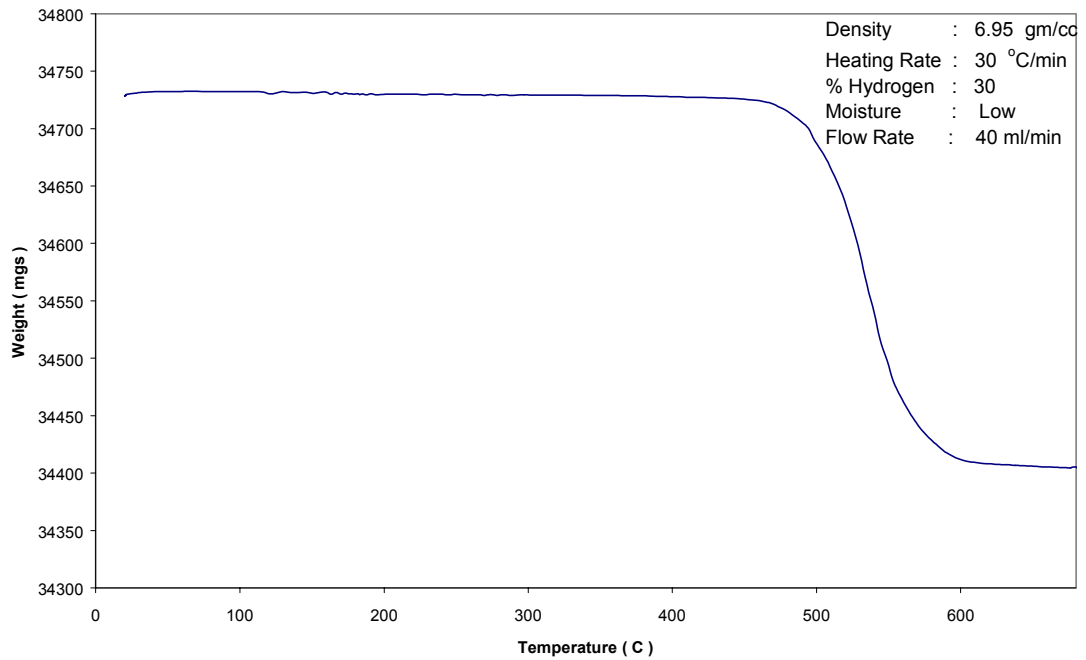
Density   : 7.04 gm/cc
Heating Rate : 30 ^{o}C/min
% Hydrogen : 30
Moisture   : Low
Flow Rate   : 40 ml/min
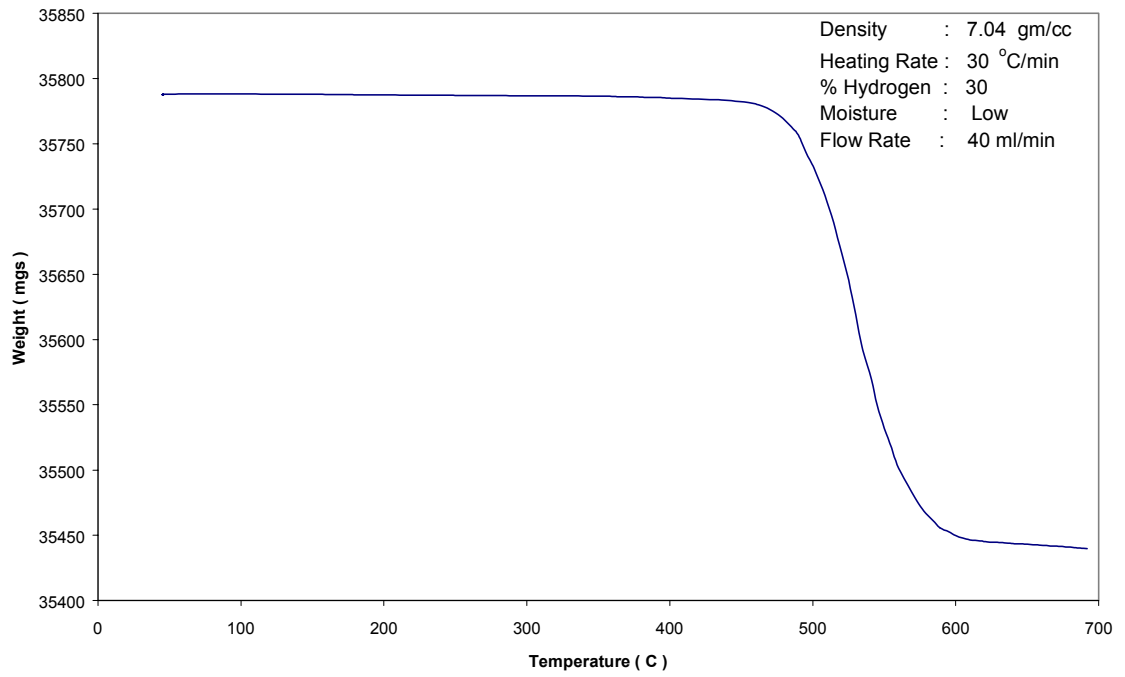
27. *Taguchi Trial No: 9; Density 7.04 gm/cc*

APPENDIX C: <u>WORKING PRINCIPLE OF FTIR</u>

FTIR or Fourier Transform Infrared Spectroscopy is an instrument used to obtain an infrared spectrum when infrared light passed through a sample. Most *dispersive* instruments use a *monochromator* to split light into a spectrum of its component wave number. A slit is used to select a narrow slice of wave numbers before it strikes the detector.
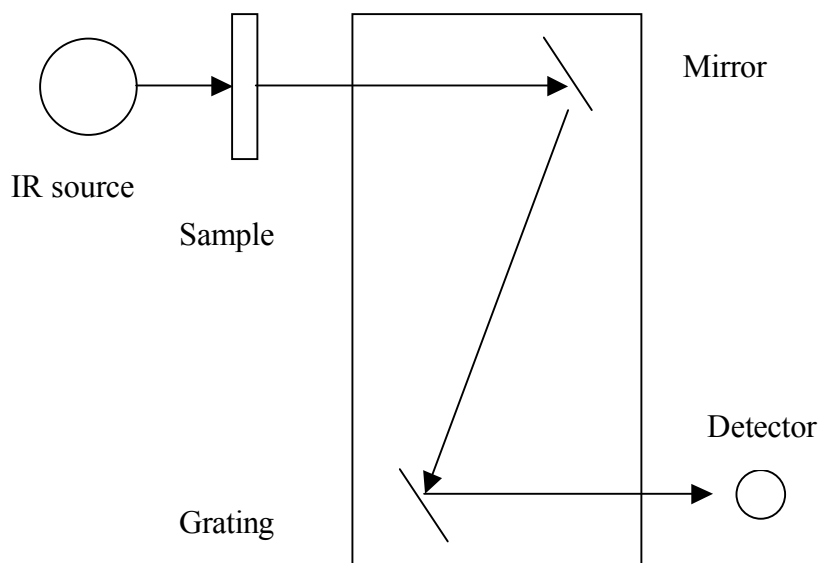
Figure C-1: Schematic of a dispersive grating infrared spectrometer

In FTIR all of the infrared radiation passes and through the sample. There are on restrictions on the wave number range that strikes the sample. The complete range of wave numbers used provides a *multiplex (or Fellgett) advantage*. It is based on fact that in an FTIR, all the wave numbers of the light are detected at once, whereas in a dispersive instrument only a small wave number range at a

time is measured. Thus, acquiring data for 10 minutes on an FTIR means all

wave numbers are observed for a full 10 minutes. In a dispersive spectrometer

each wave number is observed for only a short fraction of the 10-minute

measurement time. A schematic of a non-dispersive interferometer is shown in

Figure C-2.
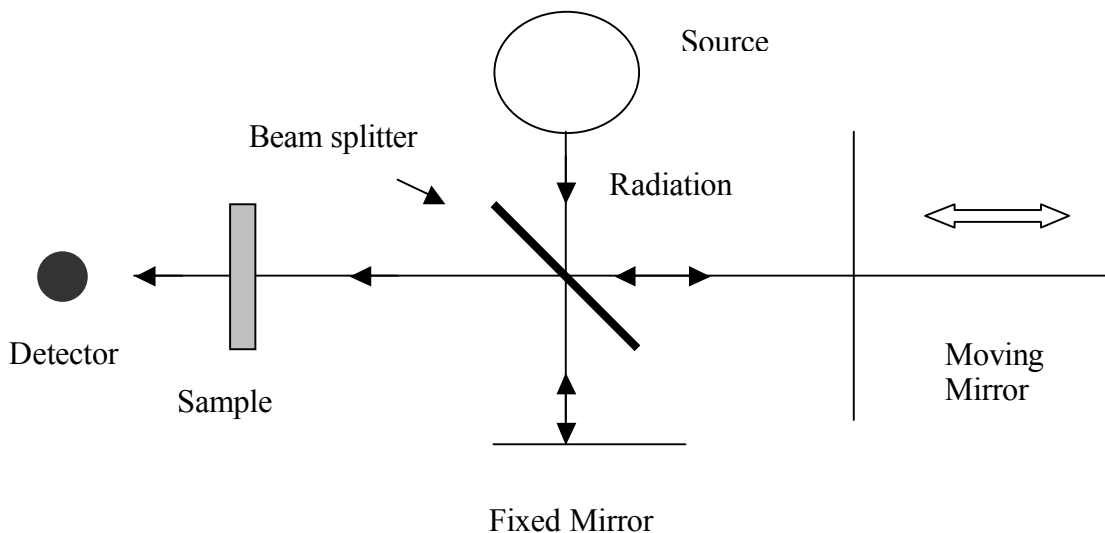
Figure C-2:   Schematic of a Michelson interferometer

The heart of most FTIRs in use today, based on the principles of Michelsons

interferometer. Light from the source, is split by the beam –splitter. One half of

the beam is transmitted to a fixed mirror and the other strikes a moving mirror.

After reflection for the respective mirrors, the two beams recombine at the beam

splitter, to interact with the sample. If the moving mirror and the fixed mirror are

at the same distance from the beam splitter, the distance traveled by the light are

the same. This condition is called as *zero path difference* (ZPD). The

displacement of the moving mirror from the ZPD (called mirror displacement (Δ)),

leads to the light traveling an extra distance. This distance is called the *optical*

path difference (δ). The relationship between mirror displacement and optical

path difference is shown in equation 1.

$$\delta \quad = \quad 2\Delta \tag{1}$$

The presence of mirror displacement leads to the interference of light.

Constructive interference takes place when the optical path difference is an

integer multiple of λ. Destructive interference occurs when the optical path

difference is $\frac{1}{2}\lambda$ or some multiple of it.

Constructive Interference: $\quad \delta \quad = \quad n\lambda \tag{2}$

Destructive Interference: $\quad \delta \quad = \quad (n + \frac{1}{2})\lambda \tag{3}$

Where, n = 0,1,2,3,4,5,6,……………

Interference leads to a light intensity is bright (constructive) and very weak

(destructive), depending on the optical path difference. If the mirror is moved at a

constant speed, the intensity of light increases and decreases smoothly. The

variation in light intensity is measured by the detector as a sinusoidal wave. A

plot of the light intensity versus optical path difference is called a *interferogram.*

Figure 61 shows a typical interferogram obtained from a FTIR. An interferogram

Fourier Transform

Voltage

Optical path Difference (cm)

92
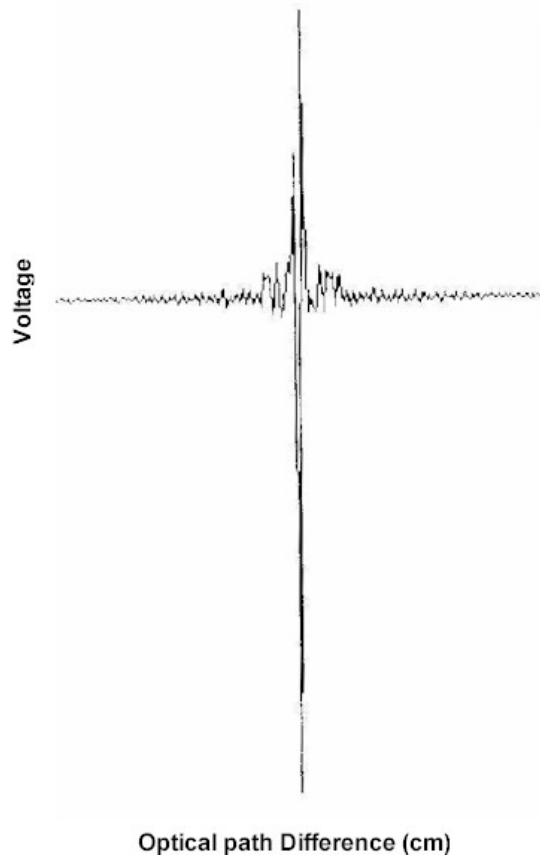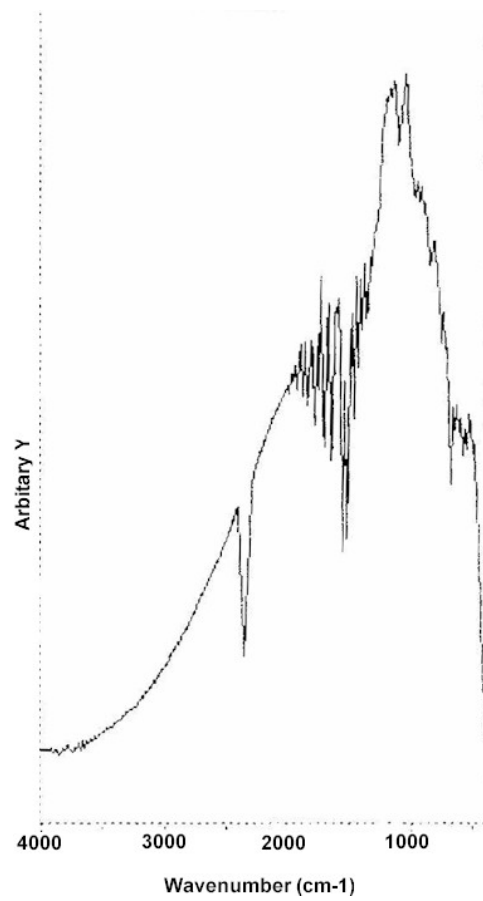
Figure C-3: Interferogram and the fourier transform

is essentially a large number of sinusoidal waves added together. According to

Fouriers theorm, any mathematical function (an x,y plot) can be expressed as a

sum of sinusoidal waves. Fourier transform calculate the infrared spectrum and

form the interferogram. Fourier tranfroms have their X units transformed. Thus,

Fourier transform inverts the interfrogram to produces an infrared spectrum.

APPENDIX D: SPECTRUMS OF EXPERIMENT A AND B

(Wave number in the X – axis Vs Absorbance in Y – axis)

Experiment A:

Background - A
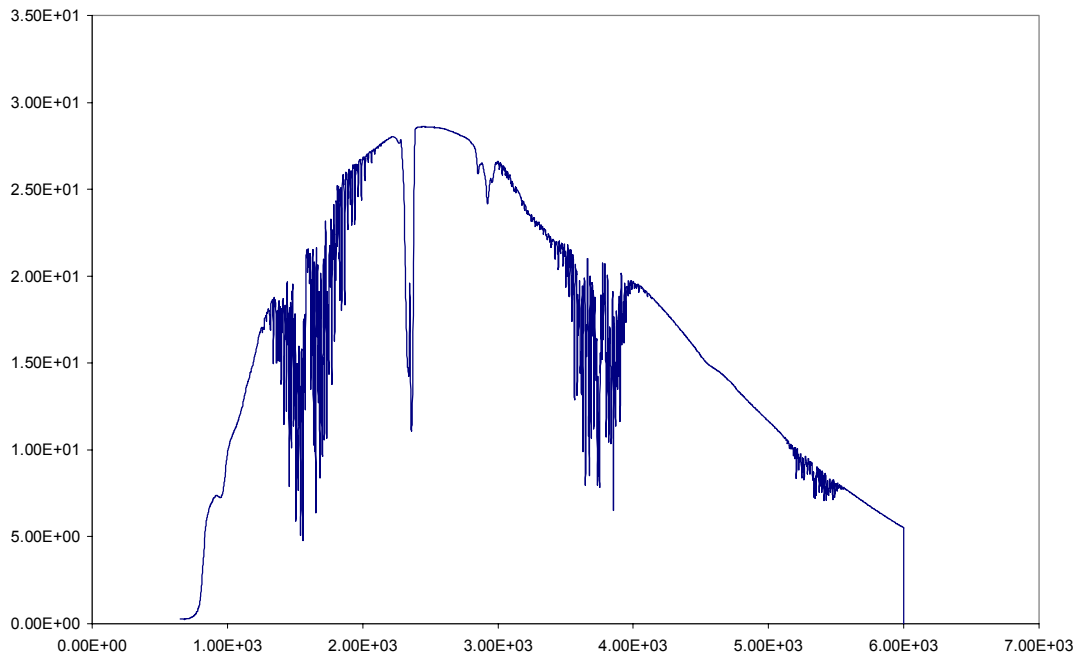
Spectra A-1
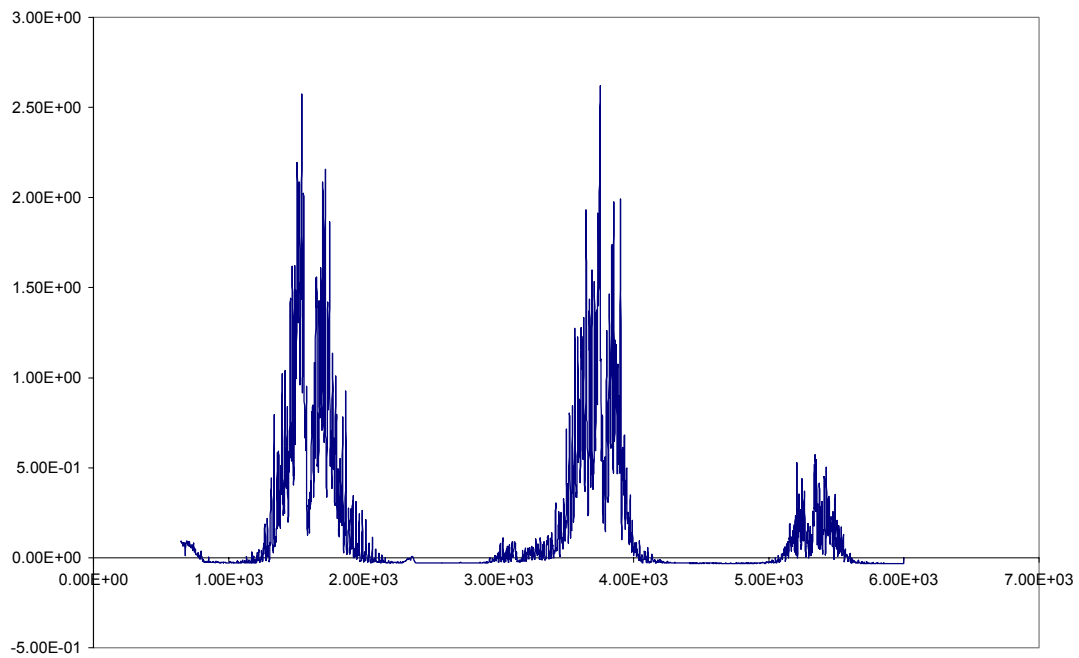
Spectra A-3
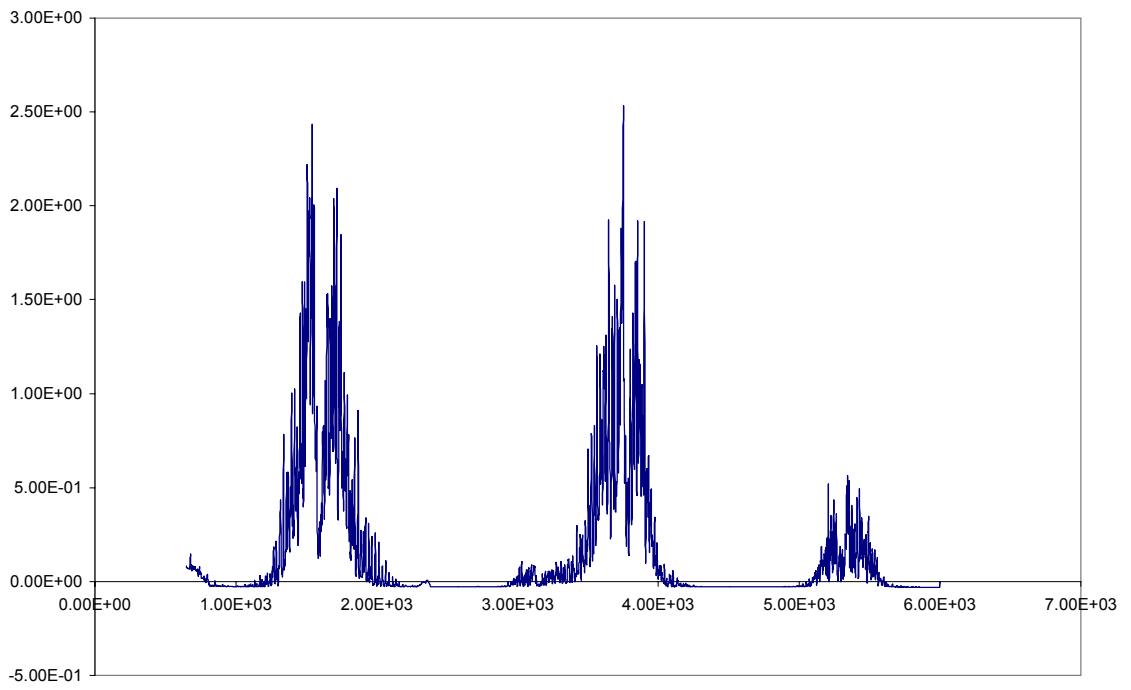
Spectra A-2
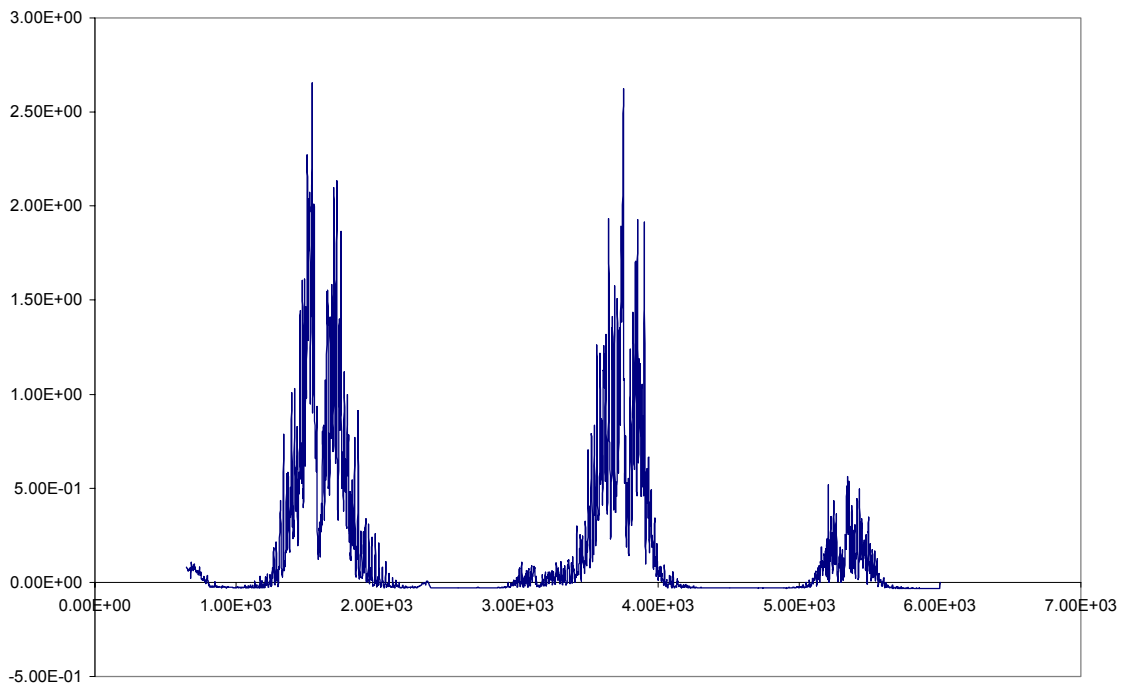
Spectra A-4
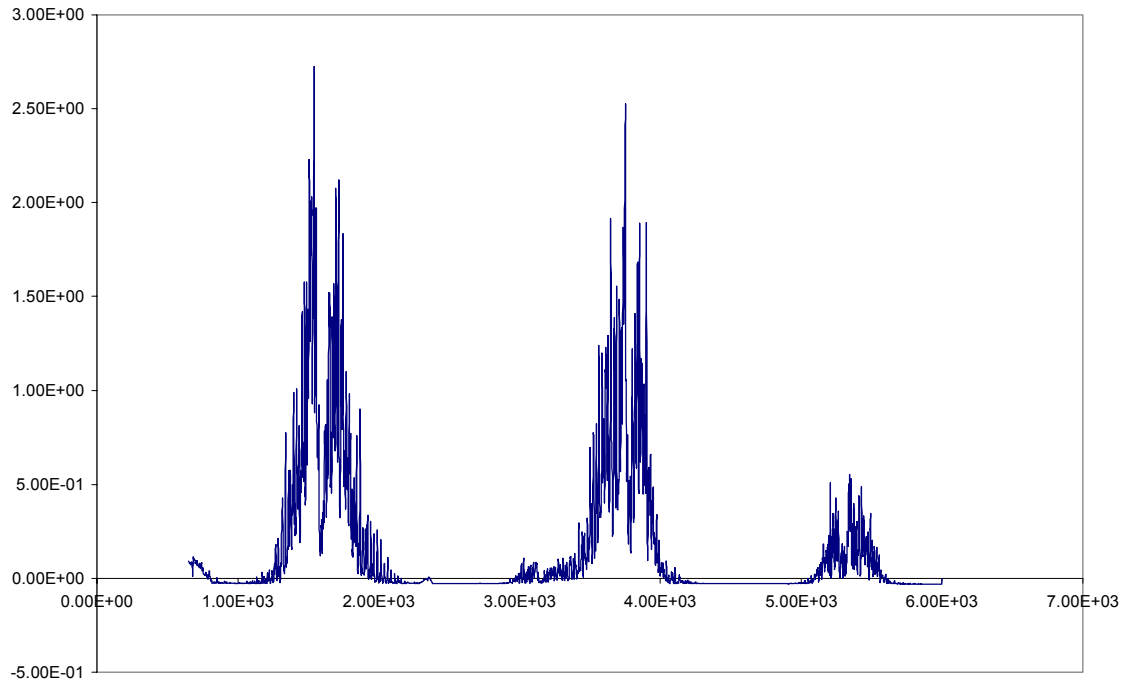
Spectra A-5
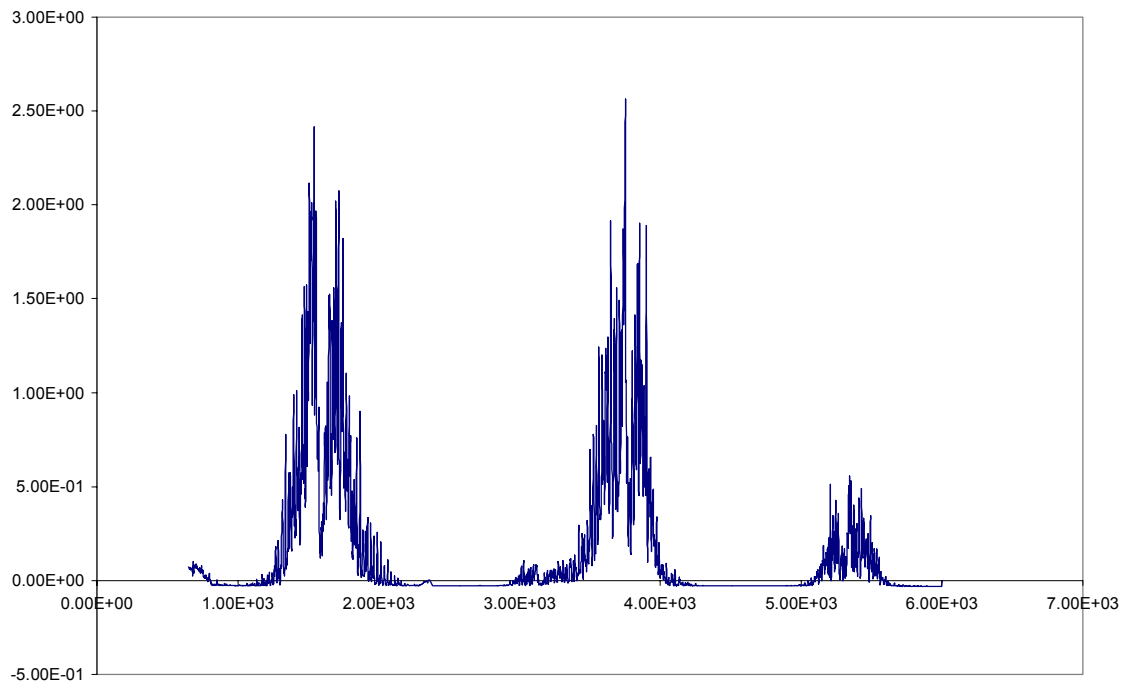
Spectra A-6
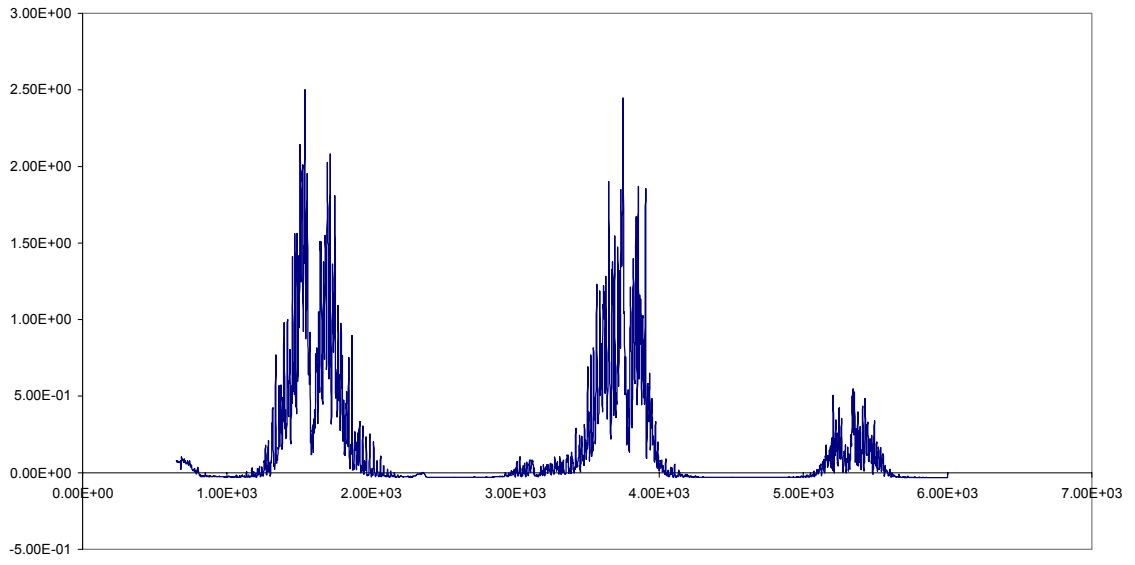
Spectra A-7
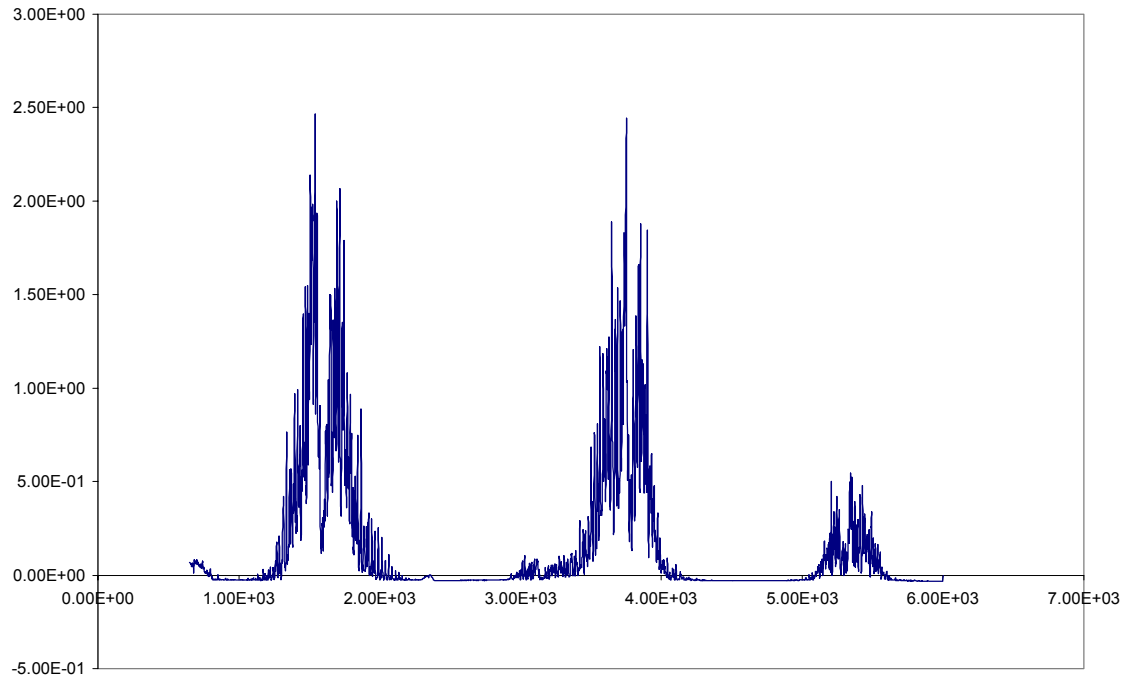
Spectra A-8
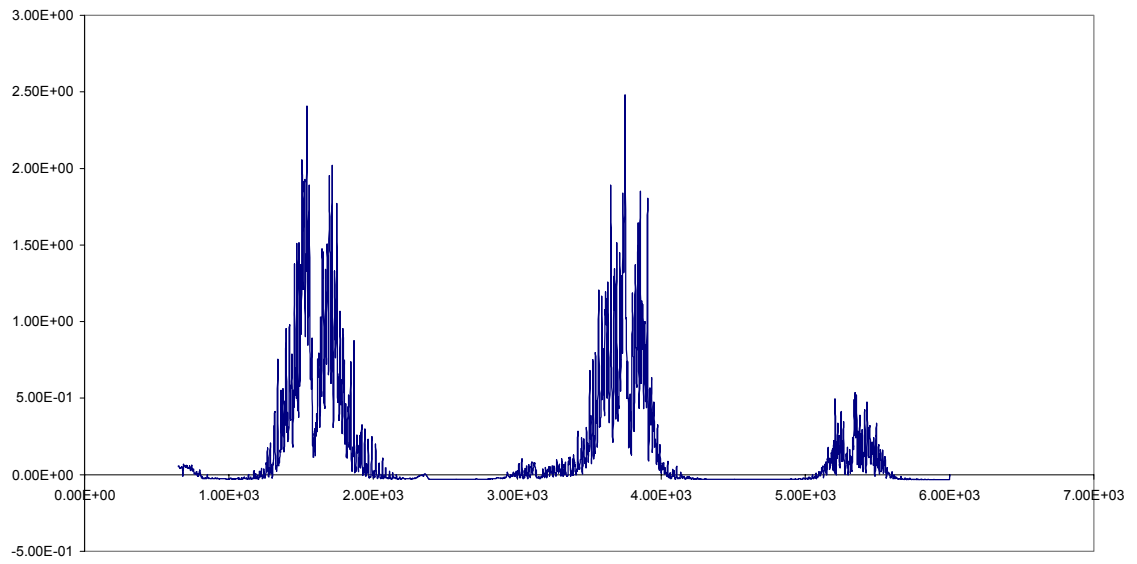
Spectra A-9
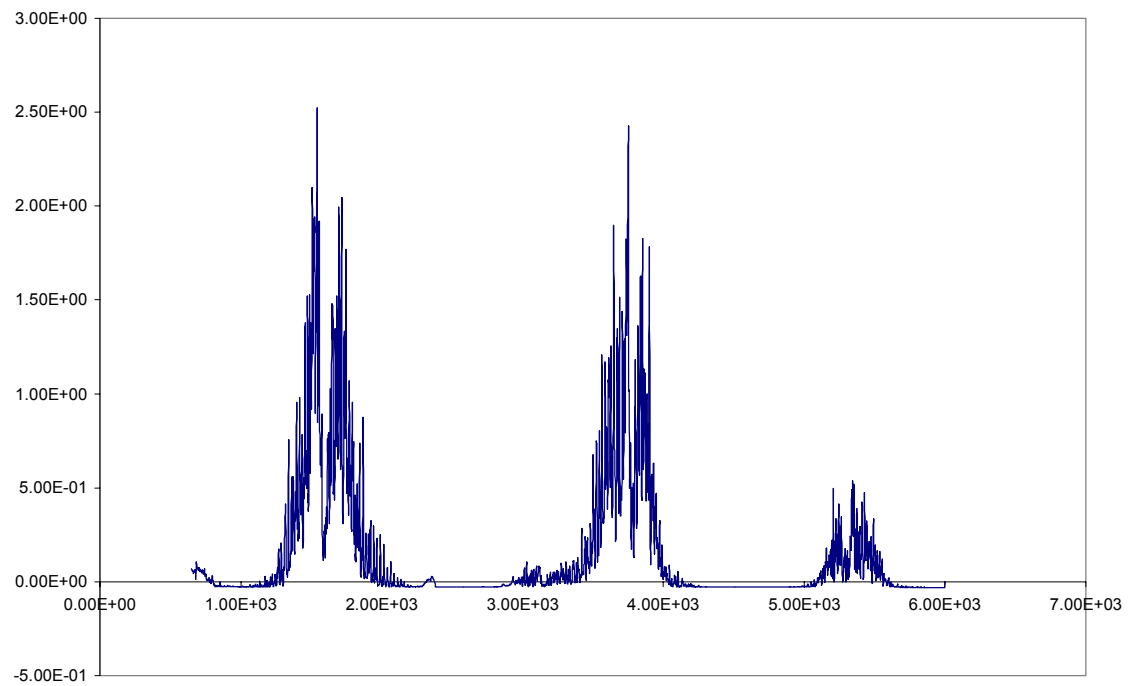
Spectra A-10

Spetra A-11

100
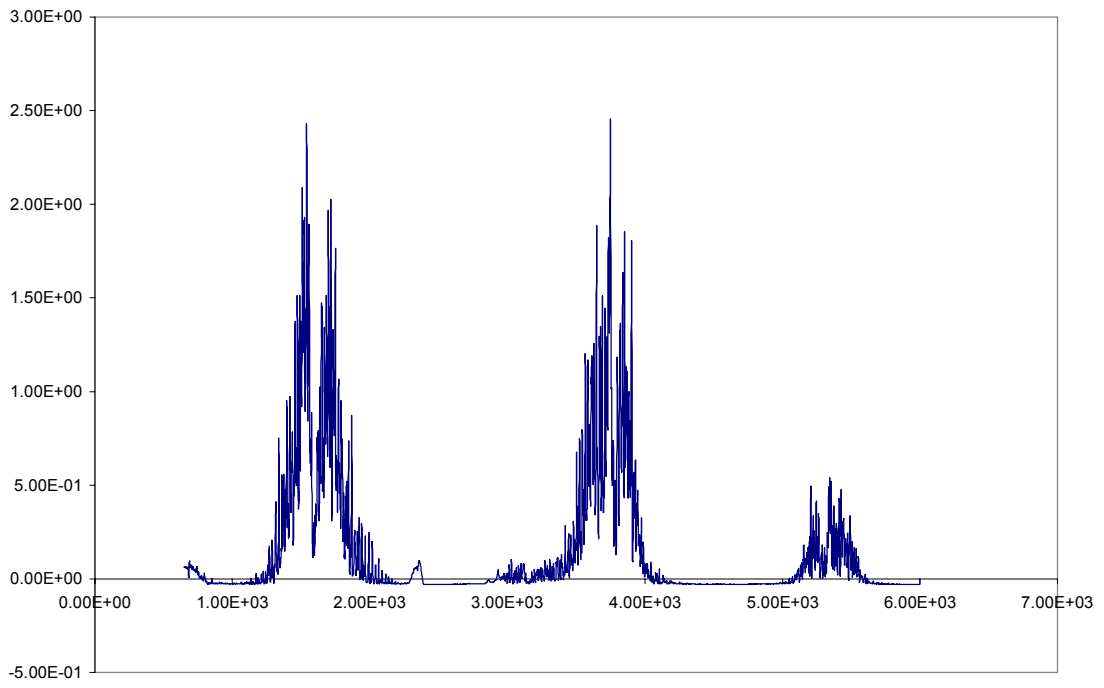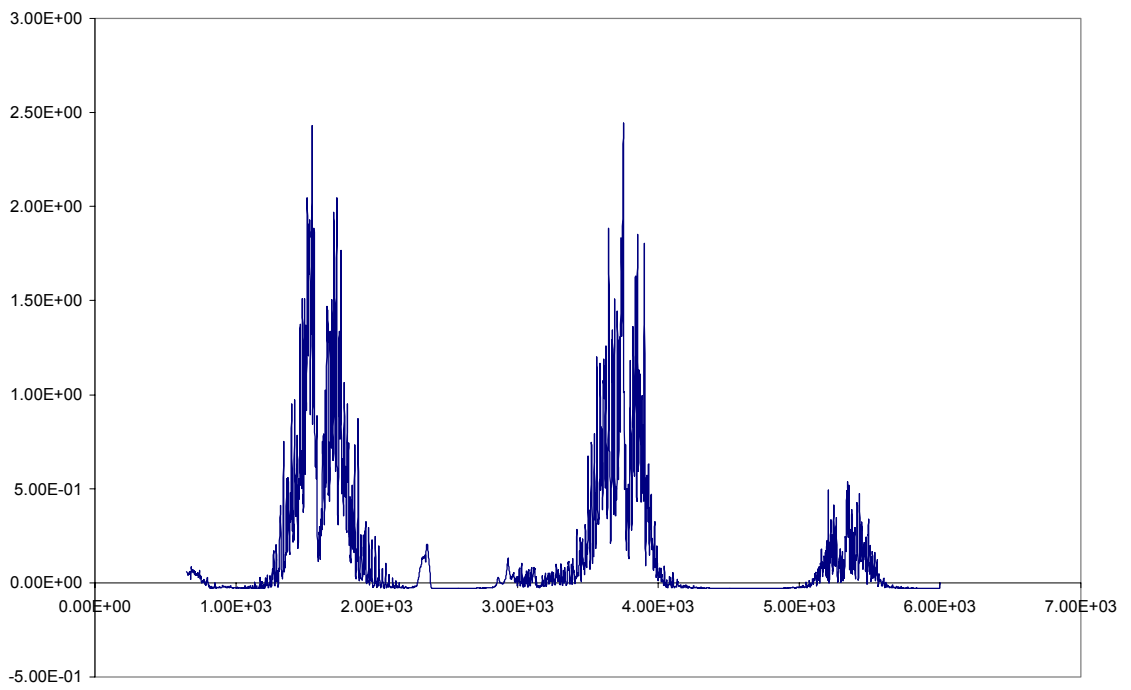
Spectra A-12

Spectra A-13

101
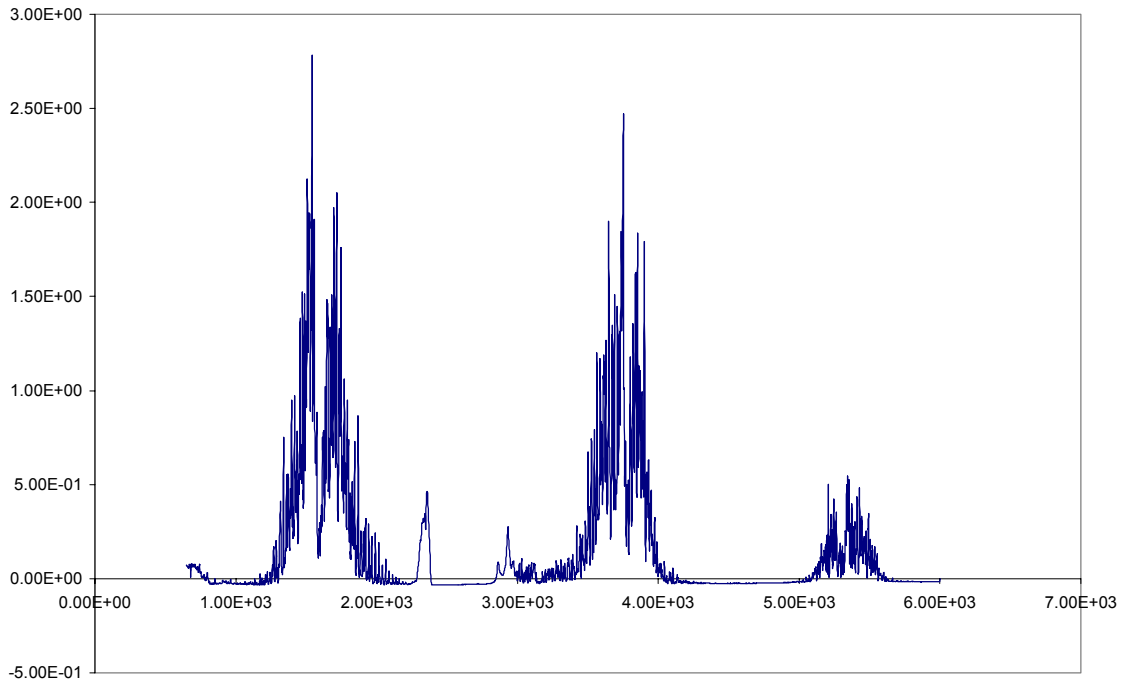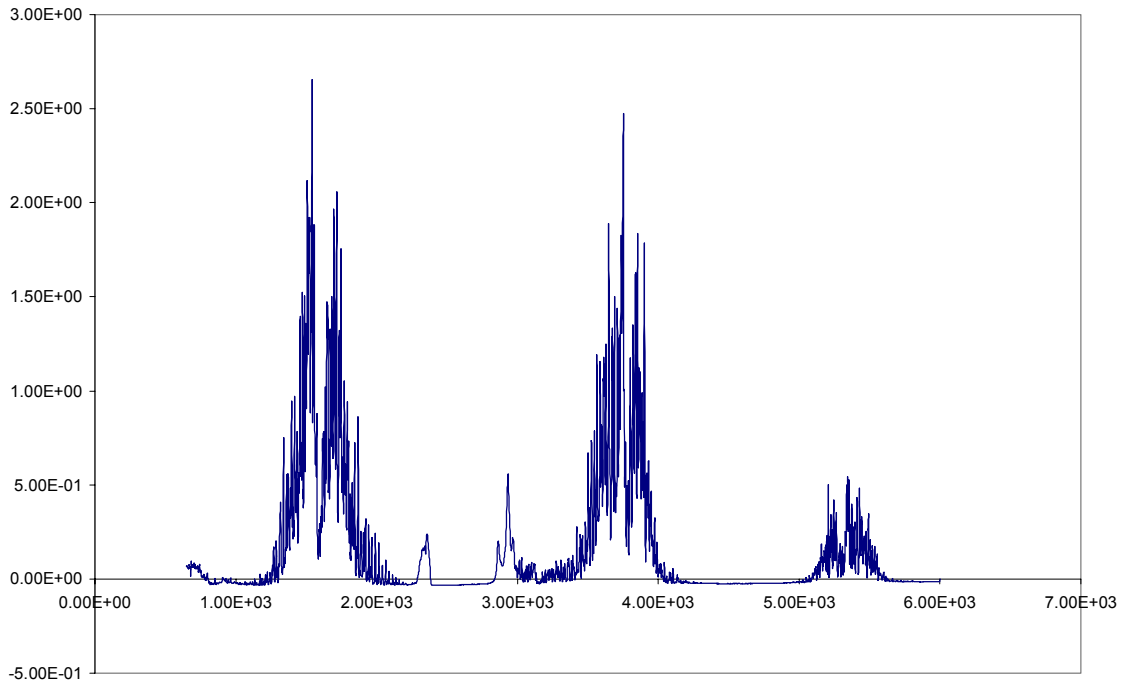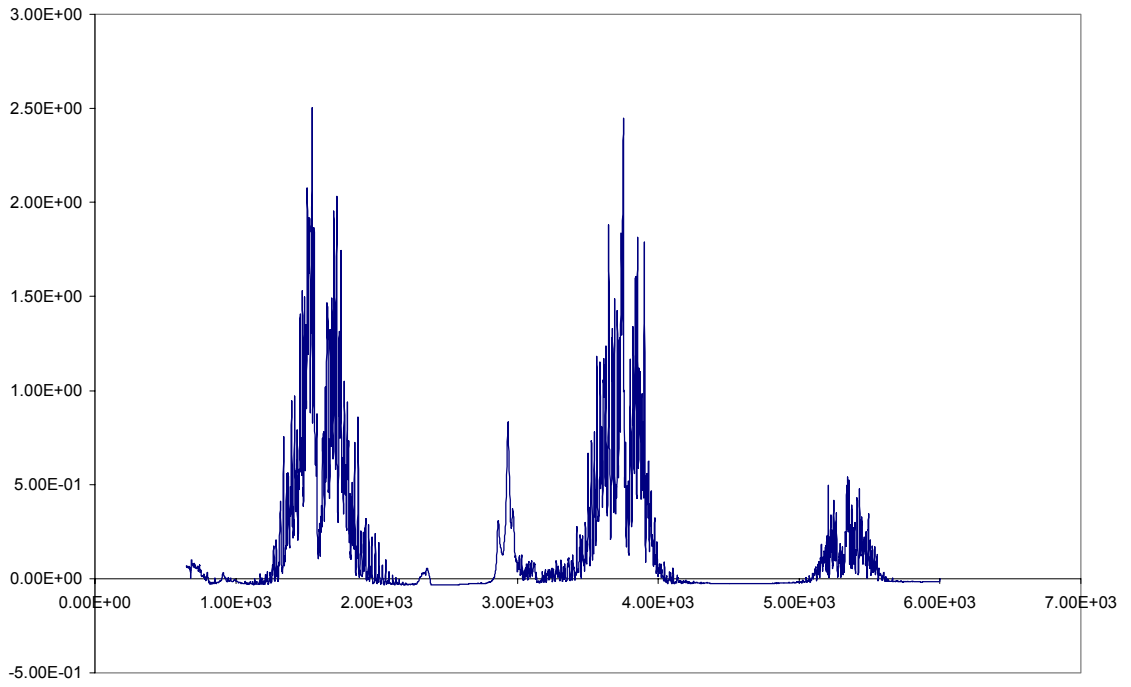
Spectra A-14

Spectra A-15
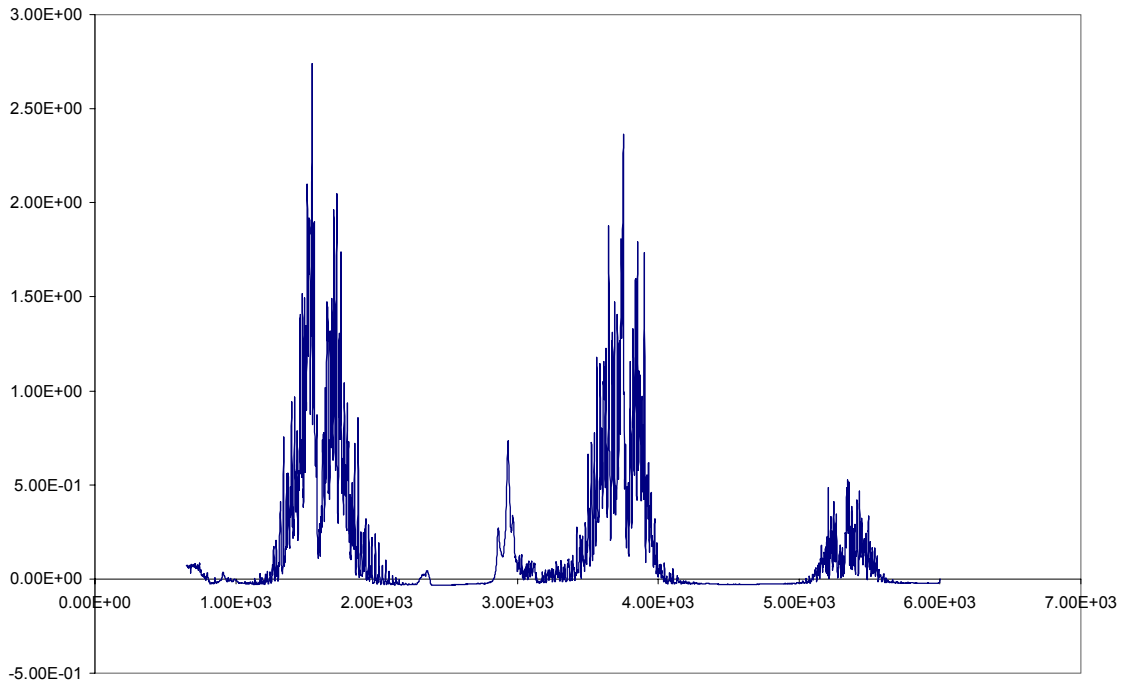
Spectra A-16

Spectra A-17

103
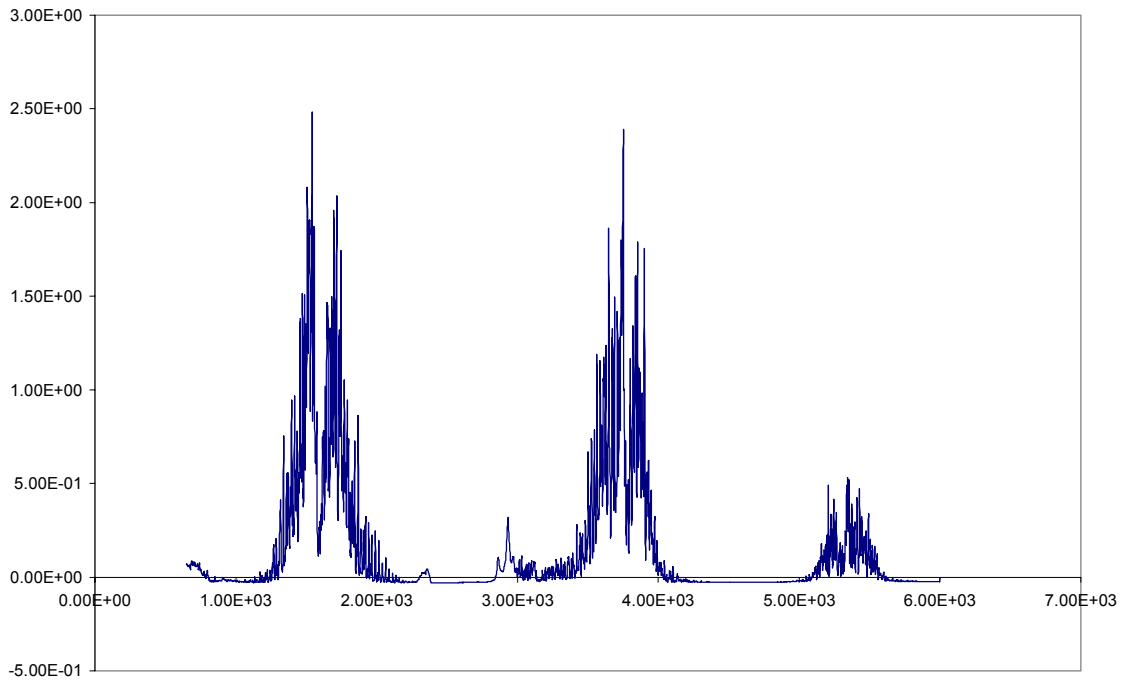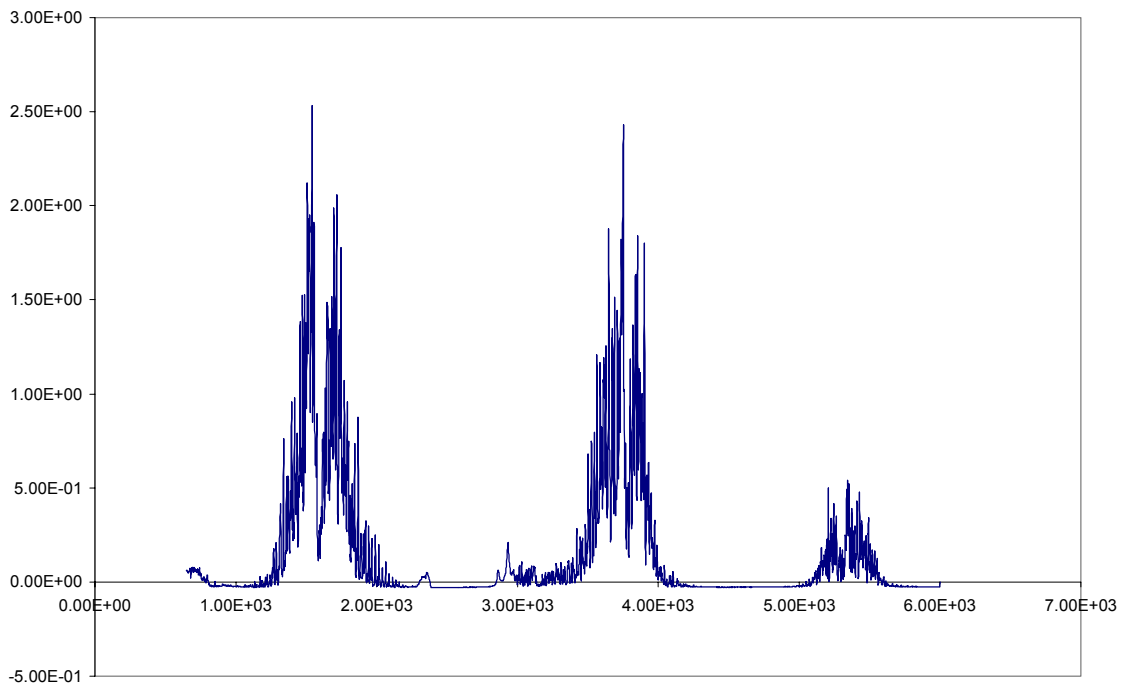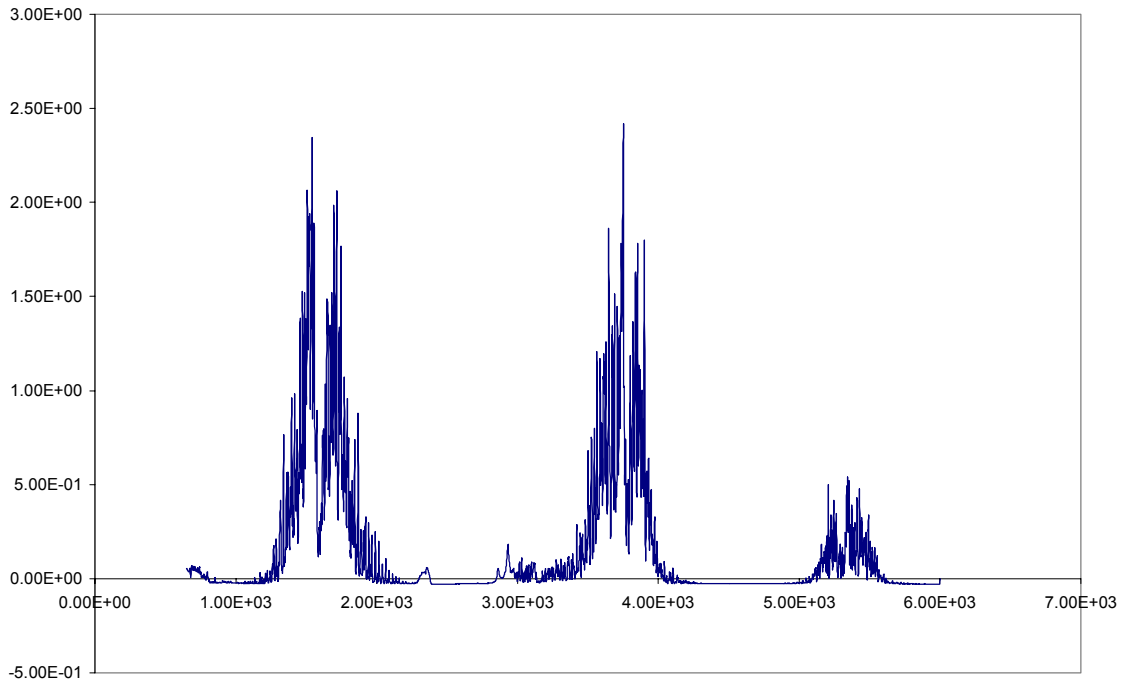
Spectra A-18

Spectra A-19
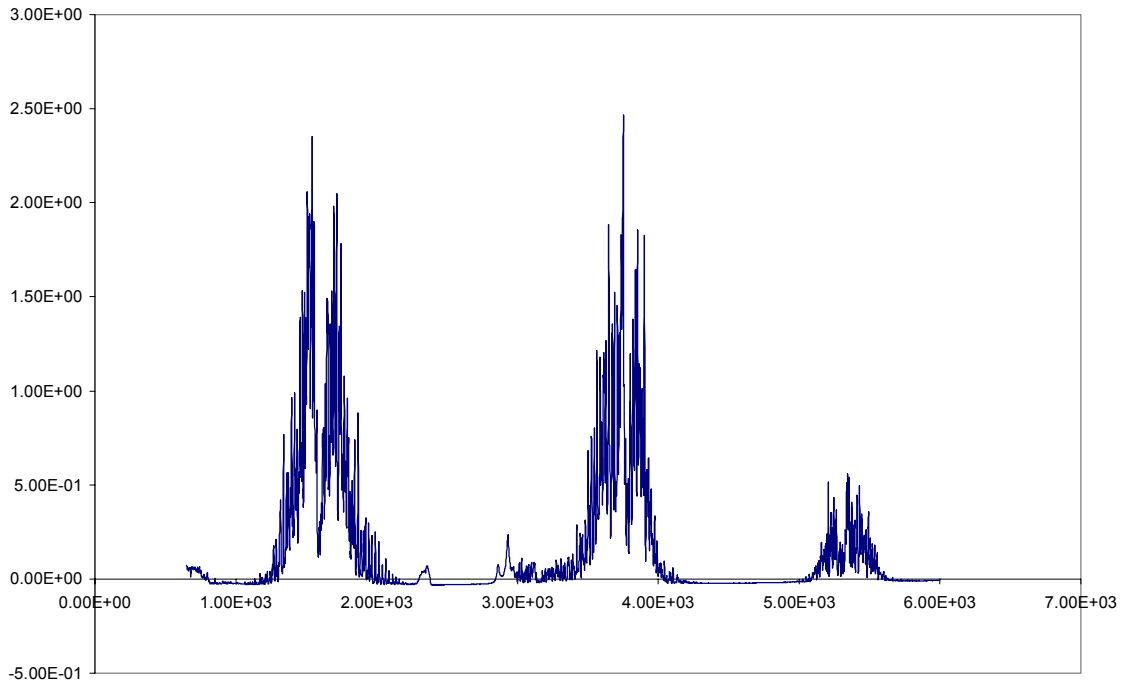
Experiment B:

Background - B
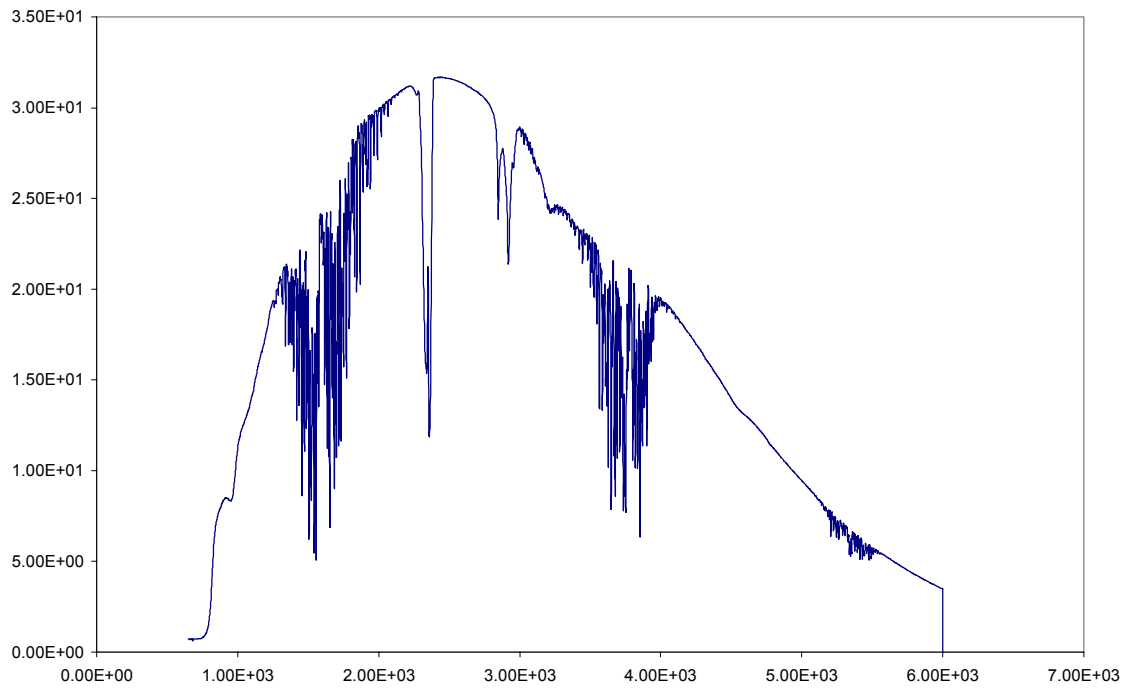
Specta B-1
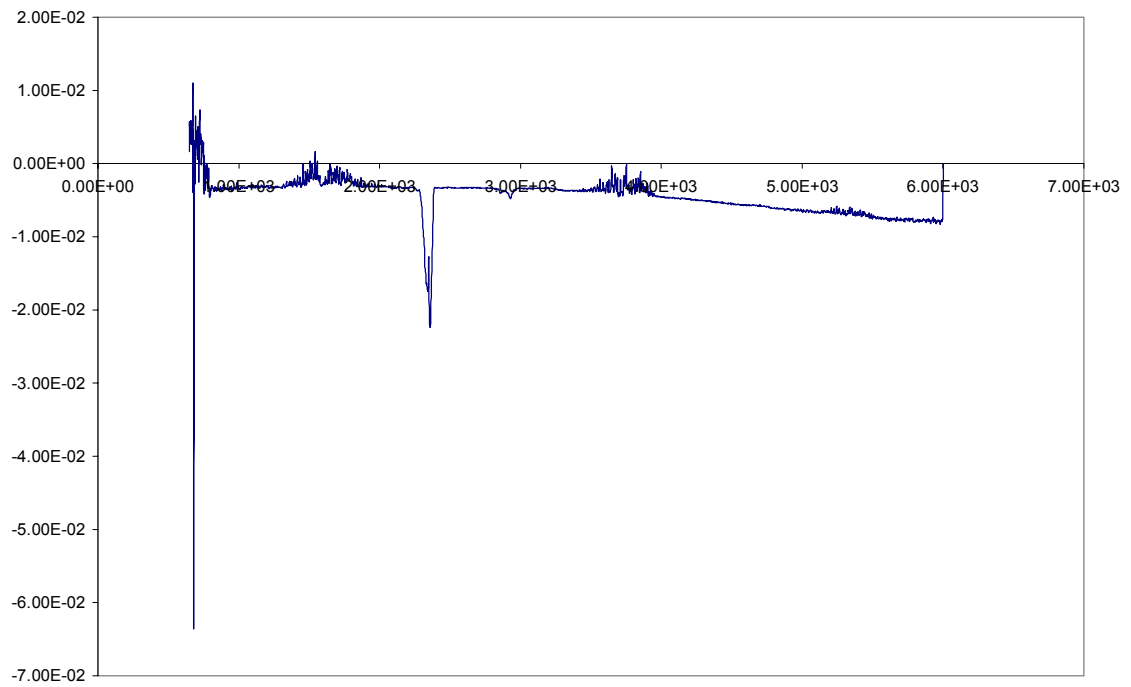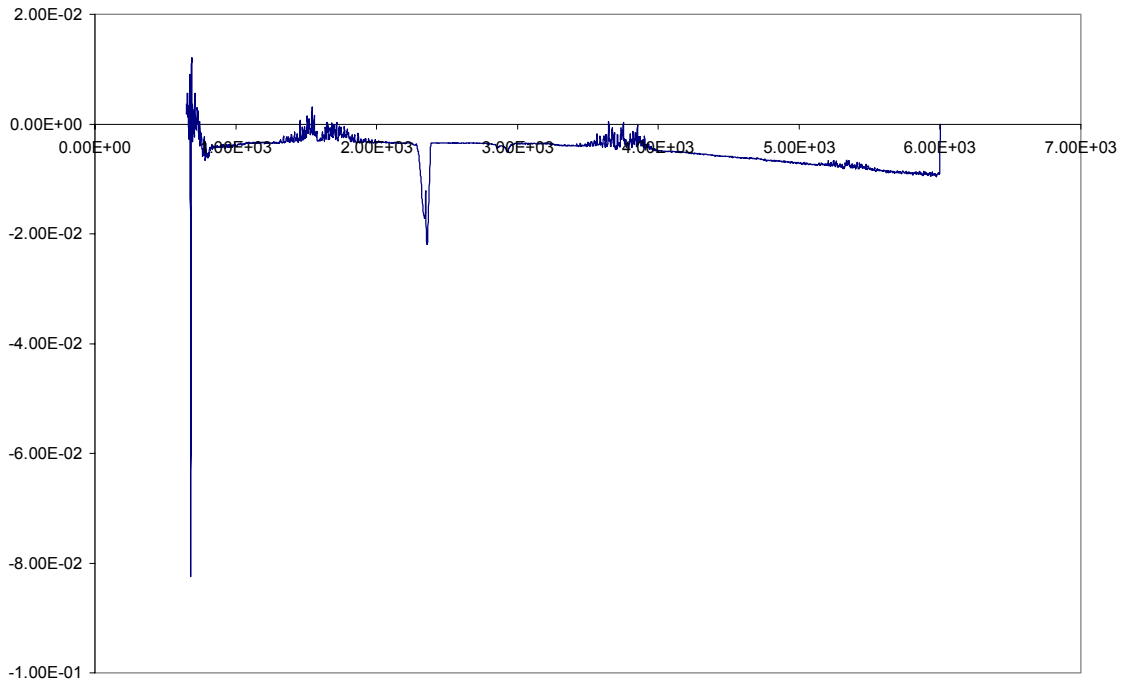
Spectra B-3

Spectra B-4
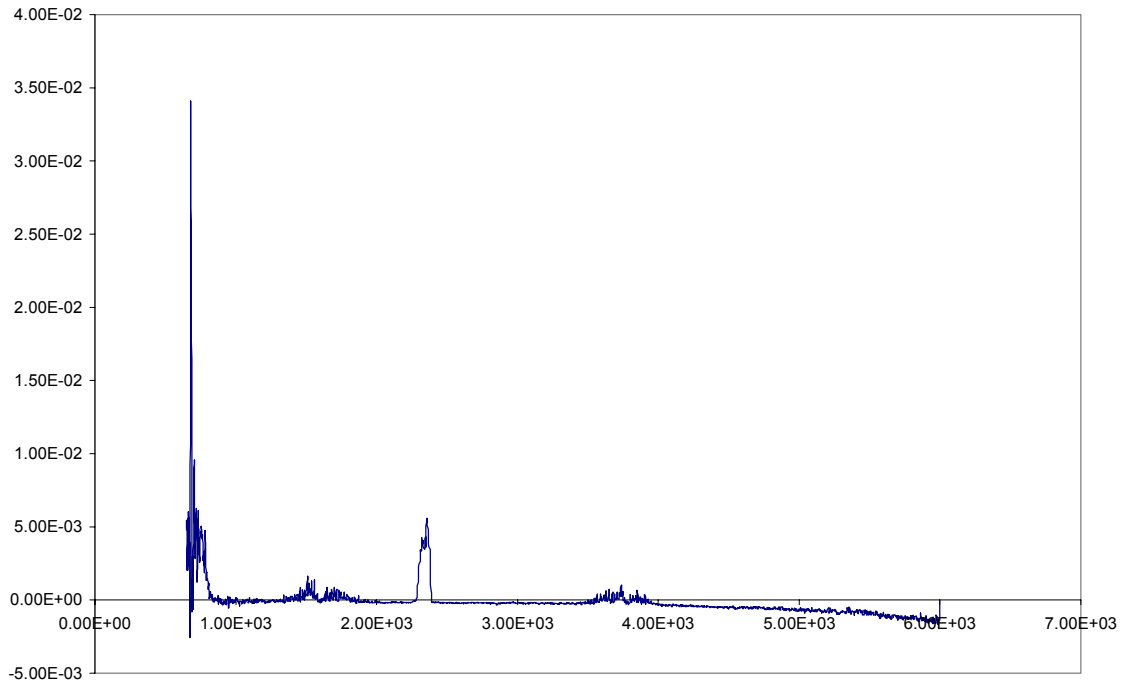
Spectra B-5
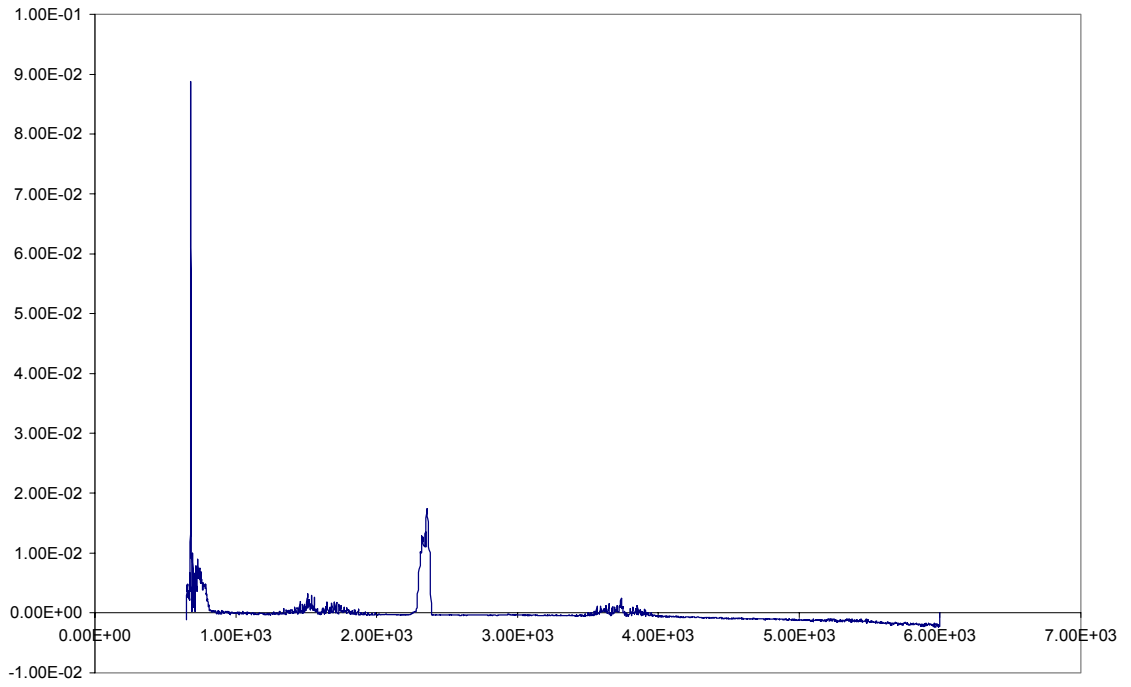
Spectra B-6
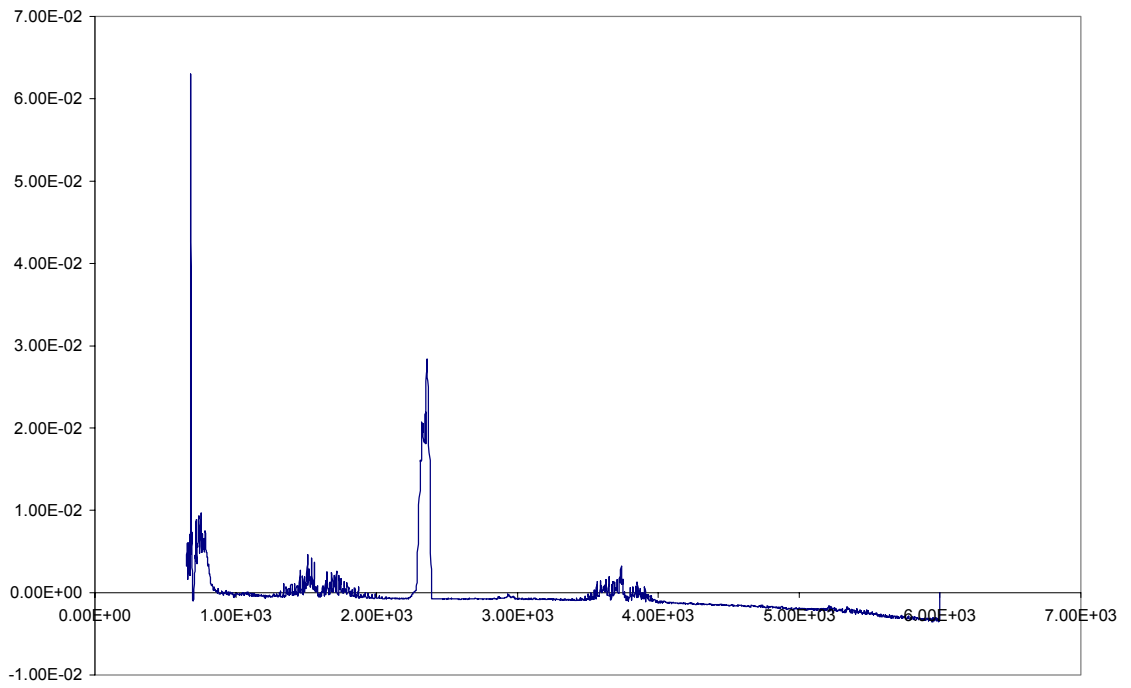
Spectra B-7
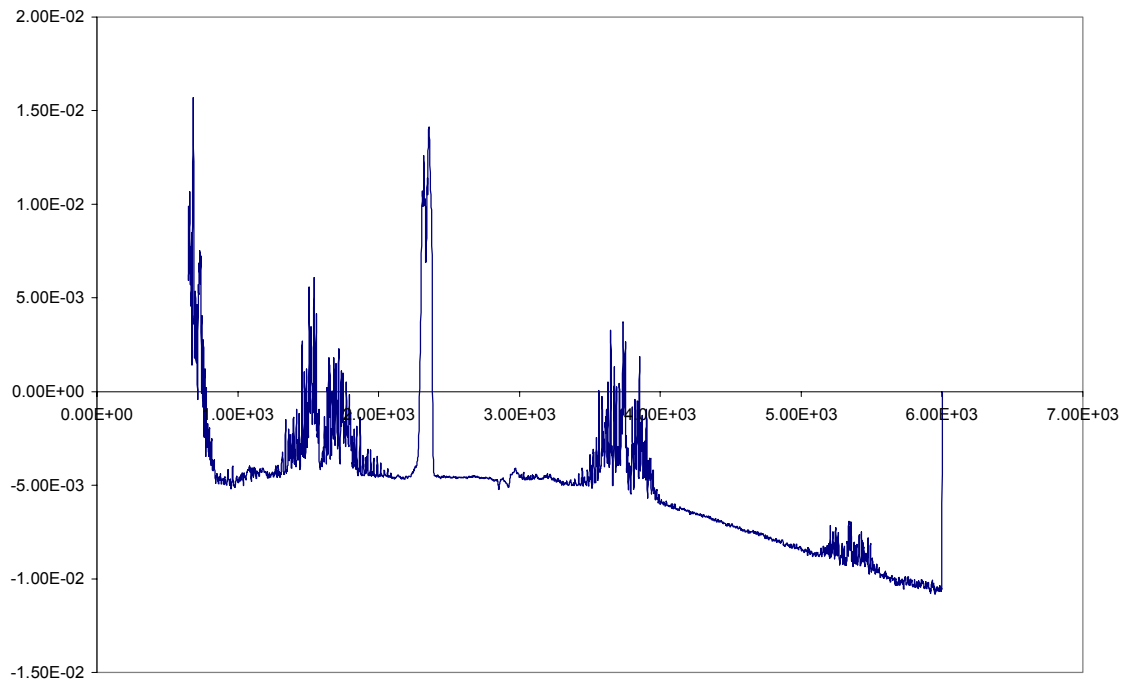
Spectra B-8

108
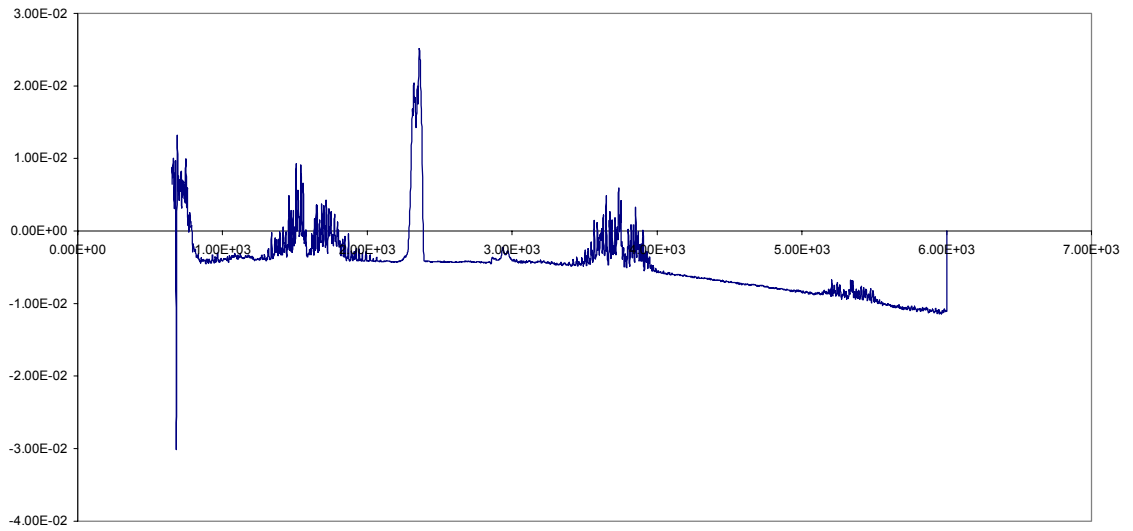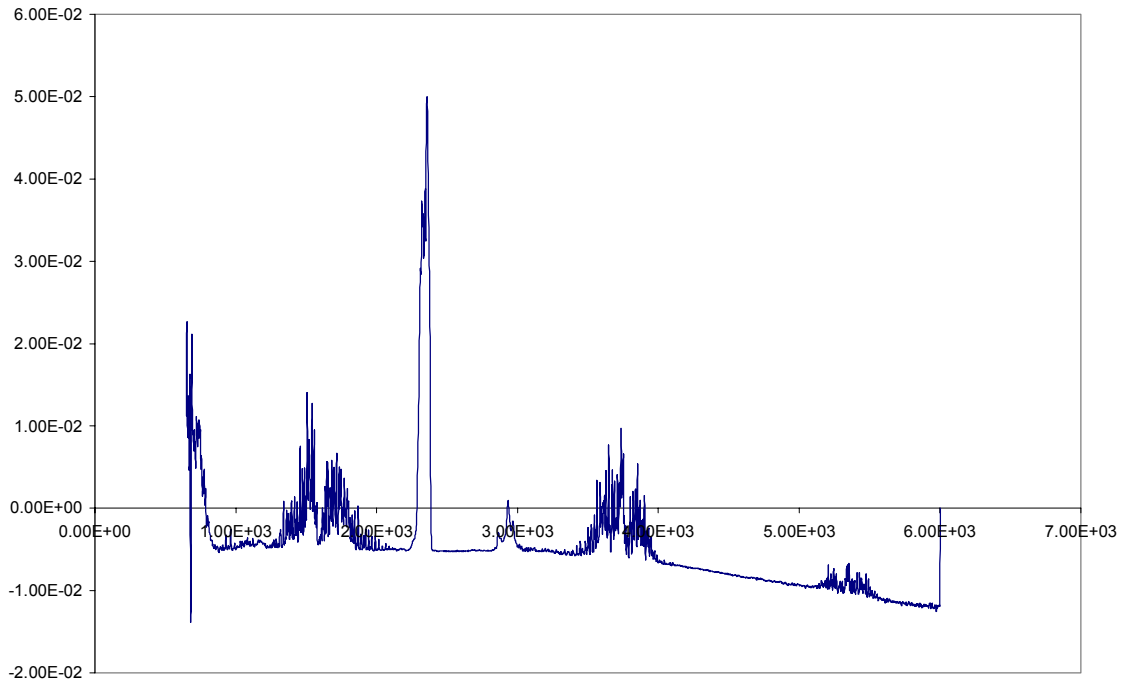
Spectra B-9

Spectra B-10
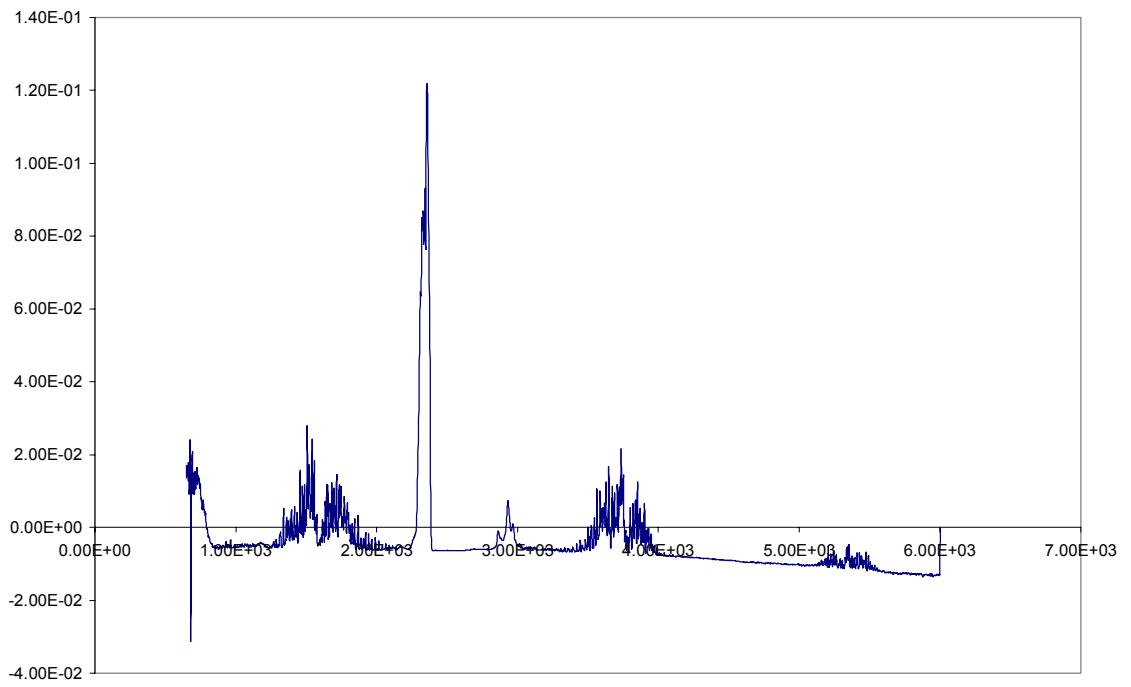
Spectra B-11
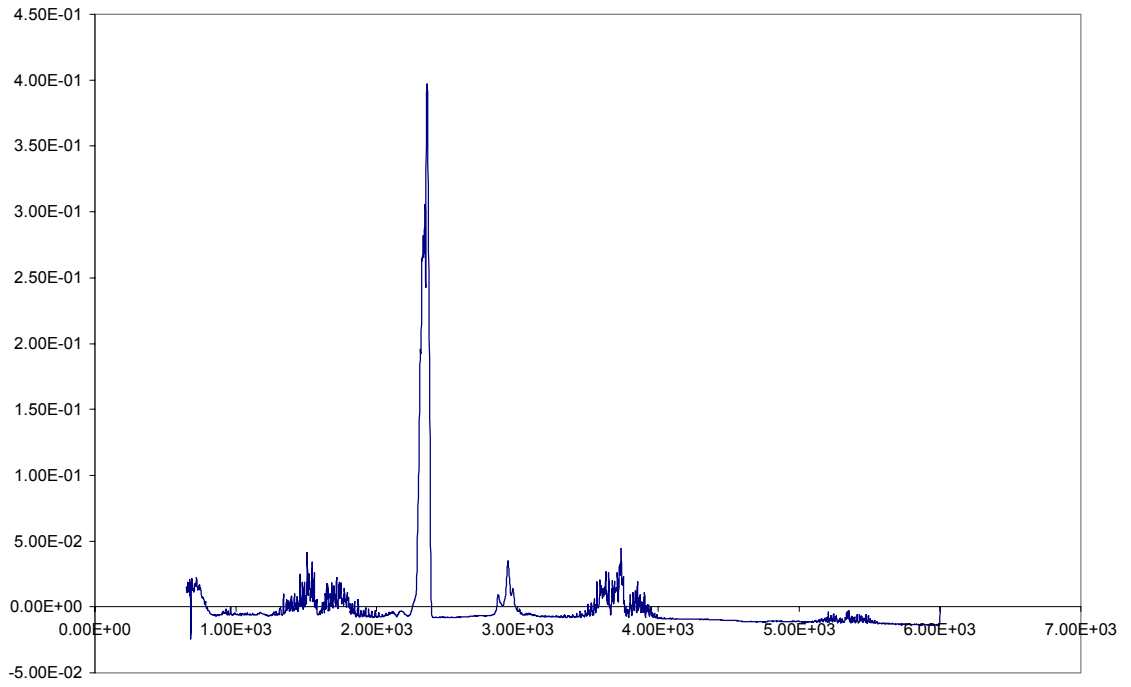
Spectra B-12
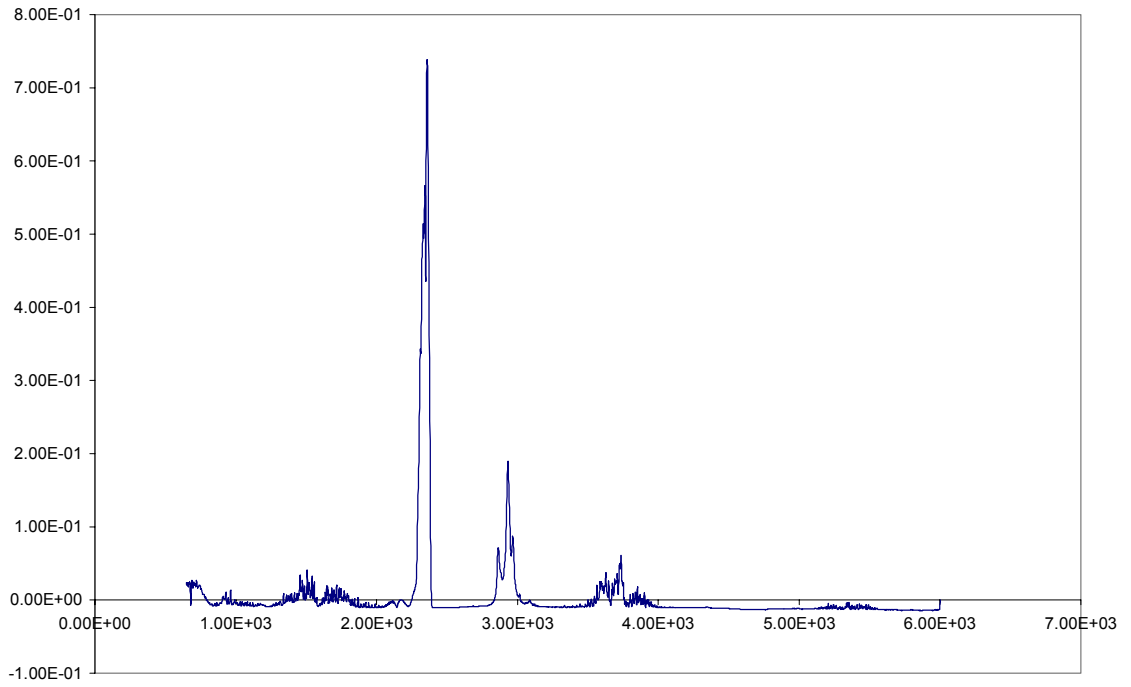
Spectra B-13

Spectra B-14

111
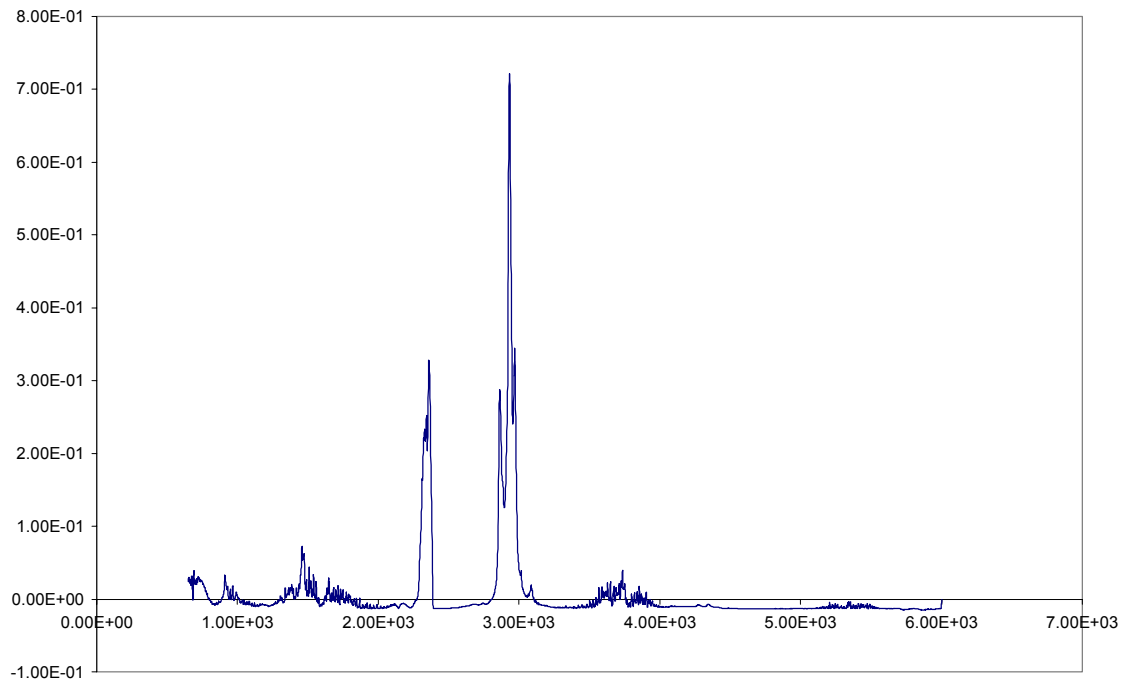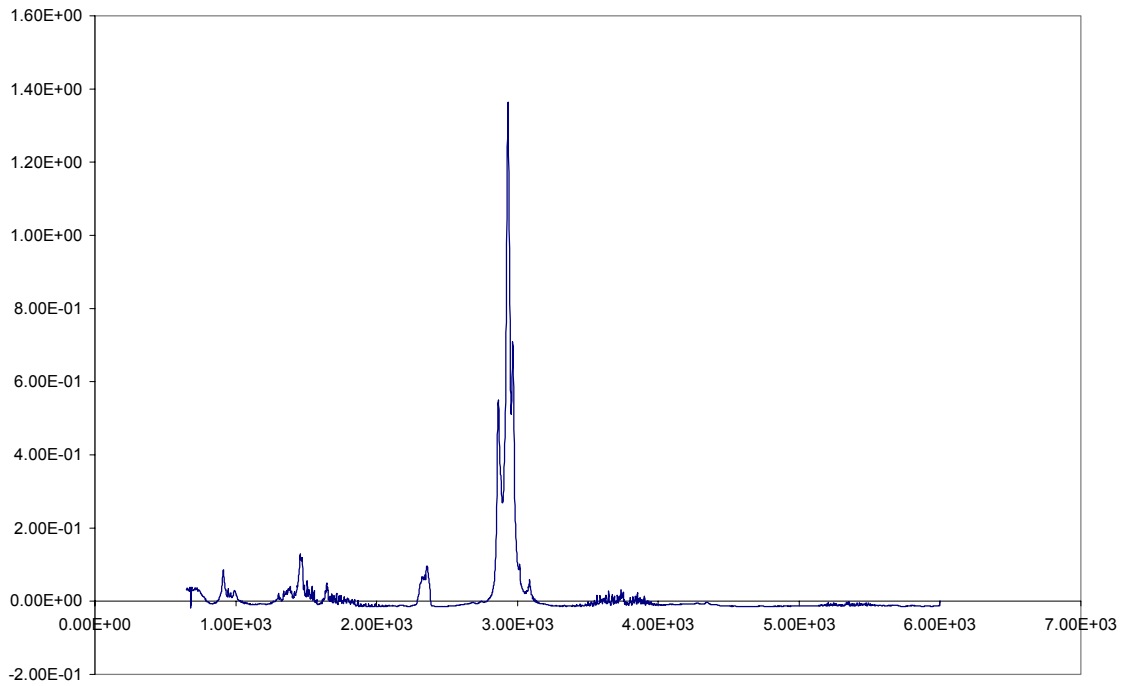
Spectra B-15

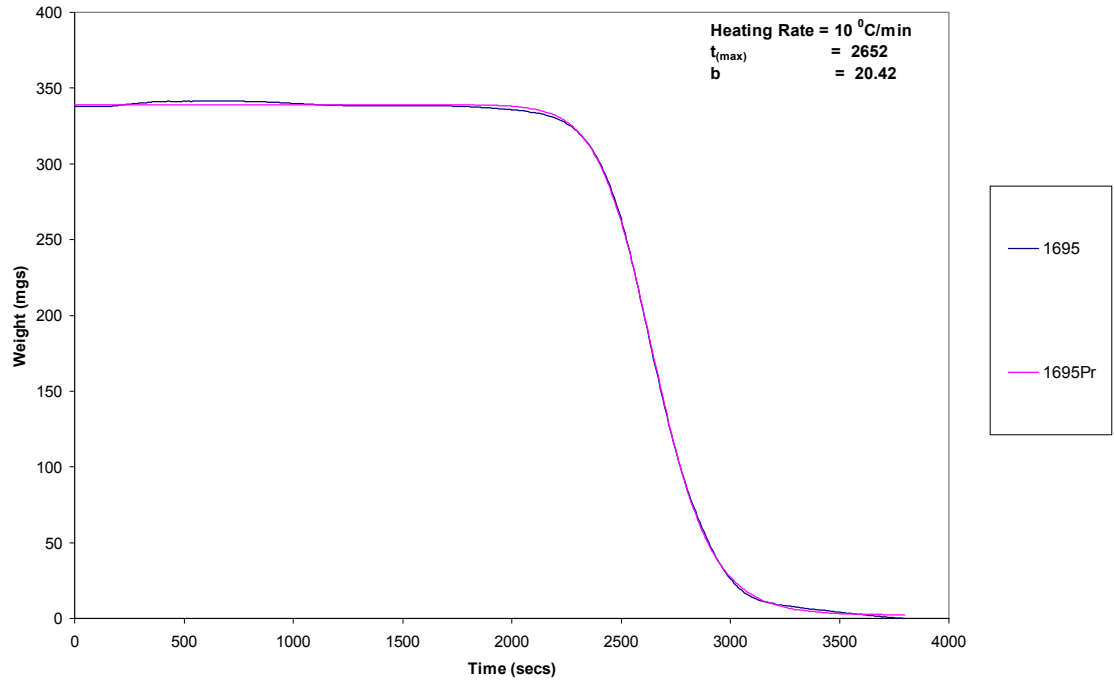**Spectra B-16**

112
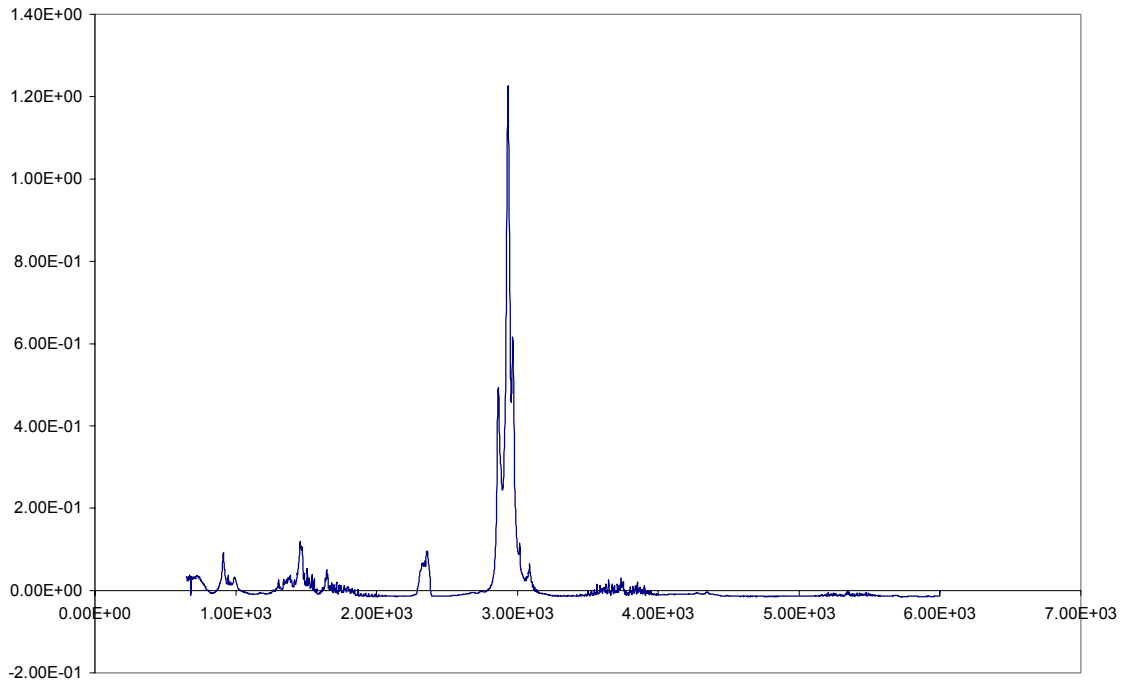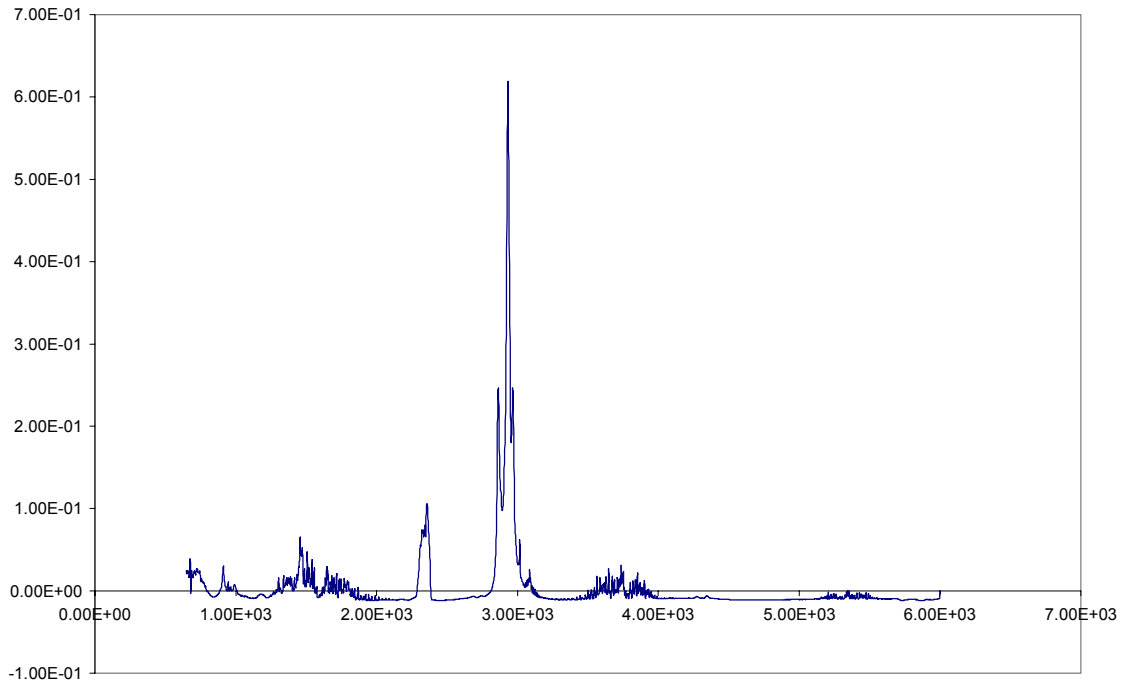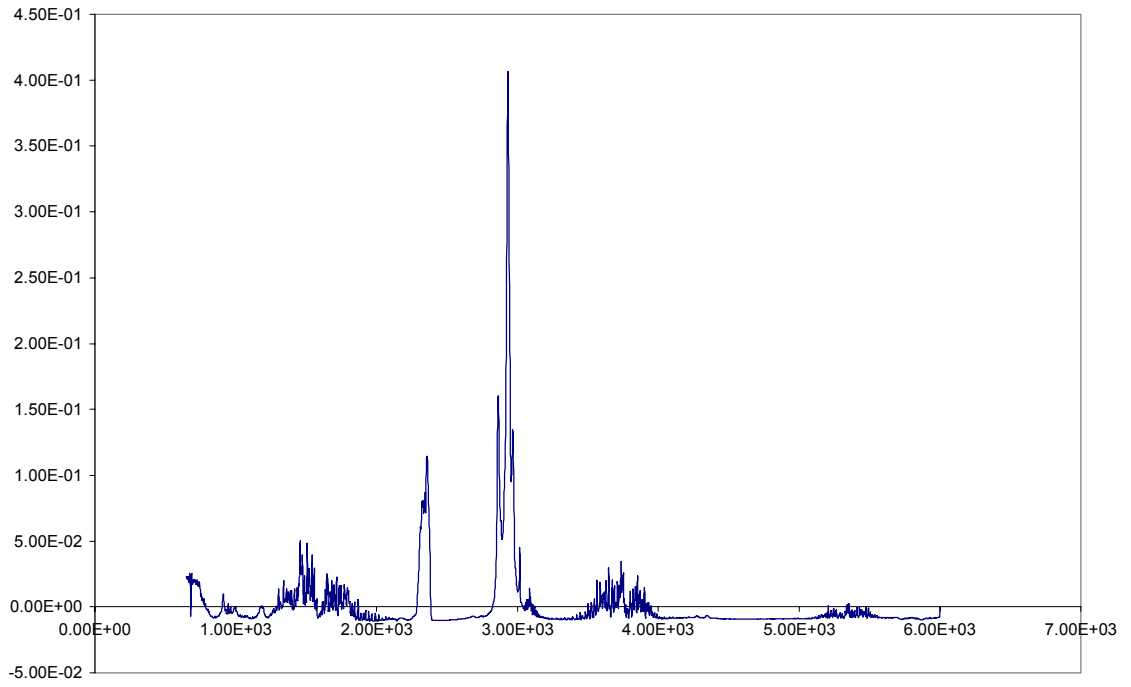
Spectra B-17

Spectra B-18
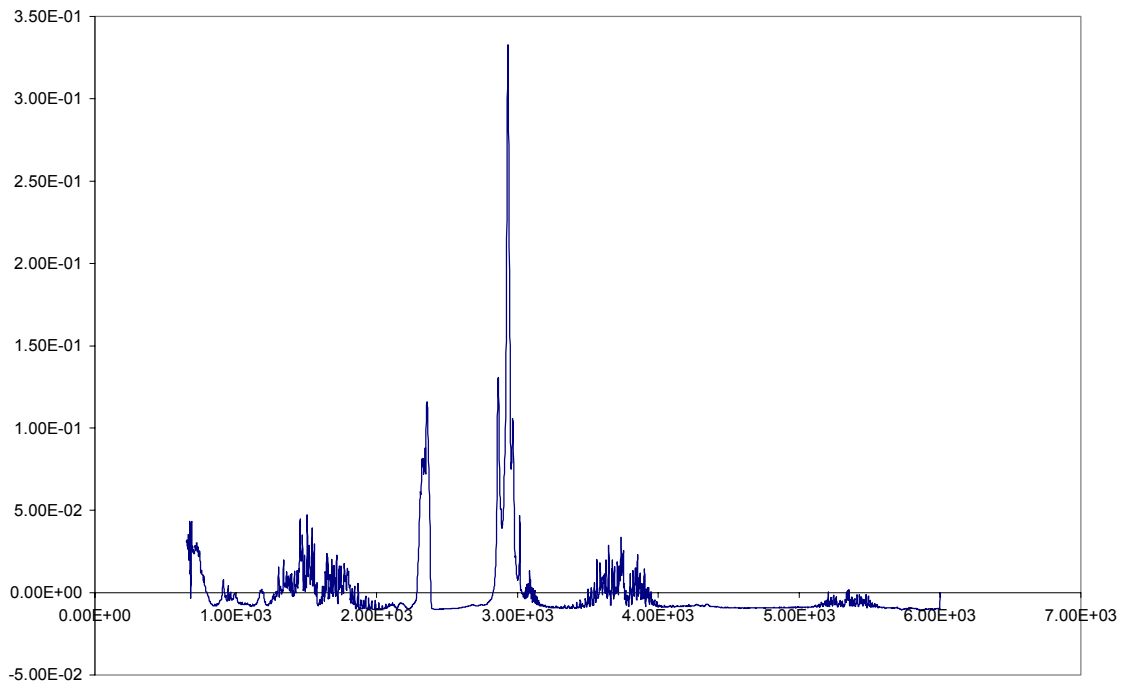
Spectra B-19
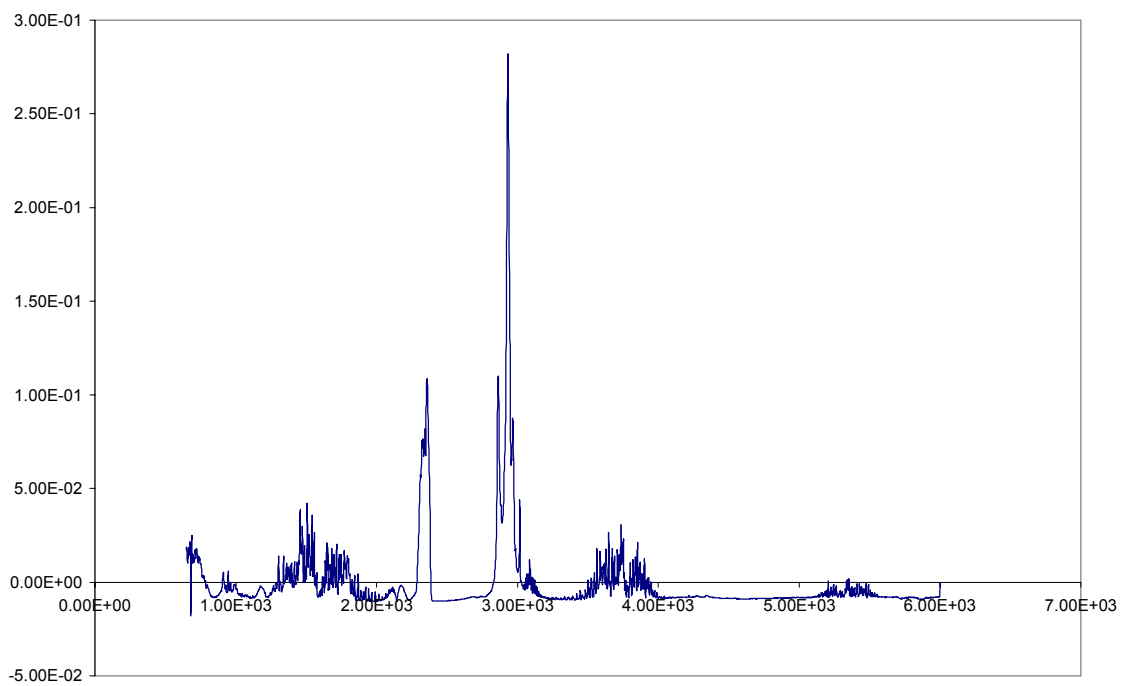
APPENDIX E: ACTUAL AND PREDICTED DATA OF THE MODEL

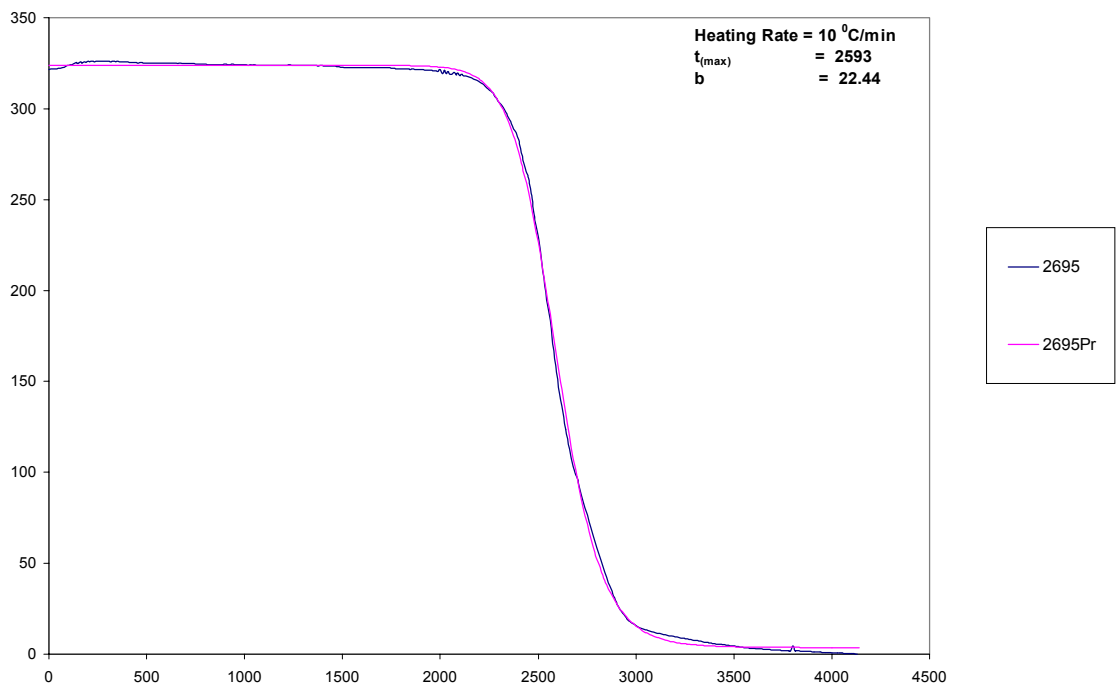**Actual Vs Predicted Weight Vs Time for Green Density 6.80 gm/cc (Trial 1)**
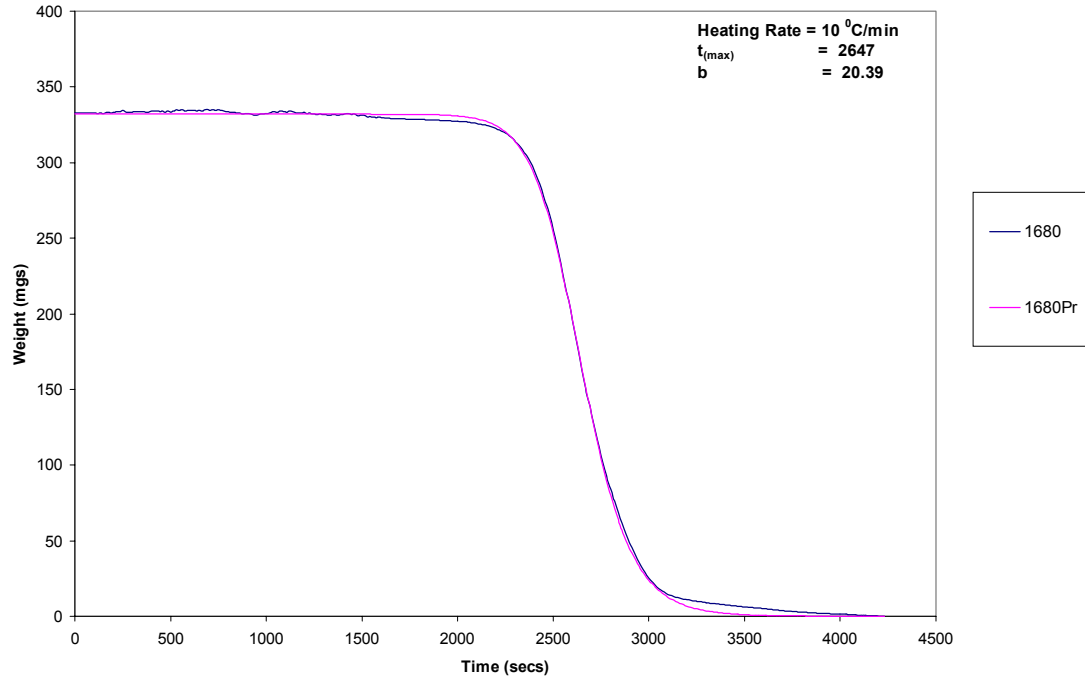
Heating Rate = 10 ^{0}C/min
$t_{(max)}$ = 2647
b = 20.39

Legend: 1680, 1680Pr

Actual Vs Predicted weight Vs Time for Green Density 6.95 gm/cc (Trial 1)

Heating Rate = 10 ^{0}C/min
$t_{(max)}$ = 2652
b = 20.42

Legend: 1695, 1695Pr

Actual Vs Predicted weights Vs Time for Green Density 6.80 gm/cc (Trial 2)

Heating Rate = 10 ^{0}C/min
$t_{(max)}$ = 2678
b = 23.64

Weight (gms)

Time (Secs)

2680

2680Pr

Actual and Predicted Weight Vs Time for green Density 6.95 gm/cc (Trial 2)

Heating Rate = 10 ^{0}C/min
$t_{(max)}$ = 2593
b = 22.44

2695

2695Pr
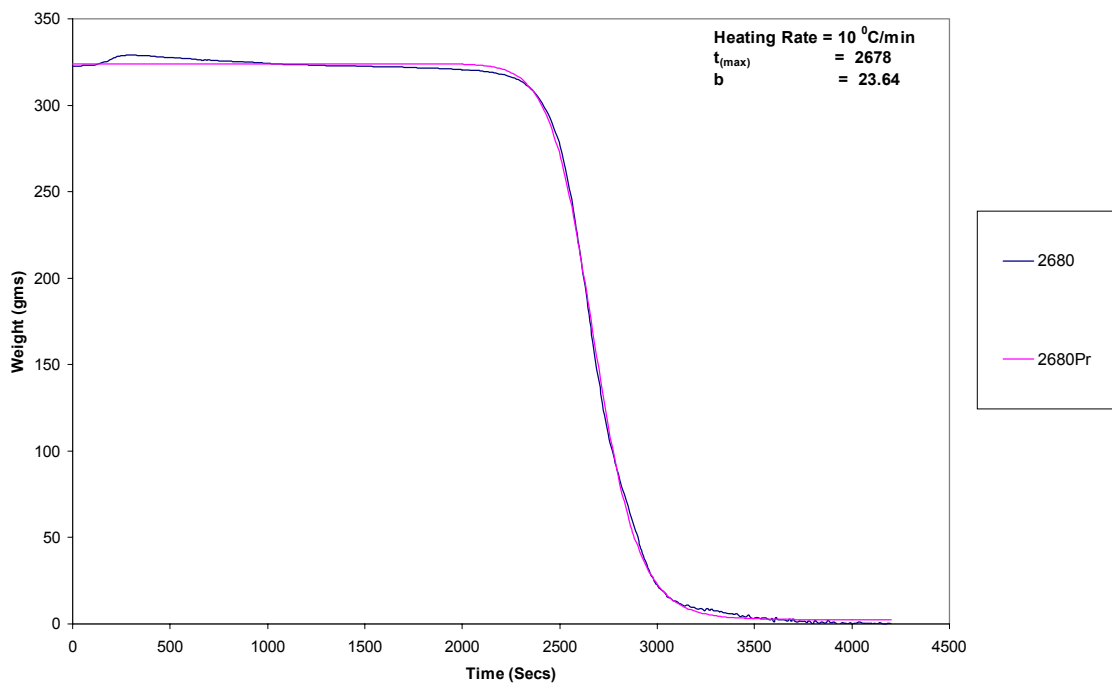
Actual and predicted weights Vs Time for Green Density 7.04 (Trial 2)
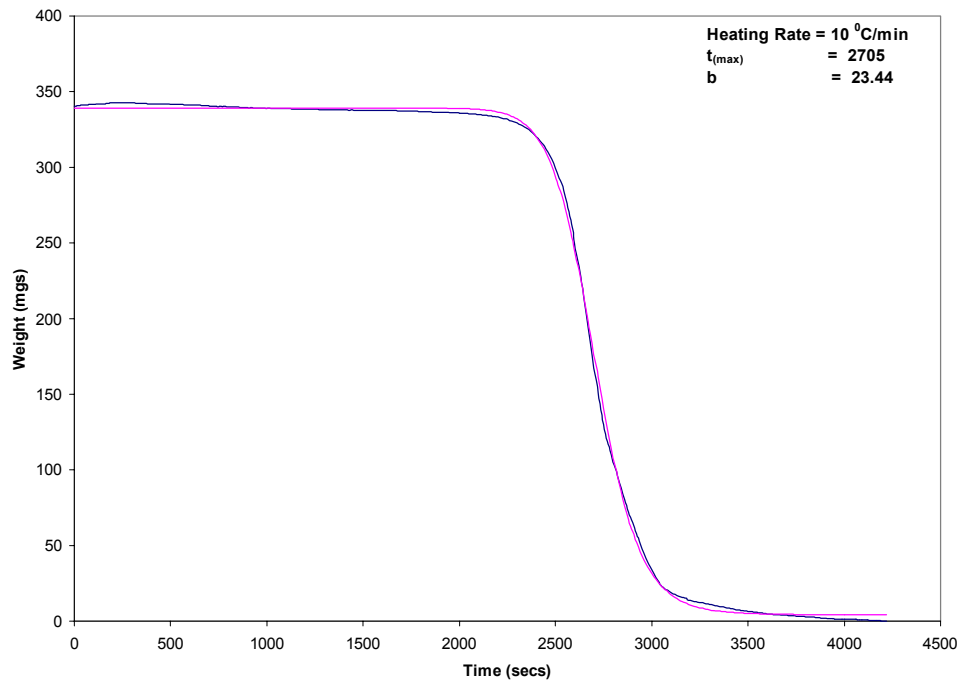
Heating Rate = 10 ^{0}C/min
$t_{(max)}$ = 2705
b = 23.44

Weight (mgs)

Time (secs)

2704

2704Pr

Actual and Predicted weights Vs Time for Green Density 6.80 gm/cc (Trial 3)

Heating Rate = 10 ^{0}C/min
$t_{(max)}$ = 2651
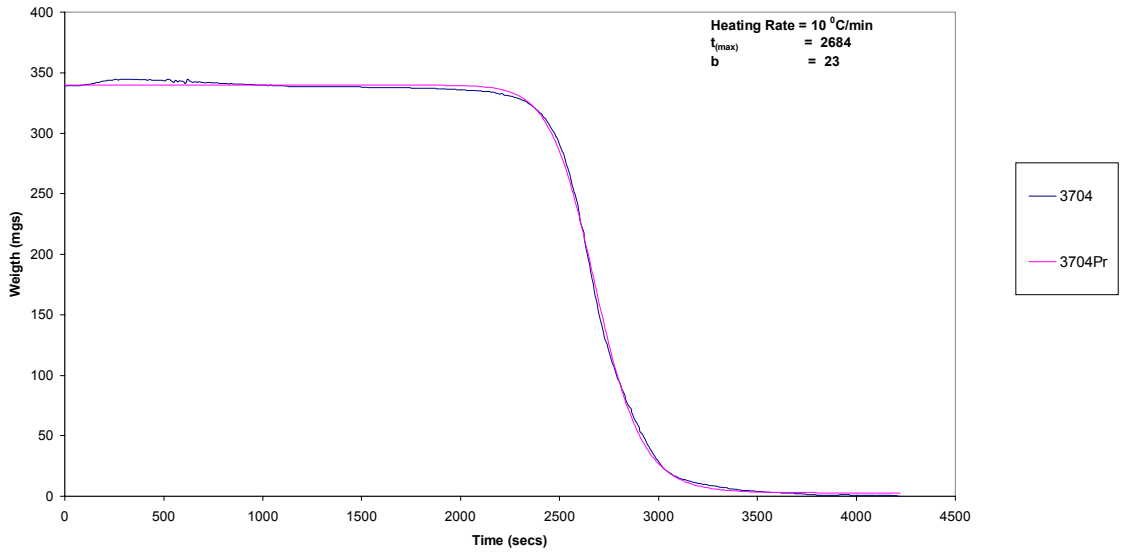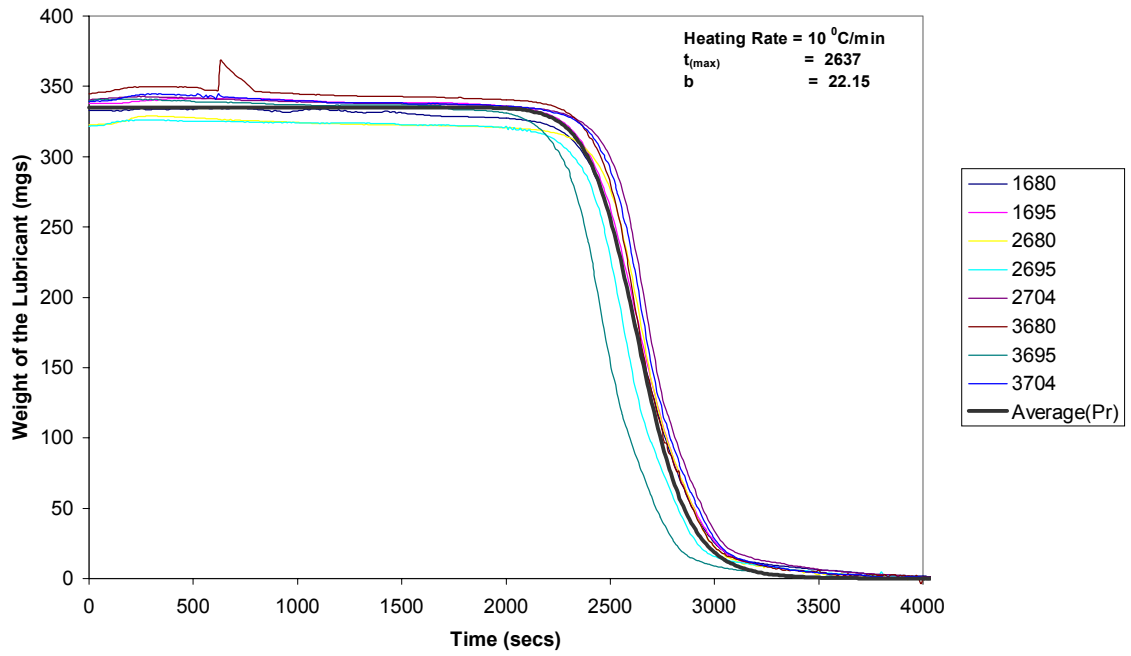b = 22.57

Weight (mgs)

Time (secs)

3680

3680Pr
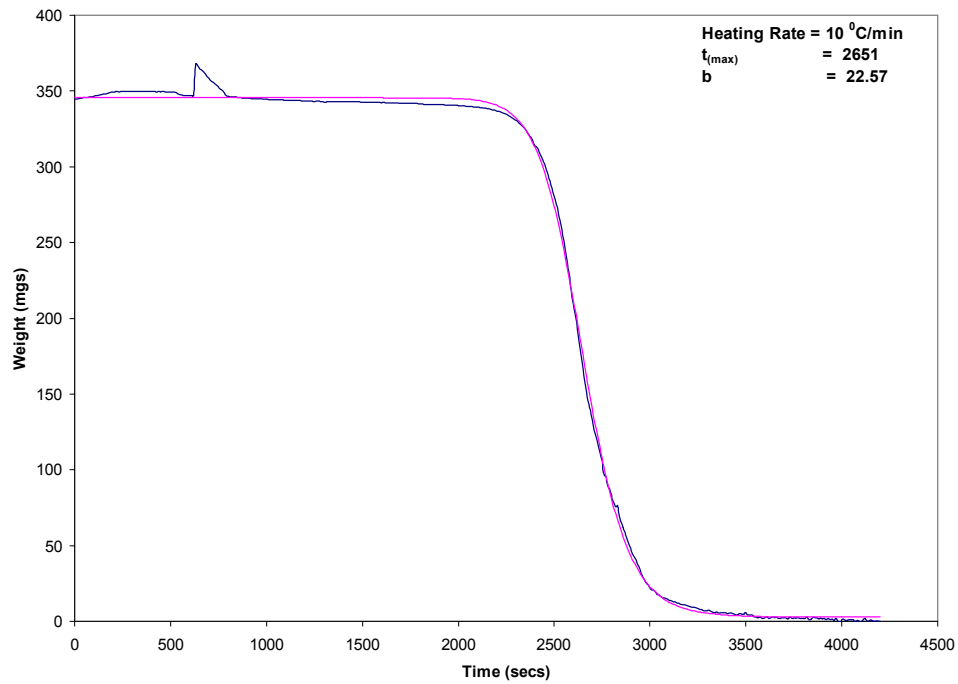
Actual Vs Predicted weight Vs Time for Green Denisty 6.95 gm/cc (Trial 3)
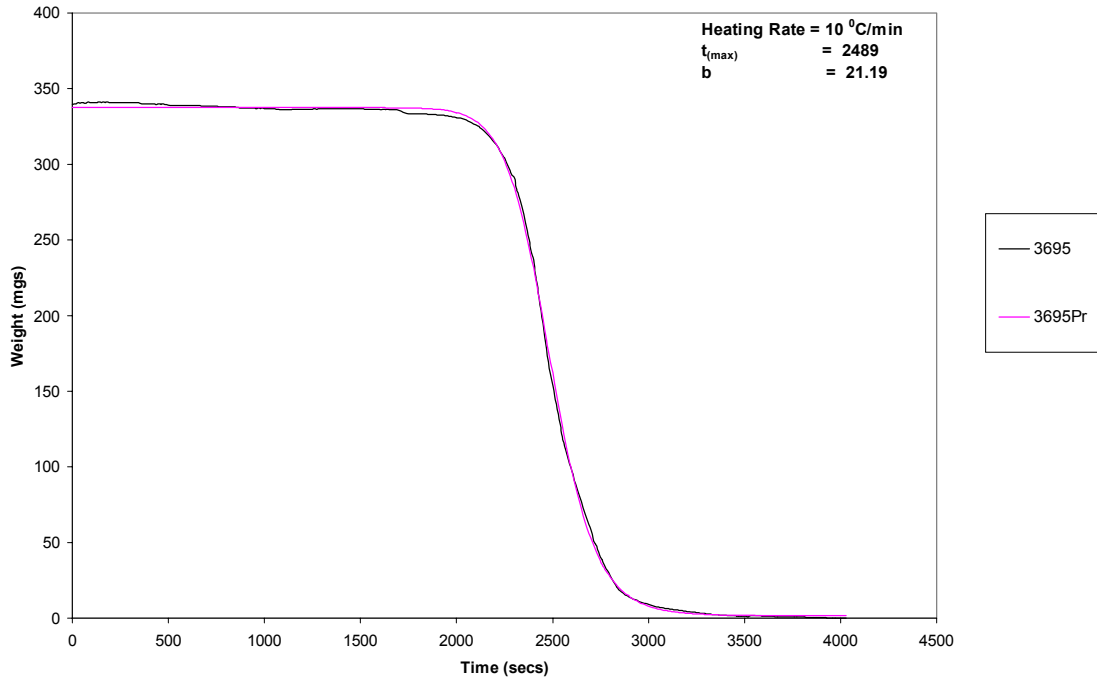
Actual Vs Predicted Weight for Green Denisty 7.04 gm/cc (Trial 3)

Actual Vs Predicted (Average of the 'b' and 'c' of the actual values)
Heating Rate ---------- 10 ^{0}C/min

Predicted Vs Actual (Average of 'c' and 'b' of the actual values)
Heating Rate -------- 30 ^{0}C/min